Modeling and Mitigation of Harmonic Distortions Caused by Mass-Distributed Harmonic Sources

by

Tianyu Ding

A thesis submitted in partial fulfillment of the requirements for the degree of

Doctor of Philosophy

in

Energy Systems

Department of Electrical and Computer Engineering
University of Alberta

Abstract

In recent years, the proliferation of energy-efficient but harmonic-producing home appliances has significantly changed the nature of power system harmonic problems. One of the main concerns nowadays is the harmonics produced by small, mass-distributed harmonic sources. Their unique random and distributed nature brings new challenges to harmonic modeling and mitigation.

This thesis presents methods to address some of the above challenges. They are (1) a method to model the collective impact of the mass-distributed harmonic sources in a secondary residential system and (2) three techniques to mitigate the harmonic distortions caused by the mass-distributed harmonic sources.

For the first subject, this thesis develops an analytical method which incorporates both the random behavior and electrical characteristic of the residential loads in order to model the collective impact of the harmonic-producing home appliances in a secondary residential system.

For the second subject, the three techniques developed in this thesis are as follows. The first one is a filtering scheme to prevent harmonics' penetration from residential distribution systems into the transmission systems. It utilizes the low-voltage tertiary winding of a distribution substation transformer to construct a low impedance path to realize harmonics' trapping. The second is an improved design method for the 3rd order high pass filter. It is established based on minimizing the filter fundamental frequency loss. This research also led to the third technique developed in this thesis, a method to create resonance-free shunt capacitors. Two configurations, the 3rd order high pass filter and C-type filter, are investigated for constructing the resonance-free capacitor. Design methods are developed, and their relative performance is studied.

Extensive analytical and simulation studies are conducted to validate the above methods. The results confirm that these methods are effective for the modeling or mitigation of harmonic distortions caused by mass-distributed harmonic sources.

Preface

This thesis is an original work by Tianyu Ding. As detailed in the following, some chapters of this thesis have been published as scholarly articles, in which Prof. Wilsun Xu is the primary supervisor and has contributed to concepts formations and manuscript composition, Prof. Hao Liang is the co-supervisor and has assisted with the mathematical derivation and manuscript composition, Xin Li has been involved in the case studies discussion.

Part of Chapter 2 of this thesis has been published as T. Ding, H. Liang, and W. Xu, "An analytical method for probabilistic modeling of the steady-state behavior of secondary residential system," *Smart Grid, IEEE Transactions on*, [to appear], DOI: 10.1109/TSG.2016.2530630.

Part of Chapter 3 of this thesis has been published as T. Ding and W. Xu, "A filtering scheme to reduce the penetration of harmonics into transmission systems," *Power Delivery*, *IEEE Transactions on,* vol. 31, pp. 59-66, Feb. 2016.

Part of Chapter 4 of this thesis has been published as T. Ding, W. Xu, and H. Liang, "Design method for third-order high-pass filter," *Power Delivery, IEEE Transactions on*, vol. 31, pp. 402-403, Feb. 2016.

Part of Chapter 5 of this thesis has been published as W. Xu, T. Ding, X. Li, and H. Liang, "Resonance-free shunt capacitors: configurations, design methods and comparative analysis," *Power Delivery, IEEE Transactions on*, vol. 31, pp. 2287-2295, 2016.

Acknowledgements

First and foremost, I would like to express my sincere gratitude to my supervisor Dr. Wilsun Xu. Without his inspiring guidance and great supervision, this research and thesis would not have been possible. I deemed it as my privilege to be his student. I am also thankful to my co-supervisor Dr. Hao Liang. His constructive feedback and insightful suggestions have contributed greatly to my research work.

Thanks also go to all my colleagues in PDS Lab. I thank Ming Dong, Pengfei Gao, Yu Tian, Qingxin Shi, Bing Xia, Yang Wang, Ricardo Torquato, Xiang Li, Benzhe Li, Xin Li, Yaxiang Zhou, Pooya Bagheri, Juncheng Wang, Tianyi Hou, Wenrui Wu, Wenhai Zhang, Haitao Hu, Yu Liu, Guangchao Geng, Xiangguo Yang, Moosa Moghimi Haji, Kunlong Chen, Ramiar Alaei, Yuanyuan Sun and Hyunjung Yong, for their help and friendship. Special thanks go to Dr. Jing Yong for her constant support and disinterested assistance during our team project.

Finally, I want to extend my deepest appreciation to my parents and my sister. They have always supported and encouraged me to do my best in all matters of life. I dedicate this thesis to them.

Table of Contents

List of Tables

List of Figures

Abbreviations

2ndHP	2nd order high pass
3rdHP	3rd order high pass
CI	Confidence interval
EV	Electrical vehicles
IDD	Individual demand distortion
IHD	Individual harmonic distortion
LL	Line to line
MCS	Monte Carlo simulation
MV	Medium voltage
NZS	Non-zero-sequence
p.u.	Per-unit
PCC	Point of common coupling
rms	Root mean square
Std	Standard
TDD	Total demand distortion
THD	Total harmonic distortion
ZS	Zero-sequence

Chapter 1

Introduction

Harmonic distortion may adversely affect both power system components and customers' devices [1-5]. Therefore, it has always been one of the main power-quality concerns since the early use of the alternating current in electrical power systems. This introductory chapter first presents an overview of the harmonics in today's power systems. Then, the problems needing to be solved are discussed. Finally, this chapter presents the scope and outline of this thesis.

1.1 Harmonics in Today's Power Systems

For decades, industrial customers have been the major harmonic producers. These loads are concentrated and connected to the utility grid through a point of common coupling (PCC). Interconnection standards have been established to limit the harmonic emission from them. To be allowed to connect to the utility grid, industrial customers must take measures to reduce the harmonics they inject into the PCC. Many effective methods are available to fulfill this need. Examples are installing harmonic filters inside the facility and using drives that generate only a small amount of harmonics. Currently, with the widespread adoption of standards such as the IEEE Std 519 [6], industrial customers inject only a few harmonics into the utility grid.

However, in recent years, a dramatic penetration of modern nonlinear electronic devices into the regularly used home appliances has occurred. More and more home appliances are becoming harmonic sources. Examples are the desktop PC, the laptop, the microwave, the LED-light, the washer, the fridge, and the vacuum. Figure 1.1 shows the measured current waveform for common home appliances [7-9], revealing that the current drawn by these home appliances is quite distorted. For some home appliances, such as the laptop and the LED-light, their current total harmonic distortion (THD) can even exceed 100%. Due to their relatively small rating, the harmonic current produced by each of such home appliances is insignificant. The collective impact of a large number of such home appliances, however, can be quite substantial. This phenomenon has been observed in field measurements conducted in residential distribution systems. For example, Figure 1.2 shows the measured current individual demand distortion (IDD) spectra of a residential feeder [9]. The only sources of harmonics in this feeder are the aforementioned nonlinear home appliances. As Figure 1.2 indicates, the harmonic currents produced by harmonic-producing residential loads have built up to a level that exceeds the IEEE Std 519 harmonic limits. Moreover, several power-quality concerns have been identified due to these mass-distributed harmonic sources. Examples are the telephone interference in new suburban areas [10], the overloading of concentric neutral cables [11], and the pipeline induction [12]. As a result, the harmonics produced by mass-distributed harmonic-producing home appliances must be treated seriously.

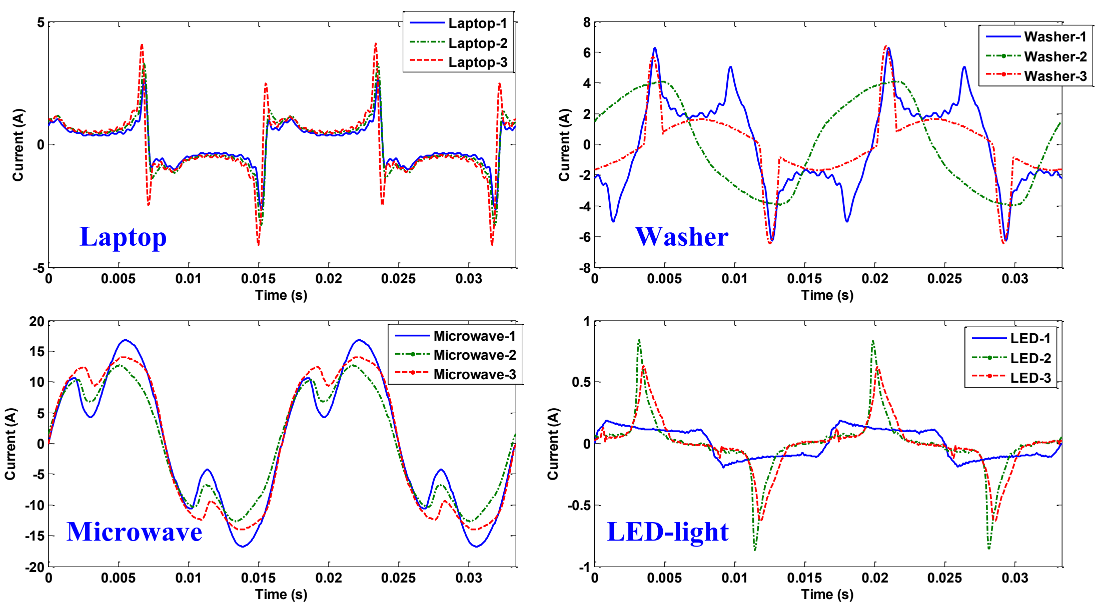

Figure 1.1: Typical current waveforms for common home appliances [7-9]

In summary, today's main harmonic sources have evolved from traditional large lumped industrial loads into numerous small nonlinear home appliances distributed in every household. This evolution has made today's power systems become systems with mass-distributed harmonic sources. Further, the unique distributed and random nature of such harmonic sources has turned the harmonic distortion management of such systems into a challenging task. Many issues need to be investigated, such as the following:

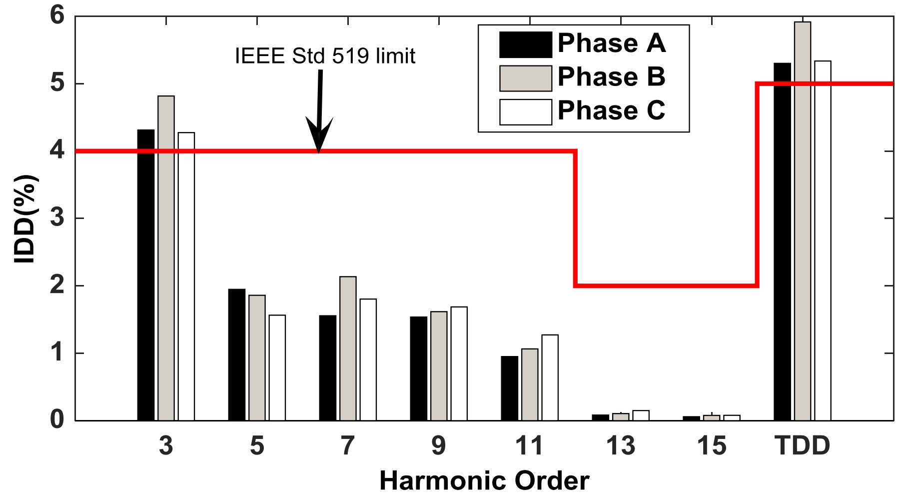

Figure 1.2: Typical IDD spectra of a residential feeder [9]

- How to show the harmonic distortion potential of a new device?
- How to impose harmonic limits on individual home appliances?
- How to select the representative locations in residential feeders for the harmonic monitoring?
- How to mitigate harmonic distortions in residential feeders?
- How to prevent harmonics' propagation from residential distribution systems into transmission systems?
- How to avoid shunt capacitor related harmonic resonance incidents due to the mass-distributed harmonic sources?
- How to select locations to implement filters for the system-wide harmonic mitigation or a single-point problem solving in a transmission system connecting several residential distribution systems?

Unfortunately, these issues cannot be satisfactorily addressed by using traditional methods or existing techniques. For example, using traditional harmonic assessment methods to predict the harmonic impact of the penetration of electrical vehicles (EVs) generally gives quite unrealistic results [13], mainly because traditional methods cannot model the random charging behavior of the EVs, which is highly affected by the driving habits of the vehicle owners.

In general, solving issues associated with systems with mass-distributed harmonic sources calls for new ideas for harmonic modeling and management.

1.2 Problem Definition

This thesis focuses on developing modeling methods to deal with the aggregation of random harmonics produced by mass-distributed home appliances, and solutions dedicated to mitigating the harmonic distortions caused by them. Four specific problems to be solved by this thesis are defined in this section.

1.2.1 Harmonic Modeling of the Secondary Residential System

Harmonic assessment is to quantify the distortion of the voltage and the current at various points in a system. It is used to determine the impact of harmonic-producing loads on a system. Proper harmonic assessment serves as the critical first step in the effective control of the harmonic distortion level. The focus of the harmonic assessment for the systems with mass-distributed harmonic sources is the residential distribution systems.

In North America, the most common distribution system supplying residential loads is of the multigrounded neutral type. An example is shown as Figure 1.3. The system can be divided into the primary system and the secondary systems. The primary system consists mainly of a multi-grounded feeder, which delivers the electrical power from the substation to the customers at various locations through the secondary systems. Each secondary system consists of a service transformer, the secondary feeder, and a number of households supplied by it. Each household has various home appliances, which may be switched on or off randomly. When nonlinear home appliances are switched on, they produce harmonic currents, which flow to the service transformer. The harmonic currents then aggregate at the primary feeder and finally propagate to the substation.

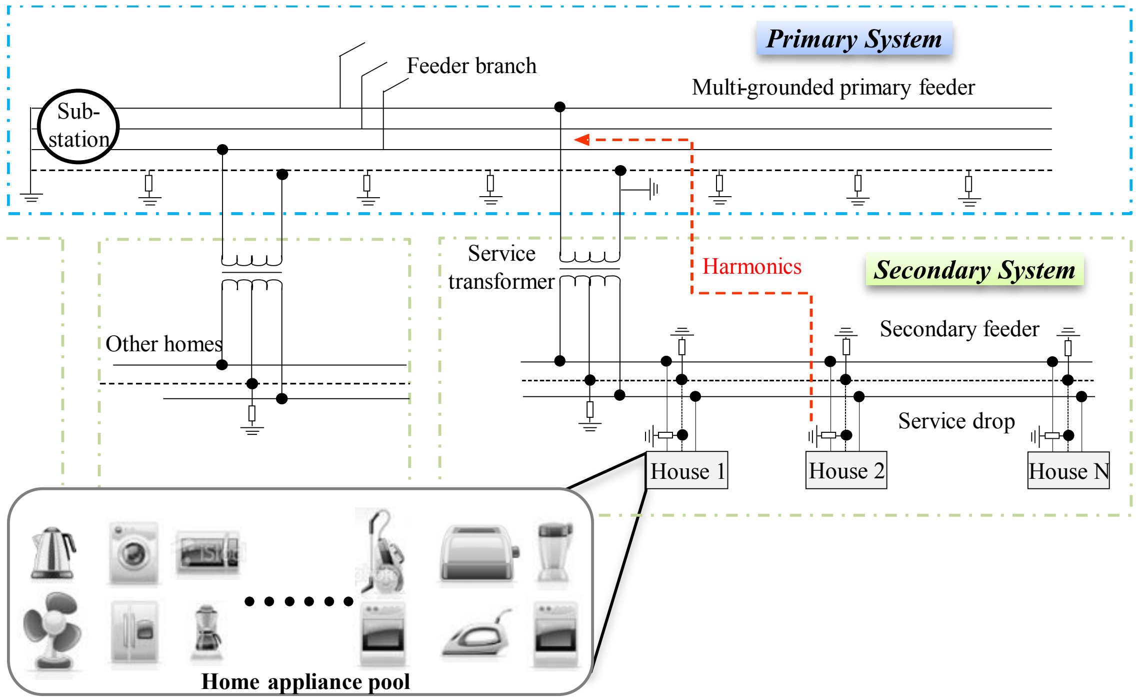

Figure 1.3: Example of a residential distribution system in North America

The harmonic assessment of the above-mentioned residential distribution system is facing four main technical challenges:

1) The randomness in the harmonic currents produced by each type of home appliances should be captured.

2) The assessment must be able to characterize the uncertainty in the aggregate harmonics produced by various home appliances.

3) The unique features of the multiphase multigrounded primary and secondary systems should be considered.

4) The assessment should be scalable, as a typical residential distribution substation serves thousands of households, while each household may have dozens of home appliances.

Previous studies have investigated various aspects of these challenges [14-19]. However, an approach for systematically addressing all of them is still not in a complete shape. As aforementioned, the harmonic distortions in residential distribution systems originate from the mass-distributed nonlinear home appliances (the bottom of the distribution system), and gradually aggregates at systems with higher voltage levels. A bottom-up approach generally fits such a characteristic and can be utilized for harmonic assessment in residential distribution systems. Its schematic view is shown as Figure 1.4.

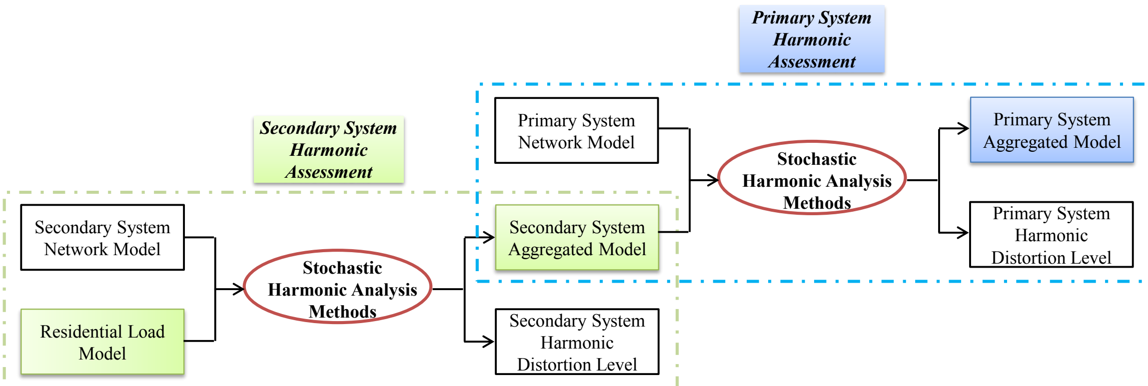

Figure 1.4: The schematic view of the bottom-up harmonic assessment approach

The bottom-up approach breaks down the harmonic assessment in residential distribution systems into two levels: the secondary system harmonic assessment and the primary system harmonic assessment. Models with different granularities can be used for the assessment of the different levels. For example, in the primary system harmonic assessment, each secondary system can be represented by its aggregate model, in which encompassed home appliances are not individually modeled.

The harmonic assessment at each level includes two tasks: (1) calculating the harmonic distortion level in various locations and (2) developing an aggregate system model for harmonic assessment of the system at a higher voltage level. One key step in implementing the bottom-up approach is to develop a method to obtain an aggregate model of the secondary residential system that can be used in the primary system harmonic assessment.

1.2.2 Reducing Harmonics' Penetration into Transmission Systems

Several power-quality concerns have been identified due to the mass-distributed harmonic sources in residential neighborhoods [10, 20-24]. A critical one is that residential distribution systems are injecting a significant amount of harmonic currents into transmission systems [23, 24]. The consequences include the tripping of transmission capacitors, the overloading of HVDC filters, and increased incidents of transmission harmonic resonances [1, 2, 4].

Currently, it is common that transmission and distribution systems are owned by different owners due to the electricity market deregulation. Therefore, the penetration of harmonic currents from distribution systems into transmission systems is becoming a sensitive issue. For example, several jurisdictions have imposed limits on such harmonics [25, 26].

So far, two types of solutions have been proposed to address this newly emerging harmonic issue. One solution is to reduce the harmonic emissions from individual electronic devices. IEC 61000-3-2 has been established for this purpose [27]. The second solution is to reduce the harmonic distortions in distribution systems through, for example, medium- and low- voltage filters [28-30]. Both solutions can reduce the amount of harmonic currents injected into the transmission systems. However, the adoption of the first solution is facing strong resistance from home appliance manufacturers, while the application of the second solution involves complex planning studies. This motivates the research on a low-complexity filtering scheme dedicated to reducing harmonics' penetration from residential distribution systems into transmission systems.

1.2.3 Design Method for Third-Order High-Pass Filter

The 3rd order high pass (3rdHP) filter is widely used to filter high order harmonics such as the 11th and 13th harmonics for both industrial systems and HVDC links [1, 31-33]. It is potentially useful for mitigating the harmonic distortions caused by mass-distributed harmonic sources.

However, in spite of its wide application in industry, a technically sound design method for the 3rdHP filter has not been established. The 3rdHP filter consists of four components. Four design conditions or equations are therefore needed to determine their parameters. So far, only two conditions (the reactive power output requirement and the tuned frequency requirement) are generally agreed upon by designers and users. These two conditions are not sufficient to determine the parameters of all four components. There is a gap to be filled to arrive at a complete design method for the 3rdHP filter.

1.2.4 Resonance-Free Shunt Capacitors

Shunt capacitors are extensively used in electric power systems due to their well-known benefits, such as the power factor improvement, the voltage support, the release of system capacity, and the reduced system losses [34-39]. However, as with any piece of electrical equipment, a number of issues are involved in the application of the shunt capacitors. A critical one is that adding shunt capacitors to the system can potentially result in the formulation of resonance circuits at or near certain harmonic orders. If sources of harmonics exist at these orders, the harmonic distortions caused by them will be significantly amplified, which is typically called the *harmonic resonance*. This is not desirable as the amplified harmonic distortions will not only damage the shunt capacitors themselves, but also cause the insulation breakdown of nearby electrical equipment, nuisance trips of relay, and the excessive harmonic torque generation, etc [1, 35, 39, 40].

In the past, the shunt-capacitor related harmonic resonance was not a major issue. As discussed earlier, the main harmonic sources used to be large industry customers. The harmonics produced by them are well controlled though interconnection standards such as the IEEE Std 519 [6, 41]. Hence, only low-level harmonic distortions were propagating in the utility grid (both the distribution system and the transmission system). Therefore, even though the shunt capacitor and the system formed a resonance circuit, the harmonic resonance was not very severe as the excitation harmonic distortions were low.

Nowadays, the shunt-capacitor related harmonic resonance must be treated seriously due to the proliferation of distributed harmonic sources and the lack of corresponding mitigation methods to prevent the harmonics produced by these sources from being injected into the utility grid. The survey presented in [42] showed that residential customers were injecting significant harmonics into distribution systems. Paper [43] indicated that in today's transmission class shunt capacitors application, resonant conditions should be avoided due to the increased harmonic currents being injected into the transmission system. The studies in [44-46] revealed that harmonic resonance is also a major concern for shunt capacitors used in systems with power electronic-based energy conversion devices such as the wind power plants and photovoltaic generations, as they also produce harmonics themselves [47-49]. Increased incidents of the shunt-capacitor related harmonic resonance have been reported [4, 6, 35, 50-52]. In some cases, for example, a shunt capacitor cannot be energized due to excessive harmonic currents, leading to a reactive power shortage in the system [40, 53].

In view of the above situation, there is a need to investigate how to prevent shunt capacitors from causing severe harmonic resonance issues, or how to make shunt capacitors resonance-free.

1.3 Thesis Scope and Outline

The scope of this thesis is to develop technically sound and practically useful solutions to address challenges in the modeling and mitigation of harmonic distortions caused by mass-distributed harmonic sources. More specifically, this thesis aims to solve the following four problems as defined in Section 1.2.

1) How to obtain an aggregate model of the secondary residential system with both the harmonic characteristic and the probabilistic behavior of the mass-distributed harmonic sources in each household considered?

2) How to reduce the harmonics' penetration from residential distribution systems into transmission systems in a way of low complexity?

3) How to determine the other two design conditions in order to arrive at a complete design method for the 3rdHP filter which is potentially useful for mitigating harmonic distortions caused by the mass-distributed harmonic sources?

4) How to make shunt capacitors immune to the severe harmonic resonance?

In order to solve these four problems, this thesis introduces several new methodologies and also conducts supporting technical studies. The following paragraphs summarize the organization of this thesis and describe the main topics and research discussed in each chapter.

Chapter 2 develops an analytical method for probabilistic modeling of the steady-state behavior of the secondary residential system. The result of the proposed method is a time-varying probabilistic PQ load at the fundamental frequency and a time-varying probabilistic Norton equivalent circuit at each harmonic frequency whose parameters are characterized by bivariate normal distributions. The three main components of the proposed method, i.e., the derivation of the state probability distributions for individual home appliance, the modeling of the aggregate secondary feeder with all home appliances, and the unscented transformation to combine the aggregate secondary feeder model and the service transformer model are given in this chapter. The effectiveness and efficiency of the proposed method are also investigated in this chapter.

Chapter 3 devises a novel filtering scheme that reduces the harmonics' penetration into transmission systems. The scheme utilizes the low-voltage tertiary winding of a substation transformer to construct a tuned low-impedance path for trapping harmonic currents. The proposed scheme is capable of trapping two zero-sequence (ZS) harmonics and three non-zero-sequence (NZS) harmonics simultaneously. The design procedure, performance evaluation and application considerations are also given in this chapter.

Chapter 4 proposes a technically-sound design method for the 3rdHP filter. The design formulas are derived in this chapter. Comparative case studies are also presented in this chapter.

Chapter 5 presents design methods to configure a shunt capacitor as a C-type or 3rdHP filter with guaranteed resonance-free performance. The concept of the resonance-free condition is introduced in this chapter. It is further used to develop design methods that lead to filter component parameters which always meet the resonance-free condition. The two filter configurations are also compared in this chapter. A major finding of this chapter is that the filter component parameters, as determined by using the proposed design methods, are independent of the system conditions. As a result, a lookup table for the filter component parameters has been created and is also given in this chapter to facilitate immediate use by industry. In addition, the usefulness of the system impedance information is investigated in this chapter. This chapter also develops optimization design methods for both the C-type filter and the 3rdHP filter configurations based on the system impedance information. The impact of adding a shunt capacitor device on other buses in a large system is also studied in this chapter.

Chapter 6 presents the motivation to decouple the component size determination and the component physical parameter determination. This chapter also provides a method to determine the capacitor size (or rating) based on the capacitor's loading conditions, and a procedure to finalize the number of branches and basic capacitor units in series to assemble a capacitor with the required capacitance and minimum voltage rating.

Finally, this thesis's main conclusions and suggestions for future research in this field are summarized in Chapter 7.

Appendix A documents detailed derivations and proofs for Chapter 5.

Appendix B presents how the RLC component cost used in Chapter 4 and Chapter 5 is obtained.

Chapter 2

Probabilistic Harmonic Modeling of the Secondary Residential System

Effective modeling of the secondary residential system is critical for the harmonic assessment of today's power systems. A key requirement for the modeling technique is the consideration of the random nature of residential loads. Previous research endeavor has revealed that for a small number of consumers (e.g., 10-20 households), the load power variations at any given time are significantly high and are directly associated with the activities of household residents [15, 54, 55]. Based on this observation, a bottom-up Monte Carlo Simulation (MCS) method is developed in [15, 54-56] to model the energy demand and the harmonic characteristic of residential loads. This technique is straightforward and versatile, but it requires a tremendous computational effort to obtain the statistical parameters, especially for the collective impact of a large group of residential loads. An alternative technique is to use load surveys [57-59]. However, it involves extensive field measurements, which generally cannot be done during the network planning stage. Also, this technique is top-down in nature and thus, has difficulties in accounting for technological advances and/or the evolution of consumer behavior in the future.

This chapter is concerned with developing a probabilistic method to model the steady-state aggregate impact of the residential loads in terms of the power consumption and harmonic injection, or, more specifically, building a time-varying steady-state aggregate secondary residential system model whose parameters are characterized bivariate normal distributions. It is organized as follows. Section 2.1 describes the problem to be addressed with the structure schematic of the secondary residential system and reviews the related work. The system model and the source of model data are introduced in Section 2.2, and the proposed analytical method is presented in Section 2.3. Section 2.4 presents the case studies used to verify the proposed analytical method, while Section 2.5 summarizes this chapter.

2.1 Problem Statement and Related Work

As shown in Figure 2.1, a secondary residential system consists of a service transformer and secondary conductors connecting various households. Each household has several home appliances, which can be categorized into two types: linear home appliances and nonlinear home appliances. Linear home appliances draw a current that is linearly related to the supply voltage, while nonlinear home appliances draw a current that is a nonlinear function of the supply voltage. Such nonlinearity is typically caused by the electronic switching, electric arcing or electromagnetic saturation [60]. All home appliances can be switched on randomly and draw power from the service transformer. However, when nonlinear home appliances are switched on, they also inject harmonic currents which gradually aggregate at the service transformer. The problem to be addressed can be formally stated as follows: to develop an equivalent steady-state model of a secondary residential system, which can characterize the random power consumption and harmonic injection of all home appliances inside the system.

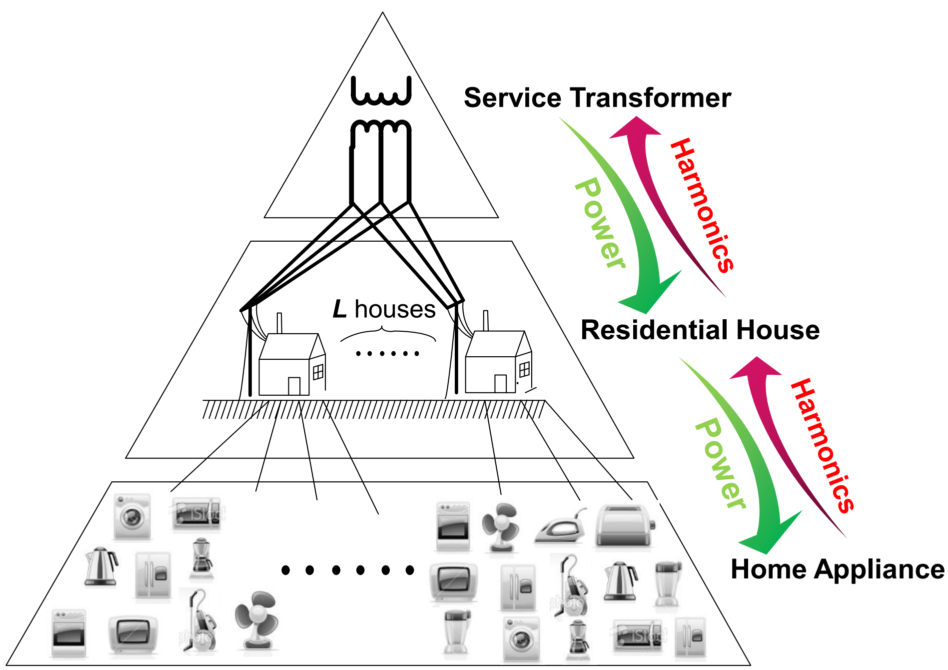

Figure 2.1: Structure schematic of secondary residential system

To address the above problem, research in three areas is involved: the steady-state electrical modeling of individual system components, random usage patterns of home appliances, and probabilistic methods for aggregate secondary residential system modeling.

Considerable efforts have been made on the subject of electrical models of all kinds of system components [60-62]. The service transformer can be modeled as a linear impedance [60]. As for home appliances, although accurate models for some specific nonlinear home appliances were proposed in [61, 62], these models are too complicated to be implemented into a system level study when these home appliances are widely spread all over the network. A more practical method that is generally considered to be accurate is to model both linear and nonlinear home appliances as PQ loads at the fundamental frequency, and as impedances and current sources, respectively, at the harmonic frequencies [60].

A body of knowledge on the random usage patterns of home appliances has been developed. According to the published works, these patterns are determined by three factors with respect to the time instants for each home appliance to be turned on [15-17, 56], the working cycle durations of each home appliance [16, 17, 54, 56], and the population of a household and the residents' lifestyle (e.g., full-time working or part-time working) [15-17, 54, 56].

Probabilistic modeling methods to deal with randomly varying harmonic-producing loads were first studied in [63]. Follow-up research works [64, 65] further found that the sum of a large number of harmonic phasors with arbitrary probabilistic distribution statistically follows a bivariate normal distribution. Reference [66] confirmed this finding based on harmonic current measurements at the medium voltage (MV) buses. In [67] and [68], the central limit theorem was applied in the prediction and analysis of the harmonic impact by the increasing penetration of EV battery chargers. However, these works either were focused on the general summation law of random harmonic vectors, or were confined to only one specific harmonic-producing load (i.e., EV charger) [67, 68]. None of these studies tried to build an aggregate model of the secondary system which would systematically consider the random and time-varying as well as the harmonic-producing behavior of residential loads.

In summary, although the individual system component electrical model, random usage patterns of home appliances, and the general summation theory of random harmonic phasors have been studied in the literature, a generic and low-complexity technique is still not in a complete shape to fulfill the need of building an aggregate secondary residential system model.

The objective of this chapter is to present a systematic and versatile technique to establish a time-varying probabilistic equivalent circuit model for the secondary residential system based on the service transformer model and the electrical model and random usage pattern model of each home appliance.

2.2 System Model

The service transformer can be modeled by its short circuit impedance as shown in Figure 2.2 [60]. As for the L households in the secondary system, each of them can be modeled by: (1) the number of residents; (2) the lifestyle of the residents (i.e. when residents are actively at home, not sleeping or away for work); and (3) all the home appliances it has. Further, each home appliance is characterized by its type (e.g., TV, fridge, microwave, etc.) which defines its electrical model and the associated activity (e.g., laundry, breakfast, cleaning, etc.). The associated activity together with (1) and (2) determines the random usage pattern model. Since secondary conductors are usually designed to have low unit impedance to avoid excessive power loss in the network, the impedance of the secondary conductors is neglected in the system model. In the following, the electrical model and random usage pattern model of the home appliance are discussed in details.

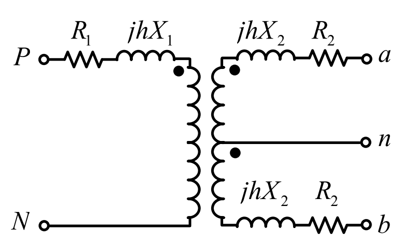

Figure 2.2: Service transformer model

2.2.1 Home Appliance Electrical Model

As discussed earlier, home appliances are classified into two types, linear and nonlinear. The electrical model for the linear home appliance is shown in Figure 2.3 [60]. The linear home appliance is modeled as a PQ load at the fundamental frequency as shown in Figure 2.3 (a) and as impedance at the harmonic frequencies as shown in Figure 2.3 (b), where h is the harmonic order. It should be noted that the home appliance may have multiple operating states with different modeling parameters. Without loss of generality, we consider a home appliance with one OFF state (denoted by the state 0) and M ON states, i.e., $m \in \{0,\ 1,\ 2,\ \cdots,\ M\}$.

(a) Fundamental frequency (b) Harmonic frequency

Figure 2.3: Electrical model for a linear home appliance in operating state m

The electrical model for the nonlinear home appliance is shown in Figure 2.4 [60]. The nonlinear home appliance is modeled as a PQ load at the fundamental frequency as shown in Figure 2.4 (a) and as current sources at the harmonic frequencies as shown in Figure 2.4 (b). As aforementioned, a nonlinear home appliance may also have different operating states which correspond to different modeling parameters.

(a) Fundamental frequency (b) Harmonic frequency

Figure 2.4: Electrical model for a nonlinear home appliance in operating state m

2.2.2 Home Appliance Random Usage Pattern Model

It has been well known that one aspect of the randomness associated with the home appliance is that when it will be switched on [15-17]. This aspect of the randomness can be characterized by the probability of a home appliance being switched on as a function of the time of day, which is called the *switch-on probability profile*. Typically, the *time of use probability profile*, which represents the probability of a household performing a specific activity during a 24-hour period, can be used as the switch-on probability profile of the associated home appliances. For example, the time of use probability profile for the cooking activity (shown as Figure 2.5) can be used as the switch-on probability profiles of kitchen home appliances such as the microwave and blender. Similarly, the switched-on probability profile of other home appliances can be determined by using the time of use probability profile of their associated activities.

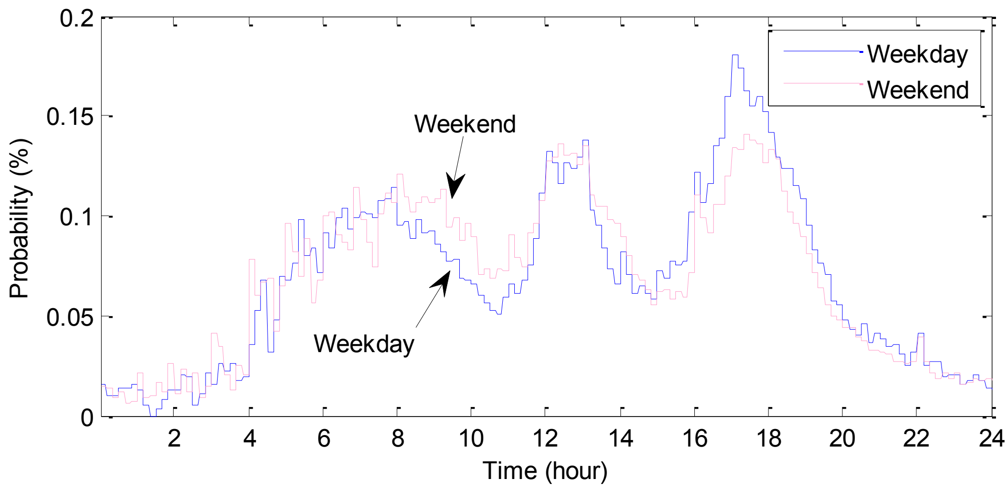

Figure 2.5: Time of use probability profile for cooking activity

Another aspect of the randomness is how long the home appliance will stay in a certain operating state (i.e., the holding time of a certain operating state). This aspect of randomness can be characterized by a probability distribution, which can be determined from statistical data and/or understanding the purpose of the usage of the home appliance [16]. For example, according to the data from the Canadian Center for Housing Technology [69], the duration of the stove staying in the ON state uniformly falls between 15 to 70 minutes. Therefore, the ON state holding time of the stove is governed by a uniform distribution with 15 and 70 as its boundaries.

The above two aspects of randomness can be further mathematically described as follows. The switch-on probability profile can be described by a time-slotted series $\{p_0[n],\ n=1,\ 2,\ ..,\ N\}$ which partitions a day into N time slots with equal duration T (e.g., $T=1\,\text{min}$ for $N=1440$), and its value in time slot *n* corresponds to the probability that the home appliance will be switched on during this time slot. The holding time of a certain operating state *m* can be described by a continuous random variable T_m governed by a bounded distribution, whose cumulative distribution function and bound are denoted by $F_{T_m}(\tau)$ and $[a_m,\ b_m]$, respectively. When the holding time in one state expires, the home appliance randomly transits to another state based on its usage pattern.

By combining all above characteristics, the random usage pattern of a multi-state home appliance can be further modeled by a non-homogeneous semi-Markov process $\{X(t),\ t\ge 0\}$ [70], where $X(t)$ represents the state of the home appliance at time *t*. Note that the process is non-homogeneous due to the time-varying usage pattern of home appliances over the day, while the semi-Markov process is used to handle general holding time distribution $F_{T_m}(\tau)$. Therefore, $\{X(t),\ t\ge 0\}$ is a right-continuous and piecewise constant process, which takes values from the set of states $\{0,\ 1,\ 2,\ \cdots,\ M\}$ and makes state transitions at time $t_1,\ t_2,\ \cdots$. It is characterized by the following.

1) The state transition matrix:

$$\mathbf{P}(t_v)=\left[p_{i,j}(t_v)\right],\ i,\ j\in S, \tag{2.1}$$

where $p_{i,j}(t_v)=P\left(X(t_{v+1})=j\,|\,X(t_v)=i\right)$ is the probability with which the process makes a transition from state i to state j at time t_v. Specifically, $p_{0,0}(t_v)=1-p_0\left[\lceil t_v/T\rceil\right]$ and $p_{0,j}(t_v)=\alpha_j p_0\left[\lceil t_v/T\rceil\right]$ for $j=1,\ 2,\ \cdots,\ M$, where

α_j is the probability for the home appliance to be in state j given it is switched on, and $\sum_{j=1}^{M} \alpha_j = 1$. Here, $\lceil t_v / T \rceil$ denotes the smallest integer no less than t_v / T.

2) The cumulative distribution function of the holding time:

$$F_{T_m}(\tau) = P\left(T_m \le \tau\right), \ \ \tau \in \left[a_m,\ b_m\right] \ \text{ and } \ m = 1,\ 2,\ \cdots,\ M \ . \tag{2.2}$$

When $m = 0$, we have $T_m = T$ with probability 1 according to the definition of the switch-on probability profile.

3) The state probability distribution in time slot n ($n = \lceil t / T \rceil$):

$$\boldsymbol{\pi}[n] = \left[P(X(t)=0),\ P(X(t)=1),\ \cdots,\ P(X(t)=M)\right]. \tag{2.3}$$

It should be noted that the expression "multi-state home appliance" here is a broad term. It can be referred to as a two-state home appliance with M=1, as well as a combination of home appliances whose running states are highly correlated. For example, a washer and a dryer comprise an extended laundry machine. The random usage pattern of this extended laundry machine can also be modeled by a non-homogeneous semi-Markov process, whose state transition diagram in a certain time slot is shown as Figure 2.6.

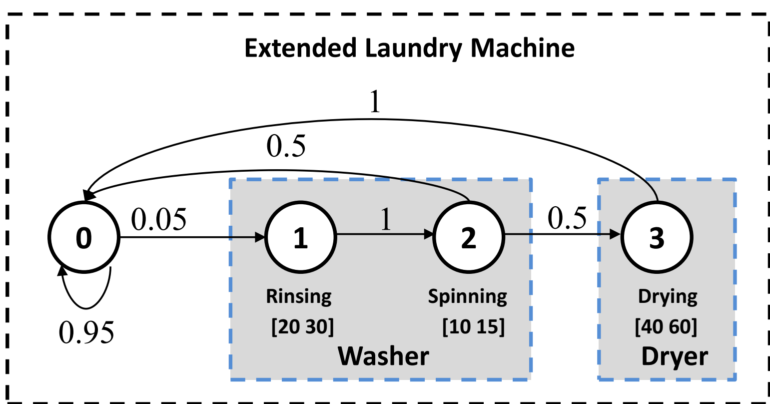

Figure 2.6: State transition diagram for the extended laundry machine

The state transition matrix in this time slot is

$$\begin{bmatrix} 0.95 & 0.05 & 0 & 0 \\ 0 & 0 & 1 & 0 \\ 0.5 & 0 & 0 & 0.5 \\ 1 & 0 & 0 & 0 \end{bmatrix}.$$

The holding time for an ON state (rinsing, spinning, or drying) is uniformly distributed within the range specified by the figures in the square brackets. In other words, the cumulative distribution functions for the ON states are $F_{T_m}(t) = \dfrac{t - a_m}{b_m - a_m}$ $\left(m = 1,\ 2,\ 3\right)$, where $\left[a_m,\ b_m\right]$ equals to $\left[20,\ 30\right]$, $\left[10,\ 15\right]$, $\left[40,\ 60\right]$ (min) for $m = 1,\ 2,\ 3$, respectively.

2.3 Proposed Analytical Method

An analytical method is developed to establish an aggregate model for the secondary residential system, given the aforementioned service transformer model and the electrical and random usage pattern models of home appliances. The main idea of the proposed method originated from the observation that the randomness in the power consumption and the harmonic injection of residential loads is due mainly to the random state switching of home appliances. For example, a microwave can be in the off, cook, defrost or fast defrost state randomly at any given time, but once its state is determined, its power consumption is deterministic, and the injected harmonic currents follow a known, deterministic spectrum. In other words, if the state probability distribution of a home appliance at a given time is determined, the probability distribution of the power consumption and the harmonic current spectrum can be calculated. Furthermore, seen from the primary side, the service transformer can be considered as an aggregator which combines two phase power consumption and harmonic injection models into one phase, based on which the central limit theorem [64, 65] can be applied to obtain the aggregate secondary system model. Figure 2.7 shows the flowchart of the proposed analytical method.

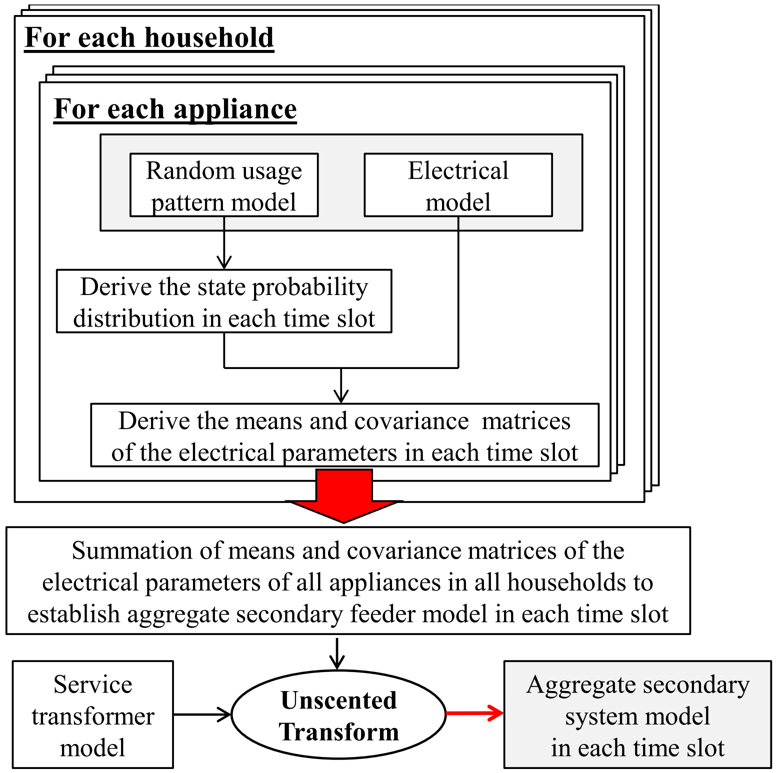

Figure 2.7: Flowchart of the proposed analytical method

The inputs of the proposed method are the random usage pattern model data and electrical model data of the home appliances, as described Section 2.2. The original non-homogeneous semi-Markov process that describes the random usage pattern model is first transformed into a non-homogeneous discrete time Markov chain [71], such that the state probability distribution of each home appliance in each time slot can be derived. Then, the state probability distribution is combined with the electrical model to obtain the means and covariance matrices of the electrical parameters (including the power consumption, harmonic current and harmonic admittance) of each home appliance in each time slot. After this procedure has been completed, two levels of aggregation are performed. The first level of aggregation is the summation of the means and the covariance matrices of the electrical parameters of all home appliances in all households to establish the aggregate secondary feeder model in each time slot. The second level of aggregation combines the service transformer with the aggregate secondary feeder model, where unscented transformation is introduced to calculate the statistics of the parameters of the final equivalent circuit. In each time slot, the parameter of the final equivalent circuit (the power consumption, harmonic current and harmonic admittance) follows a bivariate normal distribution which is characterized by the calculated mean and covariance matrix. The mean and the covariance matrix for each parameter can vary over time, corresponding to the switch-on probability profile of the home appliance. For example, Figure 2.8 gives the power consumption probability distribution for two different time slots. This figure reveals that the power consumption randomly varies in different ranges for different time slots and tends to vary in a larger power range at 20:00, when more home appliances are active compared to 7:00. The details of the key techniques involved are given in the following subsections.

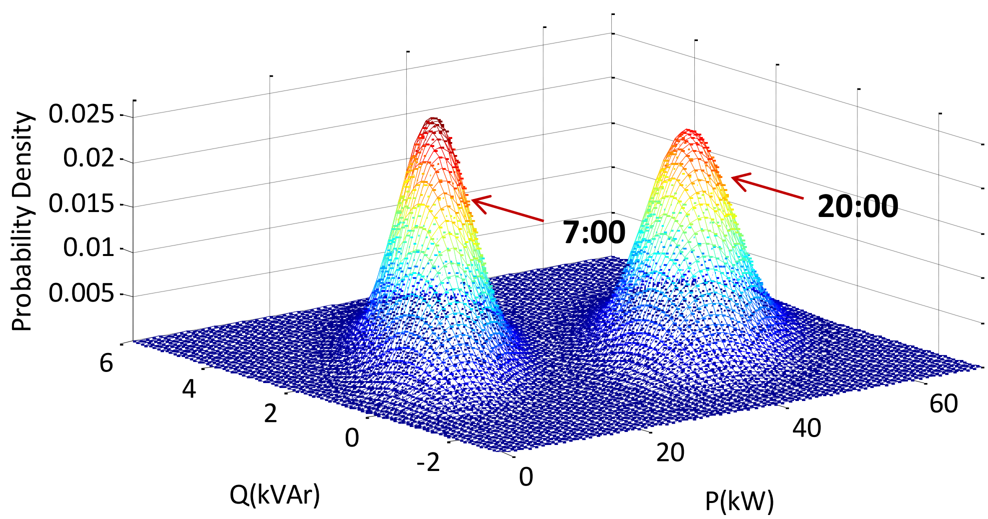

Figure 2.8: Example of power consumption probability distribution for two different time slots

2.3.1 State Probability Distribution Derivation

To obtain the state probability distribution of a non-homogeneous semi-Markov process, two key factors should be considered: (1) the initial state probability distribution; (2) updating the state probability distribution according to the time-varying state transition matrix and the random state holding time.

A. Initial State Probability Distribution

Except for the cyclically running home appliances (e.g., fridge and freezer), other home appliances typically have a period of time during a day when it is in OFF state with a high probability. For example, the coffee maker is typically in OFF state at midnight, since it is rare for people to drink coffee during their bedtime. Therefore, the state probability distribution at such a time t_0 can be represented by

$$\boldsymbol{\pi}[n_0] = \left[1\ 0 \cdots 0\right]_{1\times(M+1)}, \tag{2.4}$$

where $n_0 = \lceil t_0 / T \rceil$. Here, $\boldsymbol{\pi}[n_0]$ can serve as the initial state probability distribution for the time-varying state probability distribution calculation.

An algorithm is developed to find the initial instant t_0. It is based on the fact that, if its switch-on probability is zero for a period that is longer than the maximum time it can stay in ON states during one switch-on event, it will definitely stay in OFF state at the beginning of the consecutive time. Take the extended laundry machine shown in Figure 2.6 as an example. Suppose its switch-on probability is zero from 3:00 am to 5:00 am. Since maximum time the extended laundry machine stays in ON states $T_{\max} = b_1 + b_2 + b_3 = 30 + 15 + 60 = 105(\text{min})$, no switch-on event can happen during 3:00 am and 5:00 am. As a result, even this home appliance has been switched on before 3:00 am, it will return back to OFF state before 4:45 am, which means that this home appliance will definitely stay in OFF state at 4:46 am (corresponding to t_0). The flowchart of the developed algorithm is shown as Figure 2.9, where $p_0[n]$ and $p_0[n_{eval}]$ are the probability of the home appliance to be switched on in time slot n and n_{eval}, respectively; T is the time duration of each time slot; and $T_{\max}$ is the maximum time the home appliance can be in ON states.

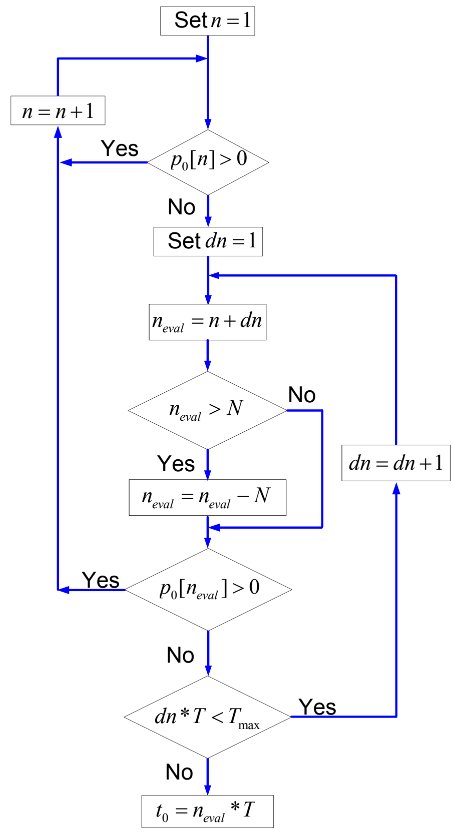

Figure 2.9: Flowchart of the algorithm to find the initial instant

B. Transformation of the Semi-Markov Process into a Discrete Time Markov Chain

Since the holding time of ON states is random, the state transition matrix $\mathbf{P}(t_v)$ of the semi-Markov process cannot be directly used to update the state probability distribution. To tackle this problem, we discretize each ON state into a series of fixed time-step sub-states whose transition probabilities are determined by the holding time probability distribution. Then the sub-state transition matrix is incorporated in the original state transition matrix to form an augmented state transition matrix, and thus, transforming the semi-Markov process into a discrete time Markov chain. Thereafter, the state probability distribution can be updated by simply multiplying the augmented state transition matrix.

The basic idea to discretize the ON state is to map the probability of a certain length holding time to the probability for a Markov chain to escape from certain states, after time slots with the same length. Based on this, the sub-state transition diagram for state m can be derived, as shown in Figure 2.10. The total number of the sub-states is determined by the longest possible holding time of state m, given by $K_m = \lceil b_m / T \rceil$, which guarantees the home appliance can transfer to other states after at most K_m time slots.

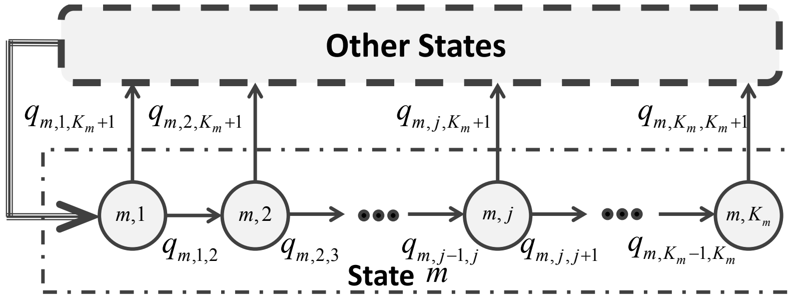

Figure 2.10: Sub-state transition diagram for state *m*

To make the sub-state transition equivalently represent the probabilistic distribution of the holding time, the probability for the process to escape from sub-state *j* should be equal to the probability that the holding time of state *m* is between *j*-1 and *j* time slots, given by

$$q_{m,j,K_m+1} = P\left(T_m \le j \cdot T \mid T_m > (j-1) \cdot T\right) = \frac{F_{T_m}(j \cdot T) - F_{T_m}((j-1) \cdot T)}{1 - F_{T_m}((j-1) \cdot T)}, \tag{2.5}$$

where $j \in \{1,\ 2,\ ...,\ K_m\}$.

Accordingly, the transition probability from sub-state *j* to sub-state $j+1$ is determined by

$$q_{m,j,j+1} = 1 - q_{m,j,K_m+1} = \frac{1 - F_{T_m}(j \cdot T)}{1 - F_{T_m}\left((j-1) \cdot T\right)}, \tag{2.6}$$

where $j \in \{1,\ 2,\ ...,\ K_m\text{-}1\}$.

For any other state transition probabilities not mentioned in (2.5) and (2.6), we have

$$q_{i,j} = 0\ . \tag{2.7}$$

Then, the sub-state transition matrix $\mathbf{q}_m$ can be built as

$$\mathbf{q}_m = \begin{bmatrix} \bar{\mathbf{q}}_m & \underline{\mathbf{q}}_{m,K_m+1} \end{bmatrix}_{K_m \times (K_m+1)}, \tag{2.8}$$

where $\bar{\mathbf{q}}_m$ is the inter sub-state transition matrix, given by

$$\bar{\mathbf{q}}_m = \begin{bmatrix} 0 & q_{m,1,2} & 0 & \cdots & 0 & 0 \\ 0 & 0 & q_{m,2,3} & \cdots & 0 & 0 \\ 0 & 0 & 0 & \cdots & 0 & 0 \\ \vdots & \vdots & \vdots & \ddots & \vdots & \vdots \\ 0 & 0 & 0 & \cdots & 0 & q_{m,K_m-1,K_m} \\ 0 & 0 & 0 & \cdots & 0 & 0 \end{bmatrix}_{K_m \times K_m}, \tag{2.9}$$

and $\underline{\mathbf{q}}_{m,K_m+1} = \begin{bmatrix} q_{m,1,K_{m+1}} & q_{m,2,K_{m+1}} & \cdots & q_{m,K_m,K_{m+1}} \end{bmatrix}^T$ is the vector of transition probabilities to other states.

With all the sub-state transition matrixes obtained, the augmented transition matrix $\mathbf{P}^A[n]$ can be built as follows:

$$\mathbf{P}^A[n] = \begin{pmatrix} p_{0,0}[n] & \overbrace{p_{0,1}[n] \quad 0 \quad \cdots \quad 0}^{K_1} & \cdots & \overbrace{p_{0,M}[n] \quad 0 \quad \cdots \quad 0}^{K_M} \\ p_{1,0}[n]\underline{\mathbf{q}}_{1,K_1+1} & \bar{\mathbf{q}}_1 & \cdots & p_{1,M}[n]\underline{\mathbf{q}}_{\mathbf{1},\mathbf{K_1+1}} \quad \mathbf{0} \quad \cdots \quad \mathbf{0} \\ \vdots & \vdots & \cdots & \vdots \\ p_{M,0}[n]\underline{\mathbf{q}}_{M,K_M+1} & p_{M,1}\underline{\mathbf{q}}_{M,K_M+1} \quad \mathbf{0} \quad \cdots \quad \mathbf{0} & \cdots & \bar{\mathbf{q}}_M \end{pmatrix}_{M_A \times M_A}, \tag{2.10}$$

where $M_A = 1 + \sum_{m=1}^{M} K_m$.

C. Algorithm to Calculate the State Probability Distribution

Based on the aforementioned techniques, the algorithm to calculate the state probability distribution for each time slot is established as follows:

Step 1: *Find the initial time* t_0, *and set* $n = \lceil t_0 / T \rceil$.

Step 2: *Initialize the state probability distribution and the augmented state probability distribution as* $\boldsymbol{\pi}[n] = \left[1\ 0 \cdots 0\right]_{1\times(M+1)}$ *and* $\boldsymbol{\pi}^A[n] = \left[1\ 0 \cdots 0\right]_{1\times M_A}$ *respectively.*

Step 3: *Set* $n_{next} = n+1$. *If* $n_{next} > N$, *then set* $n_{next} = 1$.

Step 4: *If* $n_{next} = \lceil t_0 / T \rceil$, *stop; else go to step 5.*

Step 5: *Calculate the augmented state transition matrix* $\mathbf{P}^A[n]$ *for time slot* n.

Step 6: *Calculate augmented state probability distribution for time slot* n_{next}, *given by*

$$\boldsymbol{\pi}^A[n_{next}] = \boldsymbol{\pi}^A\left[n\right]\mathbf{P}^A\left[n\right]. \tag{2.11}$$

Step 7: *Add up the sub-state probabilities to obtain the probability of each state, and thus, obtain the state probability distribution* $\boldsymbol{\pi}[n_{next}]$. *Specifically, denote the i-th element of* $\boldsymbol{\pi}^A[n_{next}]$ *and the m-th element of* $\boldsymbol{\pi}[n_{next}]$ *by* $\pi_i^A[n_{next}]$ *and* $\pi_m[n_{next}]$, *respectively. Then, calculate* $\pi_m[n_{next}] = \sum_{i=M_{m-1}+1}^{M_m} \pi_i^A[n_{next}]$, *where* $M_m = 1 + \sum_{i=1}^{m} K_i$.

Step 8: *Set* $n = n_{next}$, *and go to step 3.*

D. Cyclically Running Home Appliances

As for the cyclically running home appliances, both switch-on probabilities and holding time probability distributions are time invariant. Thus their randomness can be described by a homogenous semi-Markov process. Also, such a random process is repeated on a daily basis. Hence, the state probability distribution of a cyclically running home appliance at any time can be represented by its stationary distribution which can be calculated in the following way.

Step 1: *Use the aforementioned technique to obtain the augmented state transition matrix* $\mathbf{P}^A$, *based on the transformed homogeneous discrete time Markov chain.*

Step 2: *Calculate the augmented stationary distribution* $\boldsymbol{\pi}^A$ *by solving the following equilibrium equation:*

$$\begin{cases} \boldsymbol{\pi}^A = \boldsymbol{\pi}^A \mathbf{P}^A \\ \sum \pi_i^A = 1 \end{cases}. \tag{2.12}$$

Step 3: *Add up the sub-state probabilities which are given by* $\boldsymbol{\pi}^A$ *to obtain the probability of each state, and thus, obtain the stationary distribution* $\boldsymbol{\pi}$.

2.3.2 Aggregate Secondary Feeder Model Derivation

As the impedance of the secondary conductors is negligible, the secondary side of the service transformer (i.e., the secondary feeder) is essentially composed of home appliances connected in parallel. Correspondingly, a simplified model for the aggregate secondary feeder can be derived, whose parameters (i.e., the power consumption, harmonic current, harmonic admittance and grounding admittance) are essentially the sum of the corresponding parameters of the equivalent circuits of home appliances (given in Figure 2.3 and Figure 2.4) and the households' grounding admittance, as shown in Figure 2.11.

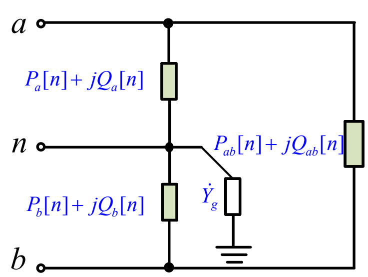

(a) Fundamental frequency

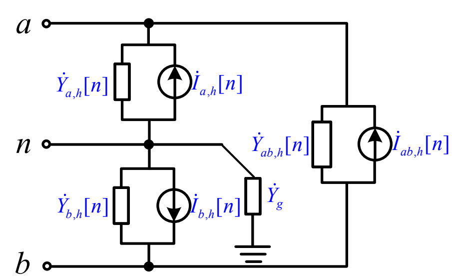

(b) Harmonic frequency

Figure 2.11: Aggregate model of the secondary feeder in time slot *n*

Since the operating state of the home appliance changes randomly, the corresponding parameters of its equivalent circuit (i.e., power consumption, harmonic current and harmonic admittance) are randomly varying. In addition, there are a large number of home appliances in the secondary system. Thus the parameters of the aggregate model are essentially the sum of a large number of random variables. In fact, all these parameters are complex numbers. As a result, according to the multivariate central limit theorem [72], the real part and imaginary part of these parameters are bivariate normally distributed. The means and covariance matrices of the real and imaginary parts of these parameters are calculated in this subsection.

Let D_l be the total number of home appliances in the l-th household ($l = 1,\ 2,\ ...,\ L$). Then, in time slot n, the power consumption of the k-th home appliance in the l-th household can be calculated as

$$\dot{S}_{l,k}[n] = \mathbf{X}_{l,k}^T[n]\mathbf{P}_{l,k} + j\mathbf{X}_{l,k}^T[n]\mathbf{Q}_{l,k}\ , \tag{2.13}$$

where $\mathbf{X}_{l,k}[n] = \left[x_{l,k,0}[n],\ x_{l,k,1}[n],\ \cdots,\ x_{l,k,M_{l,k}}[n]\right]$ is an $\left(M_{l,k}+1\right)$-vector of the state variables of the k-th home appliance in the l-th household in time slot n, with $M_{l,k}$ being the total number of ON states of the home appliance. If the home appliance is in state m, the m-th component $x_{l,k,m}[n] = 1$, while the other components $x_{l,k,j}[n] = 0$ for all $j \neq m$. Correspondingly, $\mathbf{P}_{l,k}$ and $\mathbf{Q}_{l,k}$ are the $\left(M_{l,k}+1\right)$-vectors of active and reactive power consumption of the home appliance in various states, respectively.

Based on the state probability distribution derived in the previous subsection, the mean and covariance matrix of the power consumption of the home appliance can be calculated as [73]:

$$\mu\left(\dot{S}_{l,k}[n]\right) = \boldsymbol{\pi}_{l,k}^T[n]\mathbf{P}_{l,k} + j\boldsymbol{\pi}_{l,k}^T[n]\mathbf{Q}_{l,k}\ , \tag{2.14}$$

$$\operatorname{cov}\left(\dot{S}_{l,k}[n]\right) = \begin{bmatrix} \mathbf{P}_{l,k}^T(\boldsymbol{\Lambda}_{l,k}[n] - \boldsymbol{\pi}_{l,k}\boldsymbol{\pi}_{l,k}^T)\mathbf{P}_{l,k} & \mathbf{P}_{l,k}^T(\boldsymbol{\Lambda}_{l,k}[n] - \boldsymbol{\pi}_{l,k}\boldsymbol{\pi}_{l,k}^T)\mathbf{Q}_{l,k} \\ \mathbf{P}_{l,k}^T(\boldsymbol{\Lambda}_{l,k}[n] - \boldsymbol{\pi}_{l,k}\boldsymbol{\pi}_{l,k}^T)\mathbf{Q}_{l,k} & \mathbf{Q}_{l,k}^T(\boldsymbol{\Lambda}_{l,k}[n] - \boldsymbol{\pi}_{l,k}\boldsymbol{\pi}_{l,k}^T)\mathbf{Q}_{l,k} \end{bmatrix}, \tag{2.15}$$

where $\boldsymbol{\pi}_{l,k}[n] = \left[\pi_{l,k,0}[n],\ \pi_{l,k,1}[n],\ \cdots,\ \pi_{l,k,M_{l,k}}[n]\right]$ is an $\left(M_{l,k}+1\right)$-vector, with $\pi_{l,k,m}[n]$ being the probability of state m of the k-th home appliance in the l-th household in time slot n. And in (2.15), $\boldsymbol{\Lambda}_{l,k}[n]$ is an $\left(M_{l,k}+1\right)$ by $\left(M_{l,k}+1\right)$ diagonal matrix with its m-th diagonal element being $\pi_{l,k,m}[n]$.

Then, the parameters of the aggregate model shown in Figure 2.11 are the sum of the equivalent circuit parameters of the home appliances connected by the corresponding wires. For a specific type of connection s ($s \in \{a,\ b,\ ab\}$), we have

$$\dot{S}_s[n] = P_s[n] + jQ_s[n] = \sum_{l=1}^{L}\sum_{k=1}^{D_l} \dot{S}_{l,k}[n] \cdot \mathbf{1}_s\left(s_{l,k}\right), \tag{2.16}$$

where $s_{l,k}$ represents the wires to which the k-th home appliance in the l-th household is connected (i.e., phase a and neutral (a), phase b and neutral (b), or phase a and phase b (ab)), while $\mathbf{1}_s\left(s_{l,k}\right)$ is an indicator function which equals 1 if $s_{l,k} = s$ and 0 otherwise.

Based on equations (2.14) to (2.16) and according to the property of independent random variables, the means and covariance matrices of $\dot{S}_s[n]$ can be calculated [73]. The means and covariance matrices of harmonic current ($\dot{I}_{s,h}[n]$) and harmonic admittance ($\dot{Y}_{s,h}[n]$) in Figure 2.11 can be calculated in the same way. As for the equivalent grounding admittance, it can be estimated by the number of households (L) and the typical grounding resistance of each household (r_g), given by $\dot{Y}_g = L / r_g$.

2.3.3 Aggregate Secondary System Model Derivation

Once the aggregate secondary feeder model is obtained, the next step is to combine it with the service transformer model (as shown in Figure 2.2) to establish the aggregate secondary system model. The result is a simplified equivalent circuit model as shown in Figure 2.12. At fundamental frequency, the power consumption of the whole secondary system ($\dot{S}_S[n]$) is equal to the sum of the power consumption of the secondary feeder and the power loss of the service transformer. At harmonic frequencies, nodal voltage equations can be derived for the calculation of parameters $\dot{Y}_{PN,h}[n]$ and $\dot{I}_{PN,h}[n]$.

In this subsection, the aggregation of harmonic frequency model, which is more complex, is discussed in details first. Then the aggregation of the fundamental frequency model is given. Thereafter, the method to estimate the statistics of the final aggregate model parameters is presented.

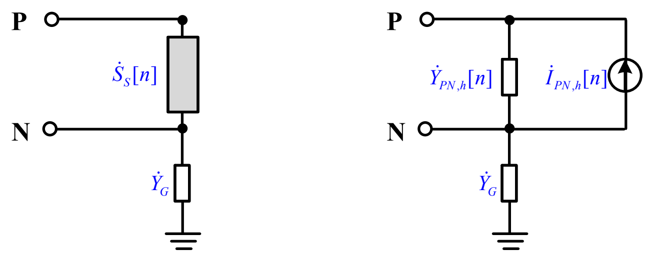

(a) Fundamental frequency (b) Harmonic frequency

Figure 2.12: Simplified equivalent aggregate secondary system model

A. Aggregation of the Harmonic Frequency Model

To establish the harmonic frequency simplified equivalent aggregate secondary system model, the nodal voltage equations are derived first for the service transformer supplying the secondary feeder represented by the aggregate model (as shown in Figure 2.13 (a)). By reducing the internal nodes, a simplified equivalent circuit is established (as shown in Figure 2.13 (b)), which is further simplified into the final aggregate model (as shown in Figure 2.12 (b)) with the characteristics of the equivalent circuit parameters being considered.

In Figure 2.13 (a), there are 5 nodes (①~⑤) and 11 branches in total. From the left side to the right side and from the upside to the downside, the first 3 branches are the three windings of the service transformer, which are denoted by the harmonic admittance of the primary winding $\dot{y}_{1,h} = 1/\left(R_1 + jhX_1\right)$ and secondary winding $\dot{y}_{2,h} = 1/\left(R_2 + jhX_2\right)$ (referred to the secondary side) and the primary to secondary winding turn ratio $N:1$. The 4th branch is the service transformer grounding resistor. The 5th to 11th branches represent the aggregate secondary feeder which has been discussed in Subsection 2.3.2.

According to Figure 2.13 (a), the branch admittance matrix for the secondary system can be obtained as

$$\dot{\mathbf{y}}_{Br,h}[n] = \begin{bmatrix} \dot{\mathbf{y}}_{T,h} & \mathbf{0} & \mathbf{0} & \mathbf{0} & \mathbf{0} & \mathbf{0} \\ \mathbf{0} & \dot{Y}_T & 0 & 0 & 0 & 0 \\ \mathbf{0} & 0 & \dot{Y}_{a,h}[n] & 0 & 0 & 0 \\ \mathbf{0} & 0 & 0 & \dot{Y}_{b,h}[n] & 0 & 0 \\ \mathbf{0} & 0 & 0 & 0 & \dot{Y}_{ab,h}[n] & 0 \\ \mathbf{0} & 0 & 0 & 0 & 0 & \dot{Y}_g \end{bmatrix}, \tag{2.17}$$

where $\dot{Y}_T = 1/R_T$, and R_T is the grounding resistance of the service transformer.

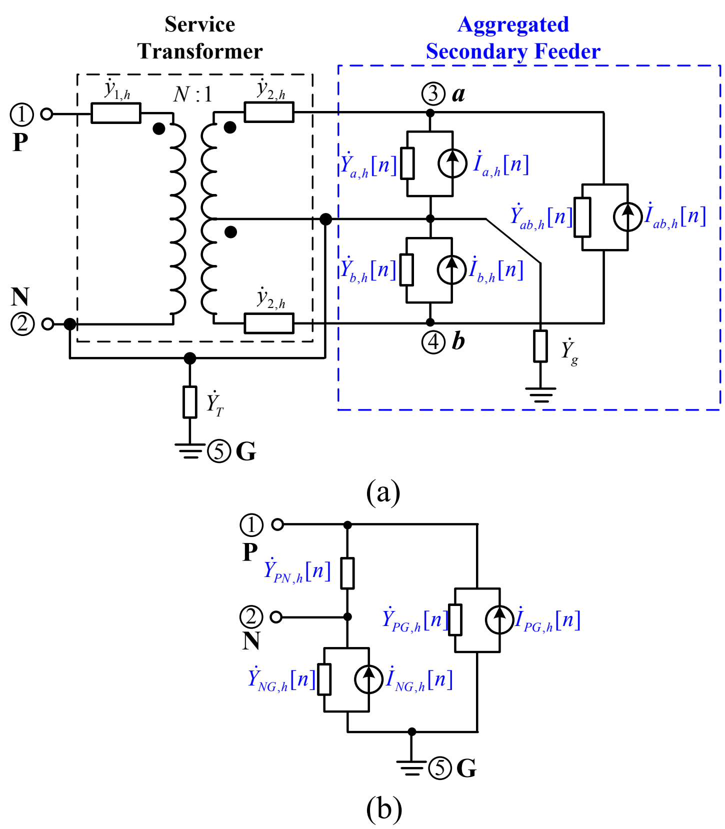

Figure 2.13: Equivalent aggregate model of the secondary system at harmonic frequency

In equation (2.17), $\dot{\mathbf{y}}_{T,h}$ is the transformer branch admittance matrix given by

$$\dot{\mathbf{y}}_{T,h} = \begin{bmatrix} \dot{y}_{T1,h} & -\dot{y}_{T2,h} & -\dot{y}_{T2,h} \\ -\dot{y}_{T2,h} & \dot{y}_{T3,h} & -\dot{y}_{T4,h} \\ -\dot{y}_{T2,h} & -\dot{y}_{T4,h} & \dot{y}_{T3,h} \end{bmatrix}, \tag{2.18}$$

where

$$\begin{cases} \dot{y}_{T1,h} = 2\dot{y}_{1,h}\dot{y}_{2,h} / \left(N^2\dot{y}_{1,h} + 2\dot{y}_{2,h}\right) \\ \dot{y}_{T2,h} = N\dot{y}_{1,h}\dot{y}_{2,h} / \left(N^2\dot{y}_{1,h} + 2\dot{y}_{2,h}\right) \\ \dot{y}_{T3,h} = \dot{y}_{2,h}\left(N^2\dot{y}_{1,h} + \dot{y}_{2,h}\right) / \left(N^2\dot{y}_{1,h} + 2\dot{y}_{2,h}\right) \\ \dot{y}_{T4,h} = \dot{y}_{2,h}^2 / \left(N^2\dot{y}_{1,h} + 2\dot{y}_{2,h}\right) \end{cases}. \tag{2.19}$$

Take the grounding point G as the reference point and number the three current source branches as the 9th, 10th and 11th branches. Then the node and branch incident matrix which does not include the current source branches is given by

$$\mathbf{A}_{Nb} = \begin{bmatrix} 1 & 0 & 0 & 0 & 0 & 0 & 0 & 0 \\ -1 & -1 & 1 & 1 & -1 & 1 & 0 & 1 \\ 0 & 1 & 0 & 0 & 1 & 0 & 1 & 0 \\ 0 & 0 & -1 & 0 & 0 & -1 & -1 & 0 \end{bmatrix}. \tag{2.20}$$

Therefore, the nodal admittance matrix can be obtained as

$$\dot{\mathbf{Y}}_{N,h}[n] = \mathrm{A}_{Nb}\dot{\mathbf{y}}_{Br,h}[n]\mathbf{A}_{Nb}^T = \begin{bmatrix} \dot{\mathbf{Y}}_{NA,h}[n] & \dot{\mathbf{Y}}_{NB,h}[n] \\ \dot{\mathbf{Y}}_{NC,h}[n] & \dot{\mathbf{Y}}_{ND,h}[n] \end{bmatrix}, \tag{2.21}$$

where

$$\dot{\mathbf{Y}}_{NA,h}[n] = \begin{bmatrix} \dot{y}_{T1,h} & -\dot{y}_{T1,h} \\ -\dot{y}_{T1,h} & \dot{y}_{T1,h} + 2\dot{y}_{2,h} + \dot{Y}_T + \dot{Y}_g + \dot{Y}_{a,h}[n] + \dot{Y}_{b,h}[n] \end{bmatrix}, \tag{2.22}$$

$$\dot{\mathbf{Y}}_{NB,h}[n] = \begin{bmatrix} -\dot{y}_{T2,h} & \dot{y}_{T2,h} \\ \dot{y}_{T2,h} - \dot{y}_{2,h} - \dot{Y}_{a,h}[n] & -\dot{y}_{T2,h} - \dot{y}_{2,h} - \dot{Y}_{b,h}[n] \end{bmatrix}, \tag{2.23}$$

$$\dot{\mathbf{Y}}_{NC,h}[n] = \left(\dot{\mathbf{Y}}_{NB,h}[n]\right)^T, \tag{2.24}$$

$$\dot{\mathbf{Y}}_{ND,h}[n] = \begin{bmatrix} \dot{y}_{T3,h} + \dot{Y}_{a,h}[n] + \dot{Y}_{ab,h}[n] & \dot{y}_{T4,h} - \dot{Y}_{ab,h}[n] \\ \dot{y}_{T4,h} - \dot{Y}_{ab,h}[n] & \dot{y}_{T3,h} + \dot{Y}_{b,h}[n] + \dot{Y}_{ab,h}[n] \end{bmatrix}. \tag{2.25}$$

Further, the nodal voltage equations can be established as

$$\dot{\mathbf{Y}}_{N,h}[n]\dot{\mathbf{V}}_{N,h}[n]=\dot{\mathbf{I}}_{N,h}[n], \tag{2.26}$$

where $\dot{\mathbf{I}}_{N,h}[n]=\dot{\mathbf{I}}_{Nex,h}[n]+\dot{\mathbf{I}}_{Nin,h}[n]$ is the nodal injection current vector which is the sum of the current injected from the primary system current source $\dot{\mathbf{I}}_{Nex,h}[n]$ and the secondary system current source $\dot{\mathbf{I}}_{Nin,h}[n]$, $\dot{\mathbf{V}}_{N,h}[n]$ is the nodal voltage with respect to the ground and

$$\begin{cases}\dot{\mathbf{I}}_{Nex,h}[n]=\begin{bmatrix}\dot{I}_{N1,h}[n] & \dot{I}_{N2,h}[n] & 0 & 0\end{bmatrix}^T \\ \dot{\mathbf{I}}_{Nin,h}[n]=\begin{bmatrix}0 & -\dot{I}_{a,h}[n]+\dot{I}_{b,h}[n] & \dot{I}_{a,h}[n]+\dot{I}_{ab,h}[n] & -\dot{I}_{b,h}[n]-\dot{I}_{ab,h}[n]\end{bmatrix}^T\end{cases}. \tag{2.27}$$

By eliminating the internal nodal voltages (i.e. node 3 and node 4 voltages), (2.26) can be transformed into

$$\dot{\mathbf{Y}}_{Ex,h}[n]\dot{\mathbf{V}}_{Ex,h}[n]=\dot{\mathbf{I}}_{Ex,h}[n]+\dot{\mathbf{I}}_{In,h}[n], \tag{2.28}$$

where $\dot{\mathbf{V}}_{Ex,h}[n]=\begin{bmatrix}\dot{V}_{N1,h}[n] & \dot{V}_{N2,h}[n]\end{bmatrix}^T$ is the external nodal voltage vector (i.e. the voltages at the node P and node N), $\dot{\mathbf{I}}_{Ex,h}[n]=\begin{bmatrix}\dot{I}_{N1,h}[n] & \dot{I}_{N2,h}[n]\end{bmatrix}^T$ is the external nodal injected current vector (i.e. the currents injected from the primary system into the node P and node N), and $\dot{\mathbf{Y}}_{Ex,h}[n]$ is the equivalent nodal admittance matrix seen between the external nodes which is given by

$$\dot{\mathbf{Y}}_{Ex,h}[n]=\dot{\mathbf{Y}}_{NA,h}[n]-\dot{\mathbf{Y}}_{NB,h}[n]\dot{\mathbf{Y}}_{ND,h}^{-1}[n]\dot{\mathbf{Y}}_{NC,h}^{-1}[n]. \tag{2.29}$$

$\dot{\mathbf{I}}_{In,h}[n]$ is the equivalent nodal injected current from the secondary system and it is given by

$$\dot{\mathbf{I}}_{In,h}[n]=\left(\begin{bmatrix}0 & 0 & 0\\ -1 & 0 & 1\end{bmatrix}-\dot{\mathbf{Y}}_{NB,h}[n]\dot{\mathbf{Y}}_{ND,h}^{-1}[n]\begin{bmatrix}1 & 1 & 0\\ 0 & -1 & -1\end{bmatrix}\right)\begin{bmatrix}\dot{I}_{a,h}[n]\\ \dot{I}_{ab,h}[n]\\ \dot{I}_{b,h}[n]\end{bmatrix}. \tag{2.30}$$

According to the physical meaning of the nodal voltage equation, the parameters of Figure 2.13 (b) can be obtained by equations (2.29) and (2.30) as

$$\dot{Y}_{PN,h}[n] = -\dot{\mathbf{Y}}_{Ex,h}[n](2,1) = \frac{\left(A_h[n]\dot{y}_{2,h}^2 + 2B_h[n]\dot{y}_{2,h}\right)\dot{y}_{1,h}}{A_h[n]\dot{y}_{2,h}^2 + N^2\left(\dot{y}_{2,h}^2 + C_h[n]\dot{y}_{2,h} + B_h[n]\right)\dot{y}_{1,h} + 2B_h[n]\dot{y}_{2,h}}, \quad (2.31)$$

$$\dot{Y}_{PG,h}[n] = \dot{\mathbf{Y}}_{Ex,h}[n](1,1) + \dot{\mathbf{Y}}_{Ex,h}[n](2,1) = 0, \quad (2.32)$$

$$\dot{Y}_{NG,h}[n] = \dot{\mathbf{Y}}_{Ex,h}[n](2,1) + \dot{\mathbf{Y}}_{Ex,h}[n](2,2) = \dot{Y}_T + \dot{Y}_g, \quad (2.33)$$

$$\dot{I}_{PG,h}[n] = \dot{\mathbf{I}}_{In,h}[n](1) = -\frac{N\dot{y}_{1,h}\dot{y}_{2,h}\left(D_h[n]\dot{I}_{ab,h}[n] + E_h[n]\dot{I}_{a,h}[n] + F_h[n]\dot{I}_{b,h}[n]\right)}{A_h[n]\dot{y}_{2,h}^2 + N^2\left(\dot{y}_{2,h}^2 + C_h[n]\dot{y}_{2h} + B_h[n]\right)\dot{y}_{1,h} + 2B_h[n]\dot{y}_{2,h}}, \quad (2.34)$$

$$\dot{I}_{NG,h}[n] = \dot{\mathbf{I}}_{In,h}[n](2) = -\dot{I}_{PG,h}[n], \quad (2.35)$$

where

$$\begin{cases} A_h[n] = \dot{Y}_{a,h}[n] + 4\dot{Y}_{ab,h}[n] + \dot{Y}_{b,h}[n] \\ B_h[n] = \dot{Y}_{a,h}[n]\dot{Y}_{ab,h}[n] + \dot{Y}_{ab,h}[n]\dot{Y}_{b,h}[n] + \dot{Y}_{b,h}[n]\dot{Y}_{a,h}[n] \\ C_h[n] = \dot{Y}_{a,h}[n] + 2\dot{Y}_{ab,h}[n] + \dot{Y}_{b,h}[n] \\ D_h[n] = \dot{Y}_{a,h}[n] + \dot{Y}_{b,h}[n] + 2\dot{y}_{2,h} \\ E_h[n] = \dot{Y}_{b,h}[n] + \dot{y}_{2,h} \\ F_h[n] = \dot{Y}_{a,h}[n]\dot{y}_{2,h} \end{cases}. \quad (2.36)$$

According to equations (2.32), (2.33), and (2.35), the model could be further simplified as shown in Figure 2.12 (b), where $\dot{Y}_G = \dot{Y}_{NG,h}[n] = \dot{Y}_T + \dot{Y}_g$.

B. Aggregation of the Fundamental Frequency Model

At the fundamental frequency, the power consumption of the whole secondary system is equal to the sum of the power consumption of the secondary feeder and the power loss of the service transformer. Accordingly, the aggregate power consumption can be derived as:

$$\dot{S}_S[n] = \dot{S}_a[n] + \dot{S}_{ab}[n] + \dot{S}_b[n] + \dot{S}_T[n]\,, \tag{2.37}$$

where $\dot{S}_T[n]$ is the power loss of the service transformer given by

$$\begin{aligned} &\dot{S}_T[n] = \left|\dot{S}_a[n] + \dot{S}_{ab}[n] + \dot{S}_b[n]\right|^2 \left(R_1^* + jX_1^*\right) / S_T \\ &+\left(\left|\dot{S}_a[n] + \dot{S}_{ab}[n]/2\right|^2 + \left|\dot{S}_b[n] + \dot{S}_{ab}[n]/2\right|^2\right)\left(R_2^* + jX_2^*\right) / S_T \end{aligned}, \tag{2.38}$$

in which S_T is the service transformer rated capacity; $R_1^* + jX_1^*$ and $R_2^* + jX_2^*$ are the per-unit short circuit impedance of the primary winding and the secondary winding respectively.

C. Estimation of Statistics of the Final Aggregate Model parameters

The statistics (means and covariance matrices) of the aggregate secondary feeder model parameters have been derived (given in Subsection 2.3.2). The relation between the final aggregate model parameters and the aggregate secondary feeder model parameters has also been established. The only step left to finalize the secondary system model is to estimate the statistics of the final aggregate model parameters. Since the functions describing the relations between the aggregate model parameters and the aggregate secondary feeder model parameters are nonlinear (see equations (2.31), (2.34) and (2.37)), unscented transformation (UT) [74] which can calculate the statistics of random variables undergoing nonlinear transformation is adopted to perform the estimation task. The basic idea of UT method is to use output samples obtained from the direct application of nonlinear functions to a set of specially selected sample inputs to estimate the output variables' statistics. Its key lies in how to produce appropriate sample inputs (that is named as sigma points) that can maintain sufficient information about the input variable's probability distribution function. The following gives a general description how the estimation is done by using the UT method.

Suppose that $\mathbf{X}$ is the vector of L-dimensional random variables with the mean $\mathbf{m}_X$ and covariance matrix $\mathbf{P}_{XX}$. The other random variable $\mathbf{Y}$ relates to $\mathbf{X}$ through a nonlinear function f. In our estimation problem, $\mathbf{X}$ is composed of the real and imaginary parts of

$\dot{S}_a[n]$, $\dot{S}_{ab}[n]$, $\dot{S}_b[n]$, $\dot{Y}_{a,h}[n]$, $\dot{Y}_{b,h}[n]$, $\dot{Y}_{ab,h}[n]$, $\dot{I}_{a,h}[n]$, $\dot{I}_{b,h}[n]$, $\dot{I}_{ab,h}[n]$; $\mathbf{Y}$ is composed of real and imaginary parts of $\dot{S}_S[n]$, $\dot{Y}_{PN,h}[n]$ and $\dot{I}_{PN,h}[n]$; and f is composed of equations (2.37), (2.31) and (2.34). With the UT method, the means and covariance matrices of random variables $\mathbf{m}_Y$ and $\mathbf{P}_{YY}$ can be obtained through the following steps [74-76].

Step 1: *Generate 2L+1 sigma vectors $\mathbf{x}_i$ (with corresponding weights W_i) according to the following:*

$$\begin{aligned}
&\mathbf{x}_0 = \mathbf{m}_X \\
&\mathbf{x}_i = \mathbf{m}_X + \left(\sqrt{(L+\lambda)\mathbf{P}_{XX}}\right)_i \qquad i = 1,\ldots,L \\
&\mathbf{x}_i = \mathbf{m}_X - \left(\sqrt{(L+\lambda)\mathbf{P}_{XX}}\right)_{i-L} \qquad i = L+1,\ldots,2L \\
&W_0^{(m)} = \lambda/(L+\lambda) \\
&W_0^{(c)} = \lambda/(L+\lambda) + (1-\alpha^2+\beta) \\
&W_i^{(m)} = W_i^{(c)} = 1/\left(2(L+\lambda)\right) \qquad i = 1,\ldots,2L
\end{aligned}, \tag{2.39}$$

where $\lambda = \alpha^2\left(L+\kappa\right) - L$ is a scaling parameter; α determines the spread of the sigma points around $\mathbf{m}_X$ and is usually set to small positive value (e.g., 1e-3); κ is a secondary scaling parameter which is usually set to 0. In equation (2.39), β is used to incorporate the prior knowledge of the distribution of $\mathbf{X}$ (for Normal distribution, $\beta = 2$ is optimal). $\left(\sqrt{(L+\lambda)\mathbf{P}_{XX}}\right)_i$ is the i-th row of the matrix square root.

Step 2: *Feed each sigma vector $\mathbf{x}_i$ to the nonlinear function to yield a set of transformed sample vectors as $\mathbf{y}_i = f\left(\mathbf{x}_i\right) \quad i = 0,1,\ldots,2L$.*

Step 3: *Calculate the mean and covariance of output variable $\mathbf{Y}$ respectively by using*

$$\begin{aligned}\mathbf{m}_Y &= \sum_{i=0}^{2L} W_i^{(m)} \mathbf{y}_i \\ \mathbf{P}_{YY} &= \sum_{i=0}^{2L} W_i^{(c)} \left(\mathbf{y}_i - \mathbf{m}_Y\right)\left(\mathbf{y}_i - \mathbf{m}_Y\right)^T\end{aligned}. \quad (2.40)$$

2.4 Verification of the Proposed Analytical Method

To verify the effectiveness and efficiency of the proposed analytical method, both the MCS method adapted from [16, 17] and the proposed analytical method are applied to a same secondary system. Simplified aggregate models are derived based on both methods, and the results are compared in this section.

2.4.1 Case Description

The system parameters are listed in Table 2.1. Each household is configured with the same set of home appliances. The home appliance random usage pattern model data are collected and derived from [77-79]. Specifically, UK 2000 Time Use Survey [77] gives the activity time of use probability profiles which are statistics of how people spend their time (when they cook, when they shower, and when they do laundry, etc.) at a 10-min resolution. They are used as the default switch-on probability profile for the associated home appliance. For example, the laundry activity time of use probability profile is assigned as the default switch-on probability profile of the washing machine. The average number of residents per household is assumed to be 2.5 based on [78]. The holding time that a home appliance stays in a certain operating state follows a uniform distribution with parameters specified in [79, 80].

Table 2.1: System Parameters

		Values
Service Transformer	Voltage (VH/VL) Rating	14.4 kV/120 V
	KVA Rating	75 kVA
	Primary Winding Resistance	0.65%
	Primary Winding Reactance	1.22%
	Secondary Winding Resistance	1.29%
	Secondary Winding Reactance	0.61%
	Grounding Resistance (R_T)	12 ohm
Number of Households (L)		10, 20
Household Grounding Resistance (r_g)		1 ohm

The residents' lifestyle (when residents are actively at home) affects the usages of home appliances. The key factor that determines the residents' lifestyle is their employment status (full-time working or part-time working). On a weekday, full-time working residents are away from home for most of the time, while part-time working residents are away from home for a shorter period. The default switch-on probability profiles cannot be used for households with residents of different lifestyles since, for example, most home appliances (except for those cyclically operating home appliances such as fridge and freezer) are definitely off for a household with full-time working residents for most of the time during a weekday. To take this into account, a calibration method can be used [80]. Here residents' lifestyle is represented by a time-slotted series $\{\mathrm{OF}[n],\, n=1,\ 2,\ ...,\ N\}$. Let OF[$n$]=1 when the household is actively occupied (e.g., morning, evening), and OF[n]=0 when nobody is at home or awake (e.g., daytime when full-time working residents are at work, midnight). The calibrated switch-on probability is given by

$$p_0^c[n] = \frac{\sum_{k=1}^{N} p_0[k]}{\sum_{k=1}^{N} p_0[k] \times \mathrm{OF}[k]} \times p_0[n] \times \mathrm{OF}[n] . \tag{2.41}$$

It has been proved in [80] that this calibration method ensures that the overall probability for switch-on events to take place over a day is constant. This is reasonable since the lifestyle will not affect the total electricity demand significantly but will have a major impact on when the electricity demand takes place. In our case study, three kinds of lifestyles are investigated, which correspond to full-time working (from 8:00 to 16:00), part-time working in the morning (from 8:00 to 12:00) and part-time working in the afternoon (from 12:00 to 16:00), respectively.

The electrical model data for home appliances are obtained from extensive tests conducted in our lab. Each test measures the supply voltage of and the current drawn by a home appliance under its normal operation. As aforementioned, if the current drawn by the home appliance is linearly related to the supply voltage, the home appliance is a linear home appliance whose fundamental frequency impedance can be calculated from the supply voltage divided by the current drawn by it. Examples are the incandescent lamp and stove. Otherwise, the home appliance is a nonlinear home appliance and it is characterized by the harmonic spectra of the current drawn by it. Examples include the freezer and microwave. Table 2.2 lists all the 28 kinds of home appliances that have been measured and their electrical model type. Detailed model data (i.e., the fundamental impedance for the linear home appliance and the harmonic current spectra for nonlinear home appliance) are documented in [80].

It should be noted that this chapter mainly focuses on the development of an effective and efficient method to model the steady-state behavior of secondary residential system in terms of the random power consumption and harmonic injection. The proposed method is independent of how the input model data are obtained. In other words, the proposed method is also capable of handling input model data obtained from other methods, such as Non-intrusive Load Monitoring [81].

Table 2.2: Measured Home appliances

Home appliance	Type	Home appliance	Type
Coffee Maker	Linear	Desktop PC	Nonlinear
Dryer	Linear	Electric Ballast Fluorescent Lamp	Nonlinear
Electric Kettle	Linear	Food Processor	Nonlinear
Electric Range	Linear	Freezer	Nonlinear
Griddle	Linear	Fridge	Nonlinear
Heater	Linear	Furnace	Nonlinear
Incandescent Lamp	Linear	Garage Door	Nonlinear
Toaster	Linear	Laptop	Nonlinear
Waffle Iron	Linear	LCD Monitor	Nonlinear
Blender	Nonlinear	LCD TV	Nonlinear
Bread Maker	Nonlinear	Microwave	Nonlinear
Compact Fluorescent Lamp	Nonlinear	Printer	Nonlinear
Copier	Nonlinear	Vacuum	Nonlinear
CRT TV	Nonlinear	Washer	Nonlinear

2.4.2 Case Study Results

To evaluate the effectiveness of the proposed analytical method, case studies are performed at two peak load time instants, 7:00 and 20:00, respectively, on a weekday. These time instants are critical for system planning and operation as they are when both the power consumption and harmonic injection from residential households are around their maximums (or peaks), which directly affect the size selection of the service transformer and service conductor.

Figure 2.14 shows the probability distributions of power consumption obtained by the proposed method and the MCS method. Both the joint distribution and marginal distributions with respect to the active power (P) and reactive power (Q) are given. In the joint distribution figures, the results associated with the proposed method and the MCS method are represented by meshed curves and green dots, respectively, while in the marginal distribution figures, the results associated with the proposed method and the MCS method are represented by the solid blue lines and green dots, respectively. As we can observe, the probability distributions obtained based on the two methods agree with each other very well. This observation also conforms to existing research works and field measurements at MV buses [66].

To take a closer look at the accuracy of the proposed method, the means and covariance matrices of the aggregate model parameters obtained by both methods are partially listed in Table 2.3 to Table 2.5, respectively, and are further compared in the following way. Since the parameters of the aggregate model are complex random variables, their means and covariance matrices are complex numbers and 2 by 2 matrices, respectively. To compare the difference between two complex numbers, each complex number is mapped into a unique 2 by 1 vector composed of its real and imaginary parts. The same operation is performed for the 2 by 2 matrix which can be mapped into a unique 4 by 1 vector. Then, the difference between two complex numbers or two matrices can be quantified by using the technique of comparing two vectors' difference. Based on the cosine similarity [82], the relative difference is given by

$$diff = \left|\frac{\mathbf{a}-\mathbf{b}}{\mathbf{a}}\right| = \left|1-\frac{\mathbf{a}\cdot\mathbf{b}}{\mathbf{a}\cdot\mathbf{a}}\right| \times 100\%, \tag{2.42}$$

where $\mathbf{a}$ and $\mathbf{b}$ are the vector mapped from the mean or covariance matrix, respectively, and $\mathbf{a}$ (i.e., the one obtained from the MCS method) is used as the reference vector.

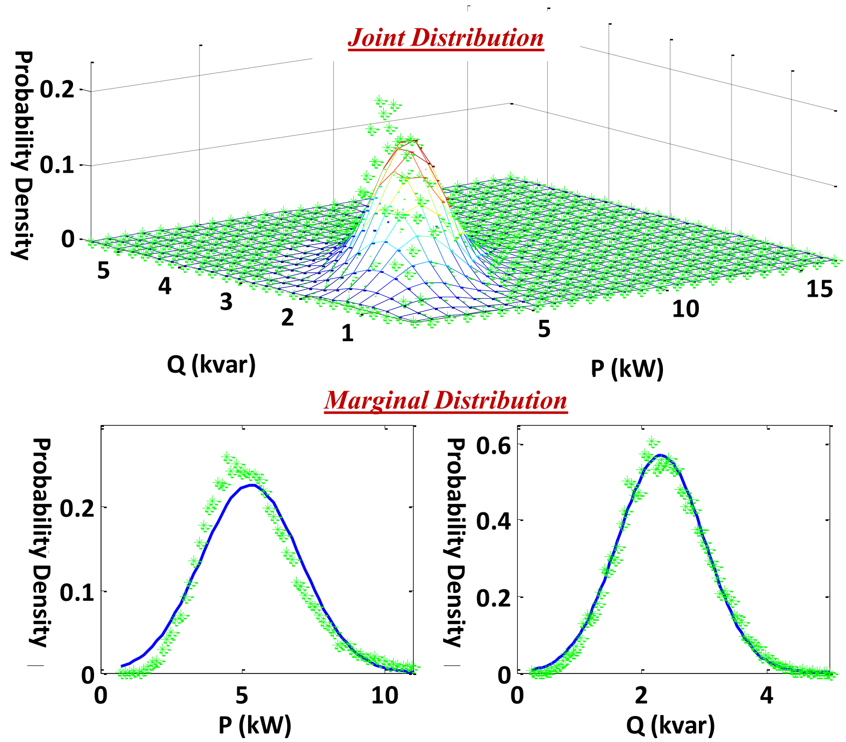

(a) 7:00

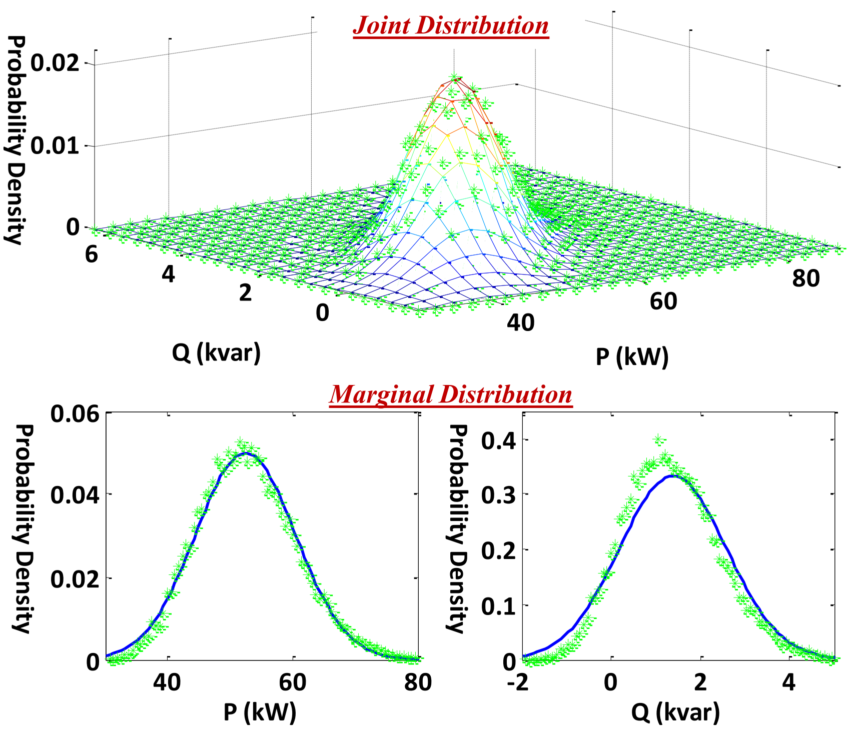

(b) 20:00

Figure 2.14: Power consumption probability distribution for a secondary system with 20 households

Table 2.3: Mean of the Aggregate Model Parameter

	Time Instant	Parameter	Proposed Method	MCS Method	*diff* (%)
10 Households	7:00	$\dot{S}_S$ (kVA)	2.6497+1.1539i	2.7131+1.1821i	2.35
		$\dot{Y}_{PN,3}$ (mS)	0.0019-0.0001i	0.0019-0.0002i	0.05
		$\dot{I}_{PN,3}$ (A)	0.0119+0.0071i	0.0123+0.0074i	3.69
		$\dot{Y}_{PN,5}$ (mS)	0.0018-0.0002i	0.0018-0.0002i	0.09
		$\dot{I}_{PN,5}$ (A)	0.0021-0.0028i	0.0024-0.0027i	3.03
	20:00	$\dot{S}_S$ (kVA)	26.0459+0.5801i	26.1233+0.4222i	0.29
		$\dot{Y}_{PN,3}$ (mS)	0.0858-0.0056i	0.0859-0.0066i	0.23
		$\dot{I}_{PN,3}$ (A)	-0.0361-0.1409i	-0.0383-0.1382i	1.38
		$\dot{Y}_{PN,5}$ (mS)	0.0835-0.0075i	0.0837-0.0093i	0.43
		$\dot{I}_{PN,5}$ (A)	0.0587-0.0438i	0.0564-0.0444i	1.92
20 Households	7:00	$\dot{S}_S$ (kVA)	5.3026+2.3101i	5.3704+2.3387i	1.26
		$\dot{Y}_{PN,3}$ (mS)	0.0037-0.0003i	0.0037-0.0003i	0.32
		$\dot{I}_{PN,3}$ (A)	0.0238+0.0142i	0.0242+0.0146i	1.87
		$\dot{Y}_{PN,5}$ (mS)	0.0036-0.0004i	0.0036-0.0004i	0.17
		$\dot{I}_{PN,5}$ (A)	0.0042-0.0056i	0.0043-0.0058i	1.86
	20:00	$\dot{S}_S$ (kVA)	52.4589+1.3862i	52.5899+1.3444i	0.23
		$\dot{Y}_{PN,3}$ (mS)	0.1722-0.0111i	0.1726-0.0154i	0.44
		$\dot{I}_{PN,3}$ (A)	-0.0727-0.2812i	-0.0781-0.2755i	1.41
		$\dot{Y}_{PN,5}$ (mS)	0.1680-0.0151i	0.1676-0.0221i	0.28
		$\dot{I}_{PN,5}$ (A)	0.1169-0.0878i	0.1121-0.0916i	0.91

Table 2.4: Covariance Matrix of the Aggregate Model Parameter for the Secondary System with 10 households

Time Instant	Parameter	Proposed Method	MCS Method	*diff* (%)
7:00	$\dot{S}_S$ (kVA^2)	[1.5407, 0.4343; 0.4343, 0.2454]	[1.5421, 0.4303; 0.4303,0.2462]	0.04
	$\dot{Y}_{PN,3}$ (10^{-3}mS^2)	[0.0150, -0.0022; -0.0022, 0.0009]	[0.0150,-0.0021; -0.0021,0.0008]	0.26
	$\dot{I}_{PN,3}$ (10^{-3}A^2)	[0.0809, 0.0232; 0.0232, 0.0118]	[0.0822, 0.0233; 0.0233,0.0124]	1.56
	$\dot{Y}_{PN,5}$ (10^{-3}mS^2)	[0.0134, -0.0023; -0.0023, 0.0013]	[0.0135,-0.0024; -0.0024,0.0012]	0.46
	$\dot{I}_{PN,5}$ (10^{-3}A^2)	[0.0035, 0.0016; 0.0016, 0.0074]	[0.0038, 0.0015; 0.0015,0.0078]	4.89
20:00	$\dot{S}_S$ (kVA^2)	[31.2210, 2.8528; 2.8528, 0.6908]	[30.5789,2.2235; 2.2235, 0.5765]	2.38
	$\dot{Y}_{PN,3}$ (10^{-3}mS^2)	[0.5739, -0.0923; -0.0923, 0.0395]	[0.5604, -0.0972; -0.0972, 0.0370]	2.02
	$\dot{I}_{PN,3}$ (10^{-3}A^2)	[0.5566, 0.0725; 0.0725,0.2943]	[0.5610, 0.0710; 0.0710, 0.3030]	1.18
	$\dot{Y}_{PN,5}$ (10^{-3}mS^2)	[0.5049, -0.0977; -0.0977, 0.0584]	[0.4950, -0.1130; -0.1130, 0.0585]	0.52
	$\dot{I}_{PN,5}$ (10^{-3}A^2)	[0.0828, 0.0099; 0.0099, 0.0850]	[0.0922, 0.0029; 0.0029, 0.0945]	9.91

Table 2.5: Covariance Matrix of the Aggregate Model Parameter for the Secondary System with 20 Households

Time Instant	Parameter	Proposed Method	MCS Method	*diff* (%)
7:00	$\dot{S}_S$ (kVA^2)	[3.0851, 0.8677; 0.8677, 0.4917]	[3.1187, 0.8604; 0.8604, 0.4914]	0.80
	$\dot{Y}_{PN,3}$ (10^{-3}mS^2)	[0.0303, -0.0041; -0.0041, 0.0016]	[0.0303, -0.0043; -0.0043, 0.0016]	0.36
	$\dot{I}_{PN,3}$ (10^{-3}A^2)	[0.1618, 0.0463; 0.0463, 0.0237]	[0.1636, 0.0461; 0.0461, 0.0239]	0.89
	$\dot{Y}_{PN,5}$ (10^{-3}mS^2)	[0.0273, -0.0046; -0.0046, 0.0024]	[0.0274, -0.0049; -0.0049, 0.0024]	0.42
	$\dot{I}_{PN,5}$ (10^{-3}A^2)	[0.0070, 0.0031; 0.0031, 0.0149]	[0.0067, 0.0026; 0.0026, 0.0154]	1.40
20:00	$\dot{S}_S$ (kVA^2)	[63.7878, 6.1726; 6.1726, 1.4393]	[63.1745, 4.5500; 4.5500, 1.1684]	1.33
	$\dot{Y}_{PN,3}$ (10^{-3}mS^2)	[1.1574, -0.1797; -0.1797, 0.0730]	[1.1336, -0.2226; -0.2226, 0.0845]	0.50
	$\dot{I}_{PN,3}$ (10^{-3}A^2)	[1.1100, 0.1434; 0.1434, 0.5861]	[1.1178, 0.1653; 0.1653, 0.5997]	1.45
	$\dot{Y}_{PN,5}$ (10^{-3}mS^2)	[1.0276, -0.1973; -0.1973, 0.1107]	[0.9855, -0.2621; -0.2621, 0.1373]	0.35
	$\dot{I}_{PN,5}$ (10^{-3}A^2)	[0.1651, 0.0198; 0.0198, 0.1692]	[0.1632, 0.0101; 0.0101, 0.1999]	8.42

The quantification results are shown as Figure 2.15 and are also partially listed in Table 2.3 to Table 2.5. Again, it can be seen that the analytical and simulation results match well with each other. The difference is mostly due to the neglect of the secondary conductor's impedance in the proposed analytical method as mentioned in Section 2.2. However, since the relative difference of all aggregate model parameters for all major harmonic orders (up to the 15th) is below 10%, the proposed analytical method can serve as an effective tool for the utility engineers to assess and study harmonic impact of residential loads.

Next we show how the random usage patterns of home appliances affect the aggregate model parameters derived from the analytical method. Figure 2.16 depicts the power 24-hour variation for two systems (20 households) with different compositions of residents' with different lifestyles [16, 17].

As for the residents who work full-time, they leave home at around 8:00 and come back at around 16:00; while for the residents who do part-time jobs, they may leave home for work in the morning from 8:00 to 12:00 or in the afternoon from 12:00 to 16:00 and stay home for the rest of the time of the day. As we can see from Figure 2.16 (a), there are two peaks of power consumption over the day, in the early morning and early evening, respectively, due to extensive household activities at that time. Also, the evening peak is more obvious as a larger number of home appliances are used by the residents.

However, when 50% residents switch to part-time working, both morning and evening peaks decrease, while the power consumption around noon increases significantly, as shown in Figure 2.16 (b). This is mainly because of the changes in the consumers' (or the residents') behavior and thus, the random usage patterns of home appliances. The ability for the proposed analytical method to capture such consumers' behavior changes is critical, especially when evaluating certain demand response programs in smart grid, e.g., time-of-use pricing for the peak load shaving.

Figure 2.17 also gives the 24-hour variation of the injected harmonic current of the secondary residential systems obtained by the proposed analytical method. It is expected that the change in the residents' lifestyle will lead to a change in the daily injected harmonic current variation of the secondary residential system, as it has an impact on when the nonlinear home appliances are switched on. It can be seen from Figure 2.17, the proposed analytical method is capable of capturing it.

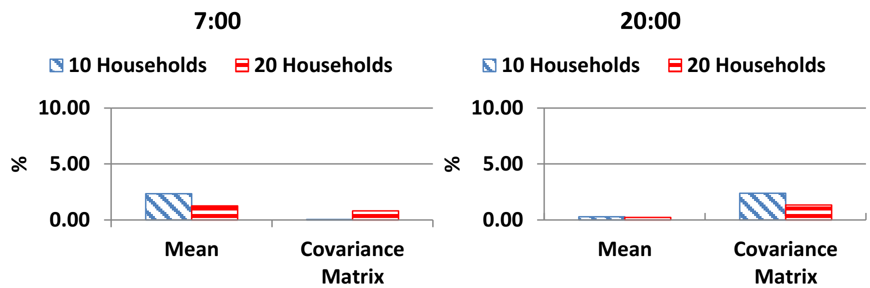

(a) Fundamental frequency power consumption

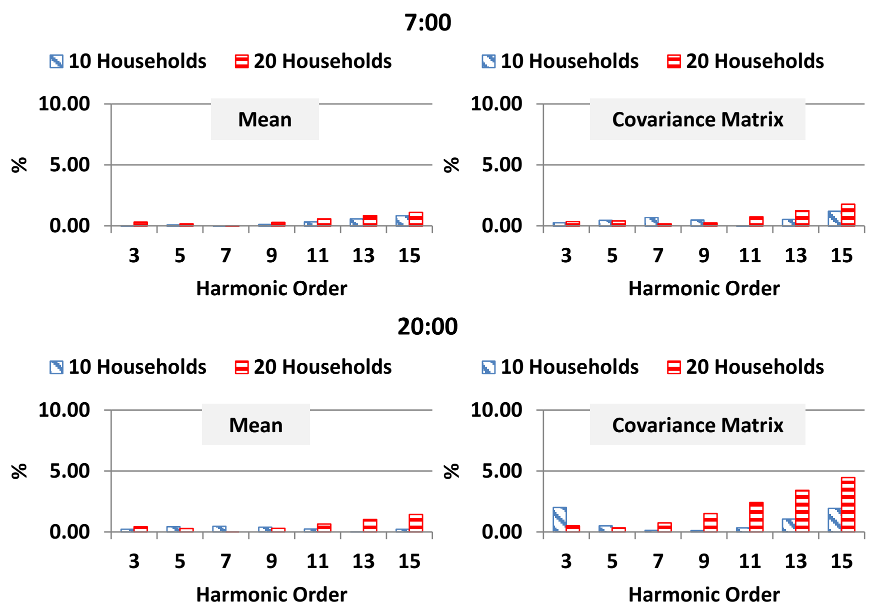

(b) Harmonic admittance

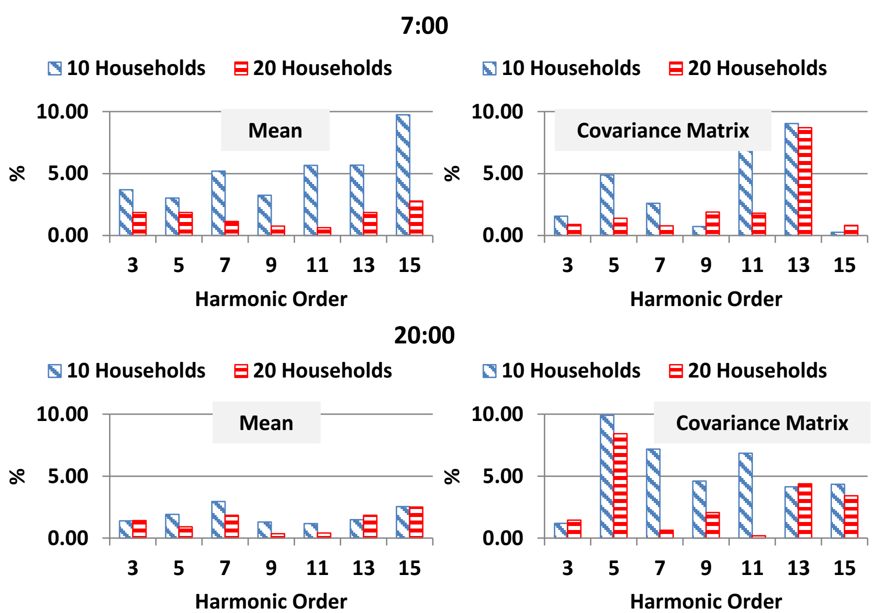

(c) Harmonic current

Figure 2.15: Relative difference for the studied cases

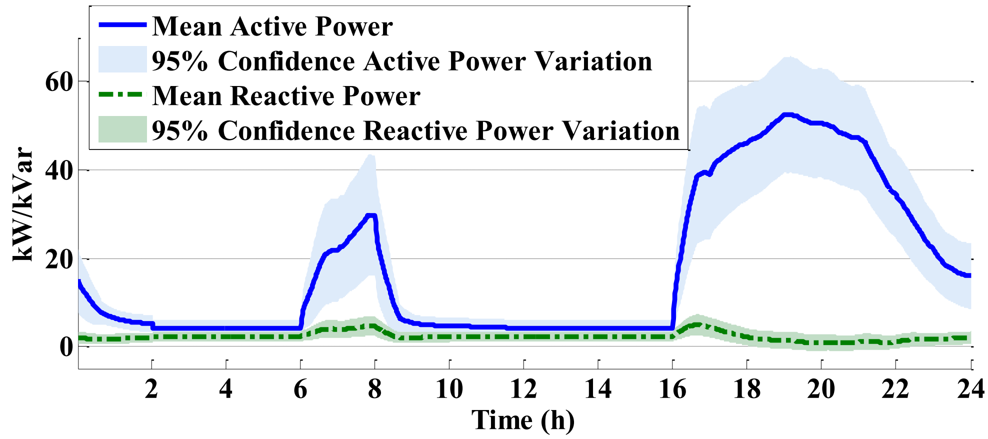

(a) All residents are full-time working

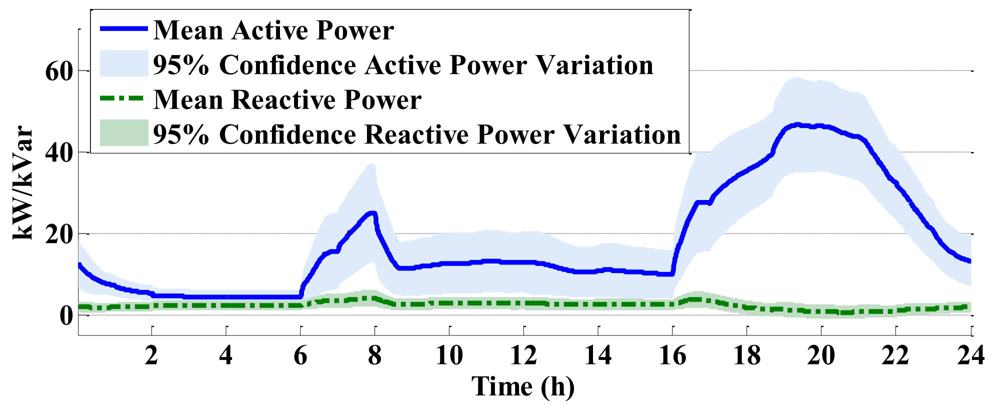

(b) 50% residents are part-time working

Figure 2.16: Power variation on a weekday for a secondary system with 20 households

In addition to the effectiveness, another significant advantage of the proposed analytical method is its time efficiency. In this work, a PC with Intel CORE i7 2.4 GHz CPU and 16 GB DDR3 RAM is used as a test platform. Both methods are coded in the Matlab 2012a environment, while MHLF [14] was called in MCS method to perform load flow and frequency scan analysis. For all the cases discussed above, it takes an average of 33 hours for the MCS method to obtain the statistics of interest (via 20,000 simulation runs to meet the 90% confidence interval (CI) convergence criterion [73]), while the time used by the proposed method is 0.01 seconds on average. The main reason is that, the MCS method relies on a large number of repetitive simulation runs under randomly generated home appliance usage profiles, which is extremely time-consuming for a typical secondary residential system with a large amount of home appliances. On the other hand, by eliminating the requirement on repetitive simulation runs, the proposed method uses an analytical model to characterize home appliance random usage patterns and thus, can significantly reduce the computational effort. Such time efficiency is expected to greatly facilitate the fast evaluation of the planning and operation strategy for the future smart grid.

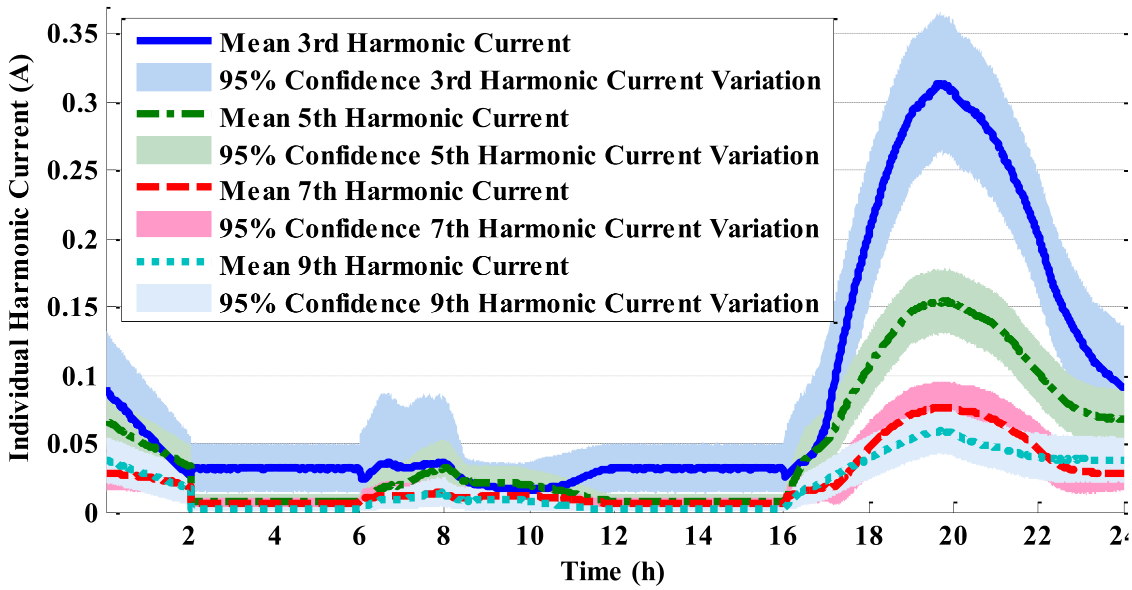

(a) All residents are full-time working

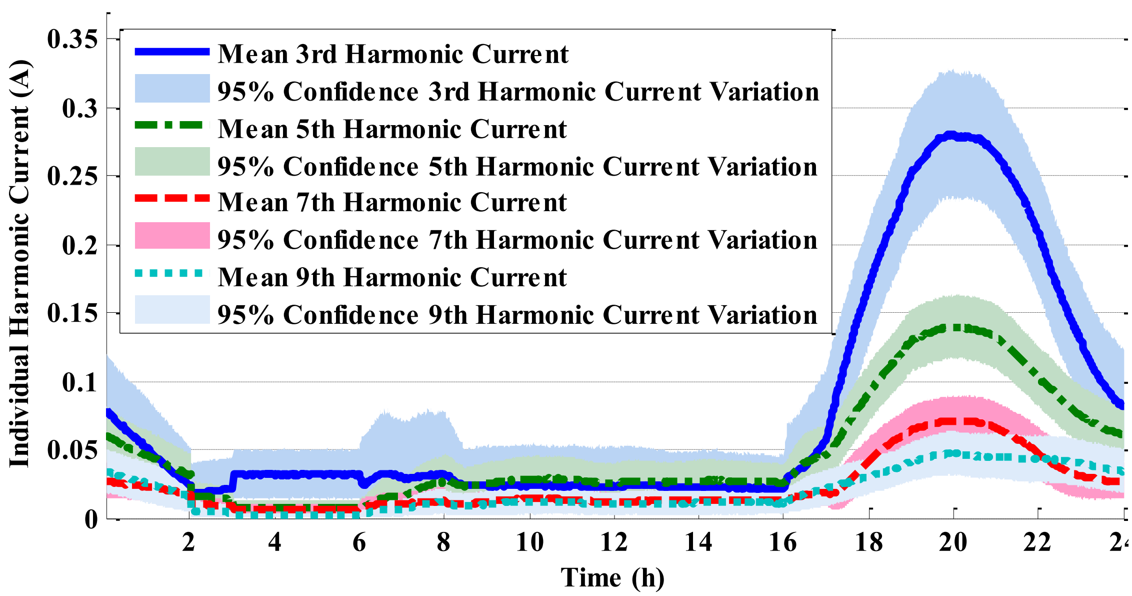

(b) 50% residents are part-time working

Figure 2.17: Individual harmonic current variation on a weekday for a secondary system with 20 households

2.5 Summary

In this chapter, an analytical method was proposed to establish a probabilistic harmonic model for the secondary residential system. This method derives the aggregate secondary system model based on the electrical model and the random usage pattern model of home appliances, to account for technological advances and the behavior evolution of consumers. The resulting model is a time-varying steady-state probabilistic equivalent circuit model whose parameters are characterized by bivariate normal distributions. The model can be easily implemented for the primary system probabilistic load flow analysis, harmonic assessment/mitigation, and demand response program evaluation. Extensive case studies based on the proposed analytical method and the MCS method confirmed the effectiveness and efficiency of the proposed method.

Chapter 3

A Filtering Scheme to Reduce the Penetration of Harmonics into Transmission Systems

The widespread adoption of energy-efficient but harmonic-producing home appliances in residential households has led to increased injection of harmonic currents into transmission systems, which could lead to transmission system power-quality issues such as the overloading of HVDC filters. As discussed in the introduction, limiting the harmonic emission of individual electronic devices and installing filters inside the distribution systems both have their own limitations in applications to reduce the penetration of harmonics produced by the mass-distributed harmonic sources into transmission systems. As Figure 3.1 reveals, the last resort to prevent harmonics from entering into transmission systems is either to install filters inside the distribution substation to bypass harmonics or to reconfigure the distribution substation transformer to block harmonics. Based on this, this chapter proposes a novel filtering scheme that utilizes the low-voltage tertiary winding of the distribution substation transformer to construct a low impedance path to trap harmonics.

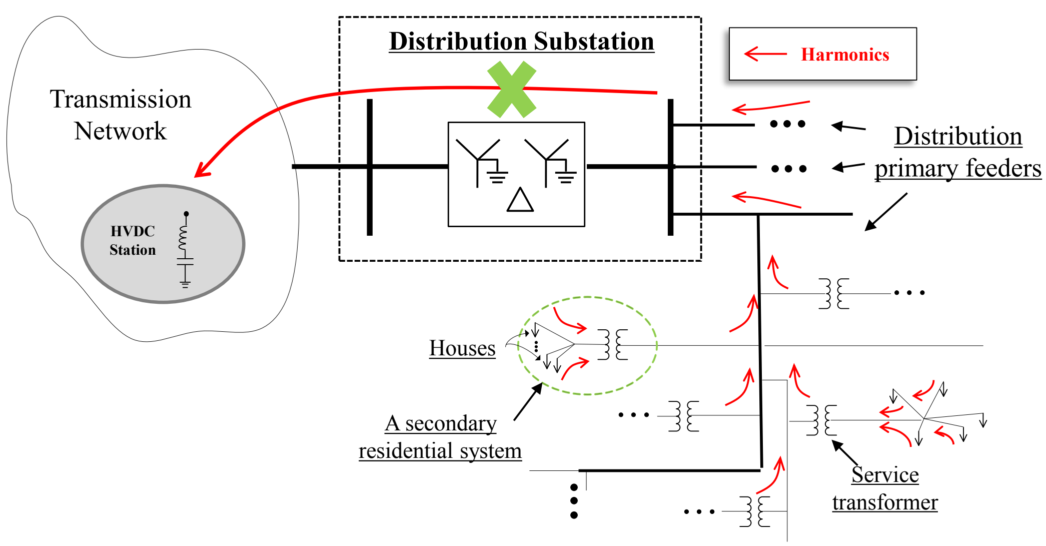

Figure 3.1: Schematic illustrating the propagation of the harmonics produced by mass-distributed harmonic sources

This chapter is organized as follows. First, a review of the techniques that are applicable for preventing harmonics from entering transmission systems is given in Section 3.1. Next, Section 3.2 presents the proposed filtering scheme, which is called as "Tertiary Winding Filter". The design method for the proposed tertiary winding filter is described in Section 3.3. Section 3.4 provides case studies that assess the performance of the proposed tertiary winding filter and its design method. Application considerations are discussed in Section 3.5, while Section 3.6 summarizes this chapter.

3.1 Review of Applicable Mitigation Schemes

Although little research work has been done in the direction of preventing harmonics from entering transmission systems, techniques that can be adopted for the purpose do exist. These techniques can be classified into two types. One is to prevent or reduce the injection of ZS harmonics into the transmission system. The other type is to deal with the positive and negative harmonics. These harmonics are collectively called as NZS harmonics in this thesis.

3.1.1 ZS Harmonic Mitigation Techniques

ZS components are dominant in the 3rd, 9th and other triple-order harmonics. Single phase non-linear loads such as energy efficient home appliances are the most significant source of ZS harmonics. It is quite common to observe high levels of ZS harmonics in a distribution substation feeding residential loads these days [10, 12].

A. Transformer Connection

The simplest way to prevent ZS harmonics' propagation into transmission systems is to configure the substation transformer’s primary side into delta or ungrounded Y connection. With such connections, there are no paths for the ZS harmonic currents to flow into the primary side. For cases where the primary side must be grounded, a grounding transformer may be installed at the primary bus to serve as the grounding point.

B. Passive ZS Filter

A shunt filter installed at the secondary side of the substation transformer can also reduce the injection of distribution system harmonics into the transmission system.

Shunt passive ZS filters create shunt low ZS impedance to trap ZS harmonics. They have various topologies (as shown in Figure 3.2) and can be broadly classified into two types.

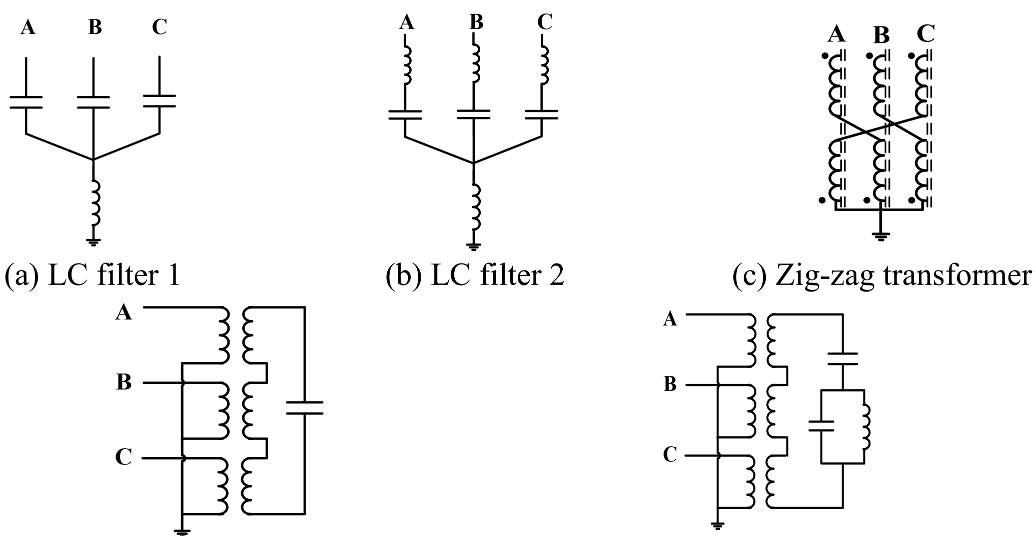

(a) LC filter 1 (b) LC filter 2 (c) Zig-zag transformer

(d) Transformer-based single tuned filter (e) Transformer-based double tuned filter

Figure 3.2: Topologies of ZS shunt filters

The first type is the LC ZS filter which only consists of capacitors and inductors. It has positive/negative sequence impedance so it affects the flow of NZS harmonics. A typical one of such filters is the star-connected capacitors grounded through an inductor (Figure 3.2 (a) [83]) which is tuned to create a low ZS impedance. The main attractive characteristic of this topology is that by adding a three-phase inductor (Figure 3.2 (b)), the capacitors can be tuned to filter positive and negative sequence harmonics as well. The drawback of this filter is that it can change the 60 Hz power flow and may result in NZS resonances [84] at other harmonic orders.

The second type of ZS filter is the transformer based ZS filter. It is developed based on the concept of grounding transformer. Such a filter behaves as open circuit at NZS so it has no impact on the normal power system operation and on NZS harmonics. A representative example is the zig-zag transformer based filter (Figure 3.2 (c) [85]). A drawback of this filter is that it needs a nonstandard transformer. Another example consists of a Yg/delta transformer with tuned capacitors and inductors inserted into the delta loop (Figure 3.2 (d)[86], (e)[87]). By the proper selection of capacitors and inductors, a ZS impedance as low as the transformer's resistance could be achieved at desired harmonics. This leads to attractive ZS filter topologies without using non-standard transformers.

It should be noted that the ZS filter can be installed at the either side of the substation transformer theoretically. However, because of high voltage, the primary side scheme is uneconomic and hard to implement. The practical implementation, therefore, is to install the ZS filter at the secondary side.

3.1.2 NZS Harmonic Mitigation Techniques

NZS components are dominant in the 5th, 7th, 11th and other non-triple order harmonics. All nonlinear loads generate NZS components.

Presently, the only known method to mitigate NZS harmonic in MV or high voltage (HV) systems is installing passive shunt filters. Commonly used LC NZS filters include the single tuned filter, the 3rdHP filter, the C-type filter, the topologies of which are shown in Figure 3.3 [28, 88-90]. These filters can be installed on the secondary side of the substation, creating a low-impedance path to trap the harmonics from the distribution systems.

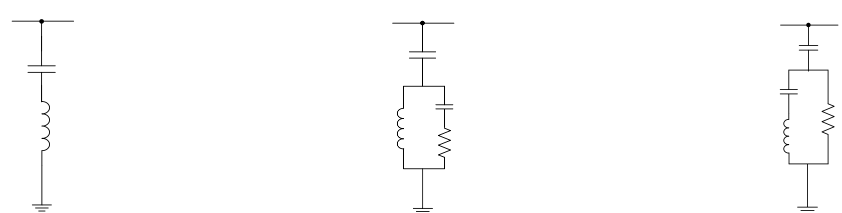

(a) LC filter 3 (b) LC filter 4 (c) LC filter 5

Figure 3.3: Topologies of LC NZS filters

3.1.3 Summary of Available Techniques

Current available techniques for preventing harmonics' entering transmission systems are summarized as shown in Figure 3.4.

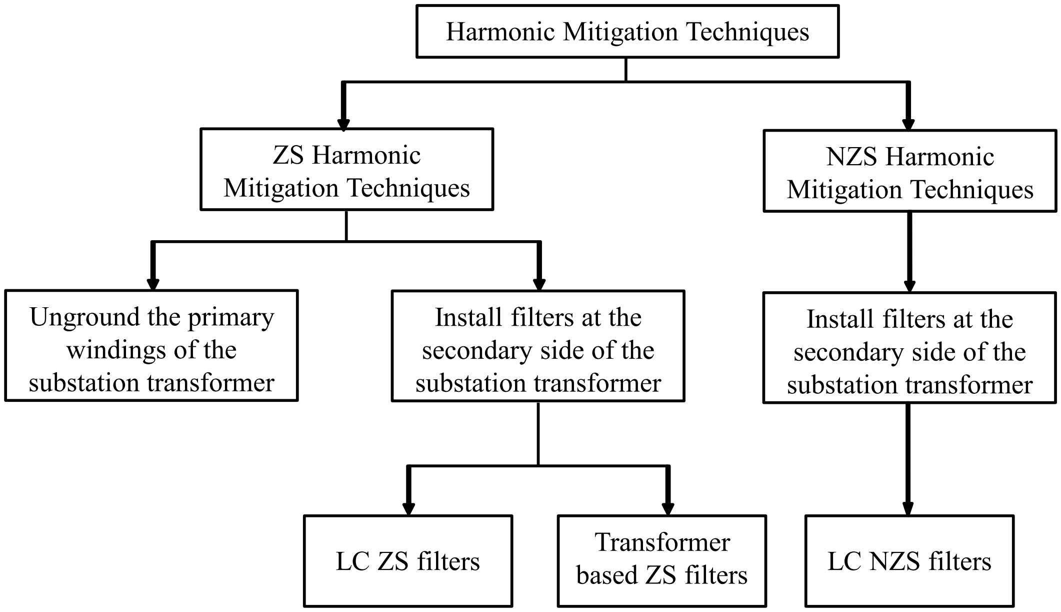

Figure 3.4: Applicable techniques summary

To prevent the harmonics from distribution systems (which usually has a wide spectrum) from entering transmission systems, both ZS harmonic mitigation techniques and NZS harmonic mitigation techniques should be used. Among the limited options, the schemes with transformer based ZS filters require a transformer of a large size to work effectively. Considering the high cost of a large transformer, all these schemes are not economical.

Compared to the scheme of the combination of the LC ZS filter and the LC NZS filter, the scheme with ungrounded primary windings and LC NZS filter is of less cost because of the absence of the LC ZS filter. However, for the cases that the grounding at the transmission side is a must, expensive HV grounding transformer should be incorporated into this scheme and this will make this scheme loose its cost advantage. Actually, the primary side winding connections of the substation transformer is usually fixed and could not be changed arbitrarily which further renders the applicability of the ungrounding scheme.

3.2 Proposed Filtering Scheme

Three winding transformers are widely used by utility companies as the distribution substation transformer. Their common connection is Yg/Yg/delta with no loads served by the delta connected tertiary winding. The tertiary winding typically has a rated voltage lower than that of the secondary winding (for example 144/25/4.16 kV). In addition, the delta connection can trap zero sequence currents [91]. Therefore, this thesis proposes to use the tertiary winding to create a filter that has a lower rated voltage and can trap zero sequence harmonics.

3.2.1 Basic Principle of the Tertiary Winding Filter

The basic idea of the proposed filter is to utilize the leakage inductance of the tertiary winding to create a low-impedance path to trap harmonic currents at tuned frequencies. This is achieved by inserting capacitors and inductors into the delta loop of the tertiary winding for ZS harmonic filtering and by connecting shunt capacitors and inductors to the tertiary winding for NZS harmonic filtering. Topology of the filter is depicted in Figure 3.5. The frequency response of a sample tertiary winding filter tuned to the 3rd and 9th ZS harmonics and 5th, 7th and 11th NZS harmonics is shown in Figure 3.6.

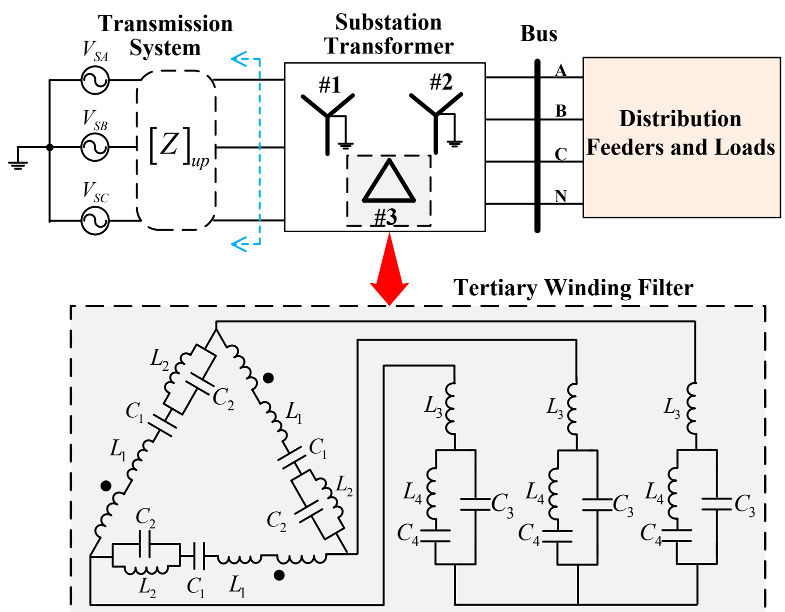

Figure 3.5: Topology of the proposed tertiary winding filter

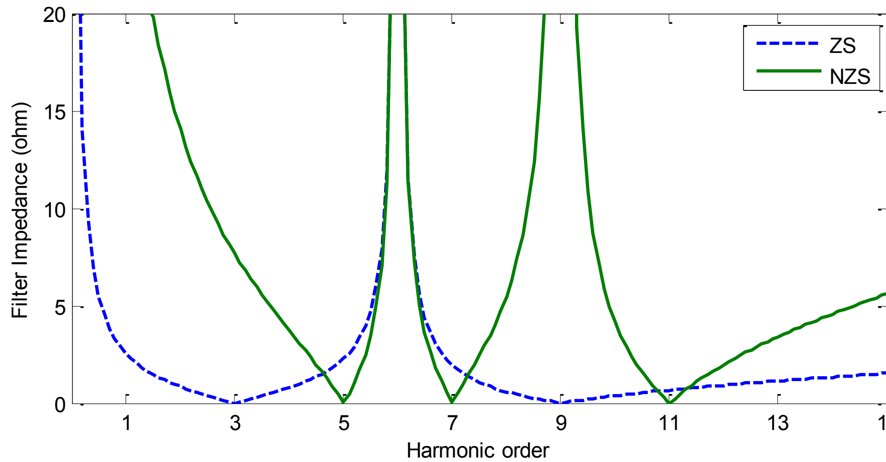

Figure 3.6: Frequency response of a sample tertiary winding filter

The equivalent circuit of the tertiary winding filter at tuned frequencies seen from the secondary side is shown in Figure 3.7. In Figure 3.7, R'_{X1} and L'_{X1} represent the resistance and the leakage inductance of the substation transformer's primary winding (referred to the secondary side); R_{X2} and L_{X2} represent the resistance and the leakage inductance of the substation transformer's secondary winding; R'_{X3} represents the resistance of the substation transformer's tertiary winding (referred to the secondary side); $Z_{Up}^{+/-/0}(h)$ represents the equivalent transmission system harmonic impedance seen at the primary side of the substation transformer (but referred to the secondary side); $Z_{Down}^{+/-/0}(h)$ and $I_{Down}^{+/-/0}(h)$ represent equivalent harmonic impedance and harmonic current source of distribution feeders and loads; ω_0 is the fundamental angular frequency (rad/s); and h represents the tuned harmonic order.

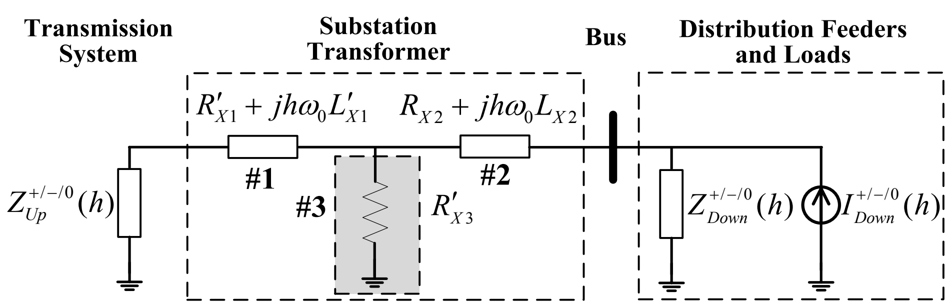

Figure 3.7: Equivalent circuit of the tertiary winding filter at tuned frequencies

It can be seen that the tertiary winding's impedance only contains the resistive component, i.e., the resistance of the tertiary winding, since the reactive component has been canceled out by the tuning capacitors. As a result, a low-impedance path separates the transmission and distribution systems. Harmonics originated from the distribution system will be bypassed by the tertiary winding before it can reach the transmission system. In addition, the typical voltage of a substation transformer tertiary winding is 4.16 kV to 13.8 kV. Low-voltage LC components can be used to construct the filter, which results in cost savings.

3.2.2 Equivalent Circuits of Tertiary Winding Filter

As shown in Figure 3.5, the tertiary winding filter is composed of two parts, i.e., the delta connected part (the delta loop) and the star connected part (the shunt components at the tertiary side).

Since the star connected shunt components behave as an open circuit in ZS, the filter's ZS equivalent circuit only consists of the delta connected components (see Figure 3.8 (a)) [92]. For NZS harmonics, the star connected components behave as a shunt connected load. Thus the filter's NZS equivalent circuit consists of both the delta and star connected components (see Figure 3.8 (b)) [92]. In the figure, *a* represents the turns ratio of the tertiary winding to secondary winding.

The filter is to be designed to achieve the following goals: (1) the delta circuit traps two ZS harmonics such as the 3rd and 9th, and (2) the star circuit in combination with the delta circuit traps three NZS harmonics such as 5th, 7th and 11th. It is important to note that due to the existence of the tertiary winding reactance, the traditional concept of multiple single-tuned filters cannot be applied in this case. A new filter topology that can cancel out the tertiary winding reactance is needed. The proposed topology that consists of multiple LC elements as shown in Figure 3.5 is able to achieve this goal.

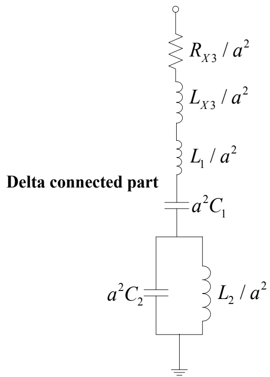

(a) Equivalent ZS circuit

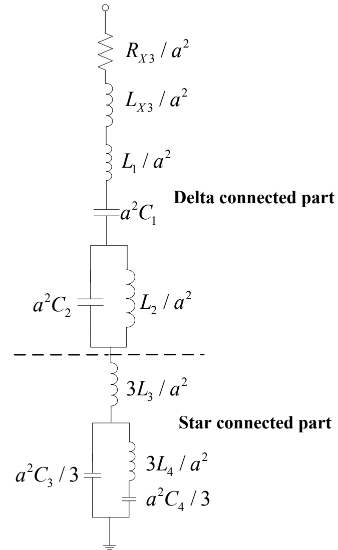

(b) Equivalent NZS circuit

Figure 3.8: Equivalent circuit of the tertiary winding filter

3.2.3 Feasibility Analysis

For the proposed filter to be effective, it is important to compare the impedance of the filter branch against that of the upstream system. This filter's impedance must be much smaller than that of the upstream impedance.

The minimum impedance of the filter branch that can be achieved at the tuned harmonics is the resistance of the tertiary winding, as the reactance is cancelled out by proper selection of the filter components. According to the typical parameters of three winding transformers, the tertiary winding resistance is comparable to the primary winding resistance. For a substation transformer, its reactance to resistance ratio is usually very high [93] which means $\omega_0 L'_{X1} >> R'_{X1}$.

Thus

$$R'_{X3} << \left|R'_{X1} + jh\omega_0 L'_{X1}\right| < \left|R'_{X1} + jh\omega_0 L'_{X1} + Z_{Up}^{+/-/0}(h)\right|. \quad (3.1)$$

The above equation means that the impedance of filer branch is far smaller than that of the upstream system. As a result, harmonics at tuned frequencies will be trapped into the tertiary side rather than propagating into the transmission system.

A rough estimation of the percentage of the harmonic current that can be trapped by the filter could be obtained by the following equation:

$$Ratio \approx \frac{h\omega_0 L'_{X1}}{R'_{X3} + h\omega_0 L'_{X1}} \times 100\% \tag{3.2}$$

where h is the tuned harmonic order.

To show the performance of the tertiary winding filter, several typical three winding transformers used by utility companies are listed in Table 3.1. The percentage of the third harmonic current that will be trapped by the filter is provided in the last column. For higher order harmonics, a larger percentage will be trapped by the filter.

Table 3.1: Trapped Ratio for Different Three Winding Transformers

Transformer Parameter					Trapped Ratio (%)
Rated Capacity[a] (MVA)	Rated Voltage[b] (kV)	Short Circuit Impedance (%)		On-Load Loss (kW)	
20/20/10	144/25/6.3	H-M	10.5	106.3	98.42
		H-L	18		
		M-L	6.5		
25/25/8	144/25/13.8	H-M	10.5	125.8	97.77
		H-L	18		
		M-L	6.5		
32/32/16	144/25/4.16	H-M	10.5	148.8	98.55
		H-L	17		
		M-L	6.5		
40/40/13.3	144/25/6.3	H-M	10.5	178.5	97.92
		H-L	17		
		M-L	6.5		
50/50/16.7	144/25/13.8	H-M	10.5	212.5	98.11
		H-L	18		
		M-L	6.5		

[a] The rated capacity of each winding;

[b] The nominal line-to-line voltage (LL-rms).

3.3 Tertiary Winding Filter Design

This section first introduces the concept of tuning sharpness and its relationship with the filtering performance. Then the design method for the tertiary winding filter with a robust filtering performance is presented.

3.3.1 Tuning Sharpness Consideration

The passive filter is said to be tuned to the frequency that makes its impedance reach its local minimum. The sharpness of the tuning is quantified by the quality factor, which is defined as the ratio of the tuned frequency to its corresponding bandwidth as follows [1]:

$$Q_r = \frac{f_r}{\Delta f} = \frac{\omega_r}{\Delta \omega} \tag{3.3}$$

where f_r is the tuned (or resonant) frequency; Δf is the half-power bandwidth, i.e., the bandwidth over which the power of vibration is greater than half the power at the tuned (or resonant) frequency f_r; $\omega_r = 2\pi f_r$ is the angular tuned (or resonant) frequency; and $\Delta\omega$ is the angular half power bandwidth.

Generally, the larger the quality factor, the sharper the tuning is. A sharp tuned filter is not desired. The reason is as follows. In practice, the system fundamental (supply) frequency may change over time, causing the harmonic frequency to change. The component capacitance and inductance may differ from the designed value due to aging, temperature effects and manufacturing tolerances [1, 39]. For a sharp tuned filter, these factors will cause a dramatic increase of the impedance at the harmonic frequency that the filter is intended to suppress. This increase greatly impairs the filter's filtering performance and can even make the filter completely incapable of filtering the harmonic of interest. Thus, in a practical application, the filter should not be too sharply tuned, and the tuning sharpness or the quality factor is an important concern in the filter design.

As Figure 3.6 shows, for the multi-tuned filter, an intuitive way to reduce the tuning sharpness is to make its parallel resonant frequencies be as far away as possible from its series resonant frequencies (the harmonic frequencies it is intended to suppress). For the proposed tertiary winding filter, this is achieved by setting the two parallel resonant harmonic orders as follows:

$$h_{p1} = \frac{1}{2}\left(h_1^{+/-} + h_2^{+/-}\right), \tag{3.4}$$

$$h_{p2} = \frac{1}{2}\left(h_2^{+/-} + h_3^{+/-}\right), \tag{3.5}$$

where $h_1^{+/-}$, $h_2^{+/-}$, and $h_3^{+/-}$ represent the three NZS tuned orders of the tertiary winding filter, respectively. Typically, $h_1^{+/-}=5$, $h_2^{+/-}=7$, and $h_3^{+/-}=11$.

It should be further noted that for the proposed tertiary winding filter, its ZS tuned orders and NZS tuned orders should satisfy the following condition:

$$h_1^0 < h_1^{+/-} < h_2^{+/-} < h_2^0 < h_3^{+/-}, \tag{3.6}$$

where h_1^0 and h_2^0 represent the two ZS tuned orders of the tertiary winding filter, respectively. Typically, $h_1^0=3$ and $h_2^0=9$.

The relationship between the parallel resonant harmonic orders or the tuned harmonic orders and the LC parameters is given in the following section.

3.3.2 Design Method

The design of the tertiary winding filter is an iterative process based on the system harmonic load flow study and the component loading assessment. The design objective is to determine the proper LC component parameters based on the transformer parameters. The flowchart of the design procedure is shown as Figure 3.9.

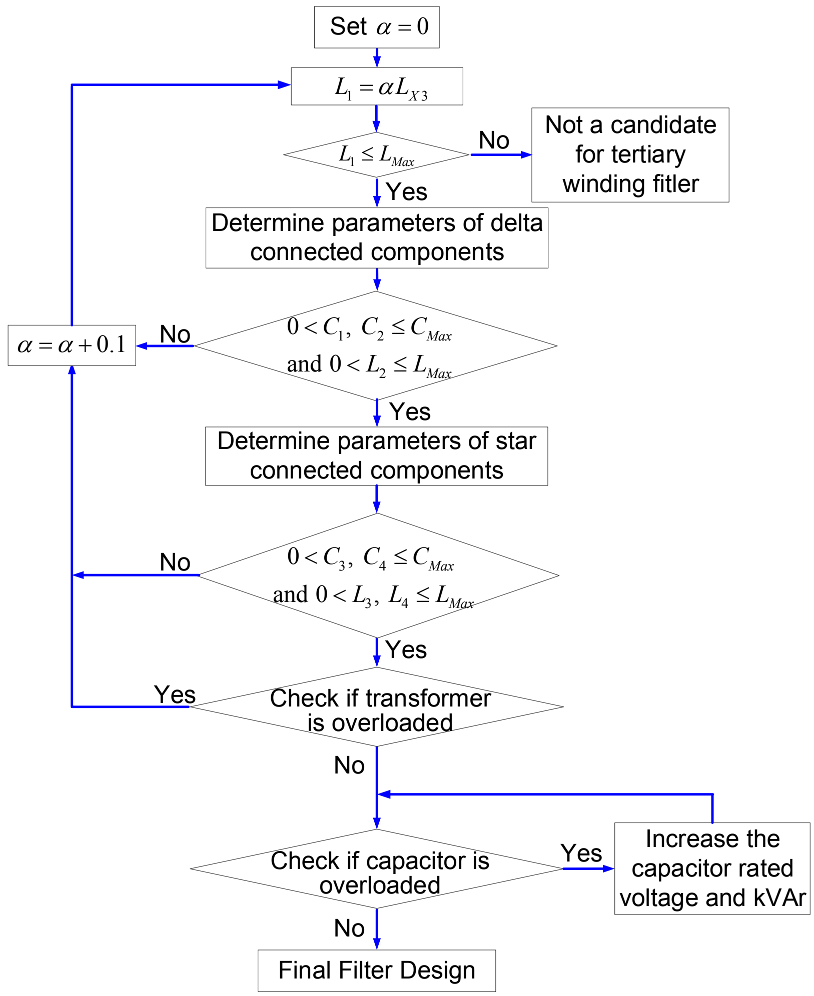

Figure 3.9: Flowchart of design procedure for the tertiary winding filter

A. LC Parameters Determination

As shown in Figure 3.9, the determination of the component parameters is done in two of the blocks. The first block is to determine the parameters of the delta connected components. Except for L_1 (which will be discussed in the Component Loading Assessment section), there are three parameters (C_1, C_2 and L_2) to be determined. Referring to Figure 3.8 (a), the ZS impedance of the filter at harmonic order h, can be expressed as

$$Z_{X3}^{0}\left(h\right)=\left(R_{X3}-j\frac{f^{0}\left(h\right)}{g^{0}\left(h\right)}\right)/a^{2}, \tag{3.7}$$

where

$$f^{0}\left(h\right)=C_{1}C_{2}\left(L_{X3}+L_{1}\right)L_{2}\omega_{0}^{4}h^{4}-\left(C_{1}L_{X3}+C_{1}L_{1}+C_{1}L_{2}+C_{2}L_{2}\right)\omega_{0}^{2}h^{2}+1, \tag{3.8}$$

$$g^{0}\left(h\right)=-C_{1}C_{2}L_{2}\omega_{0}^{3}h^{3}+C_{1}\omega_{0}h. \tag{3.9}$$

To tune the filter to trap h_{1}^{0} and h_{2}^{0} ZS harmonics means

$$\begin{cases} f^{0}\left(h_{1}^{0}\right)=0 \\ f^{0}\left(h_{2}^{0}\right)=0 \end{cases}. \tag{3.10}$$

Also, by the numerical characteristic of the parallel resonant harmonic order, we can get

$$g^{0}\left(h_{p1}\right)=0\Rightarrow C_{2}L_{2}-\frac{1}{h_{p1}^{2}\omega_{0}^{2}}=0. \tag{3.11}$$

By solving equations (3.10) and (3.11), C_{1}, C_{2} and L_{2} are determined.

With C_{1}, C_{2} and L_{2} are determined, the star connected components can be determined as follows. According to Figure 3.8 (b), the NZS impedance of the filter at harmonic order *h* can be expressed as

$$Z_{X3}^{+/-}\left(h\right)=\left(R_{X3}-j\frac{f^{+/-}\left(h\right)}{g^{+/-}\left(h\right)}\right)/a^{2}, \tag{3.12}$$

where

$$f^{+/-}(h) = A\omega_0^6 h^6 - B\omega_0^4 h^4 + D\omega_0^2 h^2 - (3C_1 + C_3 + C_4)$$
$$\begin{cases} A = C_1C_2C_3C_4\left(L_{X3}+L_1+3L_3\right)L_2L_4 \\ B = C_1C_2\left(\left(C_3+C_4\right)\left(L_{X3}+L_1+3L_3\right)+3C_4L_4\right)L_2 + C_3C_4\left(C_1\left(L_{X3}+L_1+L_2+3L_3\right)+C_2L_2\right)L_4 \\ D = C_1\left(3C_2+C_3+C_4\right)L_2 + \left(C_3+C_4\right)\left(C_1\left(L_{X3}+L_1\right)+\left(3C_1L_3+C_2L_2\right)\right)+\left(3C_1+C_3\right)C_4L_4 \end{cases}$$

(3.13)

$$g^{+/-}(h) = -E\omega_0^5 h^5 + F\omega_0^3 h^3 - (C_1C_3 + C_1C_4)\omega_0 h$$
$$\begin{cases} E = C_1C_2C_3C_4L_2L_4 \\ F = C_1C_2C_3L_2 + C_1C_2C_4L_2 + C_1C_3C_4L_4 \end{cases} . \quad (3.14)$$

The filter is tuned to filter $h_1^{+/-}$, $h_2^{+/-}$, and $h_3^{+/-}$ NZS harmonics, therefore,

$$\begin{cases} f^{+/-}\left(h_1^{+/-}\right)=0 \\ f^{+/-}\left(h_2^{+/-}\right)=0 \\ f^{+/-}\left(h_3^{+/-}\right)=0 \end{cases} . \quad (3.15)$$

By the sharpness tuning constraint and the characteristic of NZS impedance given by equation (3.12), we have

$$g^{+/-}\left(h_{p2}\right) = 0 \Rightarrow \frac{C_3C_4}{C_3+C_4}L_4 - \frac{1}{h_{p2}^2\omega_0^2} = 0 . \quad (3.16)$$

By solving equations (3.15) and (3.16), C_3, C_4, L_3 and L_4 are determined.

B. Component Loading Assessment

The parameters determined by using equations (3.10), (3.11), (3.15) and (3.16) may not necessarily pass the component loading criteria. There are two such criteria to be considered. One is related to the capacitor. According to IEEE Std 18-2012 [94], a capacitor has loading limits on V_{rms}, V_{peak}, I_{rms} and kVAr. Another is related to the substation transformer. The transformer shall not be overloaded because of its filtering function. The inductors are commonly custom made and their construction takes into account the maximum harmonic currents passing through them.

The flowchart of Figure 3.9 represents the proposed method to address the overloading issue. There are two main ideas contained in this chart. The first is that the capacitor criteria are met by using capacitors with higher voltage and kVAr ratings. This is a common industry practice and it significantly reduces the complexity of the filter design process. In addition, a limit on the value of capacitance (C_{Max}) is imposed to ensure that the value is reasonable and the capacitors are available in the market.

The second idea is an iterative process that ensures the transformer is not overloaded. For this purpose, the equivalent loading index developed in [87] is used to check transformer overloading. The index converts the harmonic currents passing through the transformer into an equivalent 60Hz current that produces that same heating effect. With this index, one can determine the loading level of a transformer with the harmonic effects included.

The transformer loading level can be controlled or adjusted through the compensation inductors L_1. Varying this component is functionally equivalent to changing the ZS and NZS tertiary reactance of the transformer. As a result, the combined ZS and NZS 60Hz and harmonic currents flowing through the transformer can be adjusted. Note that the 60Hz current is a main component affecting the transformer loading level. In the flowchart, inductor L_1 is adjusted by using iterative parameter α. It is gradually increased (i.e. the equivalent ZS and NZS reactance of the transformer is gradually increased) until they reach the maximum inductance (L_{Max}) which is set to ensure the inductor is practically feasible to be manufactured. This process essentially scans the various L_1 to find filter component parameters that will not cause transformer overload. Typical substation transformers have at least a 20% loading margin. So it is common that the filter component parameters can be found without going through the iterative process (L_1 =0). On the other hand, a heavily loaded transformer may not be able to take harmonic currents. In this case, the iterative process produces no solution. This means that the transformer is not a candidate for installing the tertiary winding filter.

3.4 Case Studies

In this section, simulation studies on a generic distribution system are first conducted to validate the proposed filter and its design procedure. Then the robustness of the filtering performance of the proposed filter is investigated by using the MCS method. Finally, the performance of the proposed filter when installed throughout a transmission system is further examined.

3.4.1 Validation Studies

This subsection conducts simulation studies on the test system #1, a generic distribution system supplying residential loads, which are evenly distributed along five feeders. Figure 3.10 depicts the network configuration of the test system #1, in which each section block consists of three secondary systems serving 10 residential houses. Table 3.2 gives the main parameters of the test system #1.

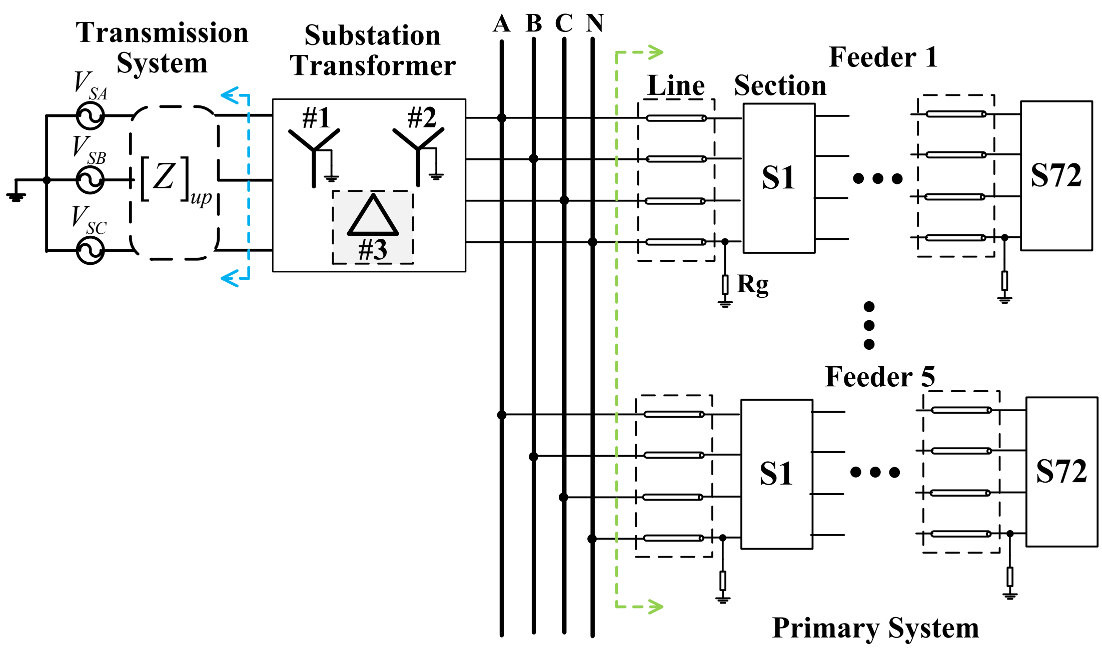

Figure 3.10: Network configuration of the test system #1

Table 3.2: Main Parameters of the Test System #1

System Parameters		Values	
Transmission System	Voltage level (LL-rms)	144 kV	
	Equivalent impedance	$Z_{+/-}$=10.18+j32.95 ohm	
		Z_0=2.42+j33.63 ohm	
Substation Transformer	Rated Capacity	20 MVA/20 MVA/10 MVA	
	Rated Voltage (LL-rms)	144 kV/25 kV/6.3 kV	
	Connection Type	Yg/Yg/Delta	
	Short Circuit Impedance	H-M	10.5%
		H-L	18%
		M-L	6.5%
	On-Load Loss	106.3 kW	
Main Trunk	Number of Feeders	5	
	Power Line Type	Overhead line	
	# of Sections per Feeder	72	
	Length of Each Section	0.12 km	
	Grounding Span	100 m	
	Grounding Resistance (R_g)	15 ohm	

A. Tertiary Winding Filter Design Results

The introduced iterative process (Figure 3.9) is employed to determine the final filter design. Table 3.3 presents the parameters and ratings of the designed tertiary winding filter component.

Table 3.3: Designed Tertiary Winding Filter

Delta Connected Part	L_1	Value (mH)	/
		Rating I_{rms} (A)	/
	C_1	Value (uF)	946.57
		Rating V_{rms} (kV)	0.69
	L_2	Value (mH)	0.34
		Rating I_{rms} (A)	432.83
	C_2	Value (uF)	567.94
		Rating V_{rms} (kV)	0.91
Star Connected Part	L_3	Value (mH)	0.43
		Rating I_{rms} (A)	392.24
	C_3	Value (uF)	193.71
		Rating V_{rms} (kV)	3.43
	L_4	Value (mH)	1.50
		Rating I_{rms} (A)	135.29
	C_4	Value (uF)	82.22
		Rating V_{rms} (kV)	3.68

B. Simulation Results

The network components (the substation transformer and overhead lines) are modeled as linear impedance. The secondary systems are modeled by the aggregate model developed in Chapter 2. They are all employed in a multiphase harmonic power flow program [14] to perform the simulation studies.

In order to establish a sound understanding of the proposed filter performance, the simulation results for both the case without the tertiary winding filter and the case with the tertiary winding filter are shown in Figure 3.11 to Figure 3.14.

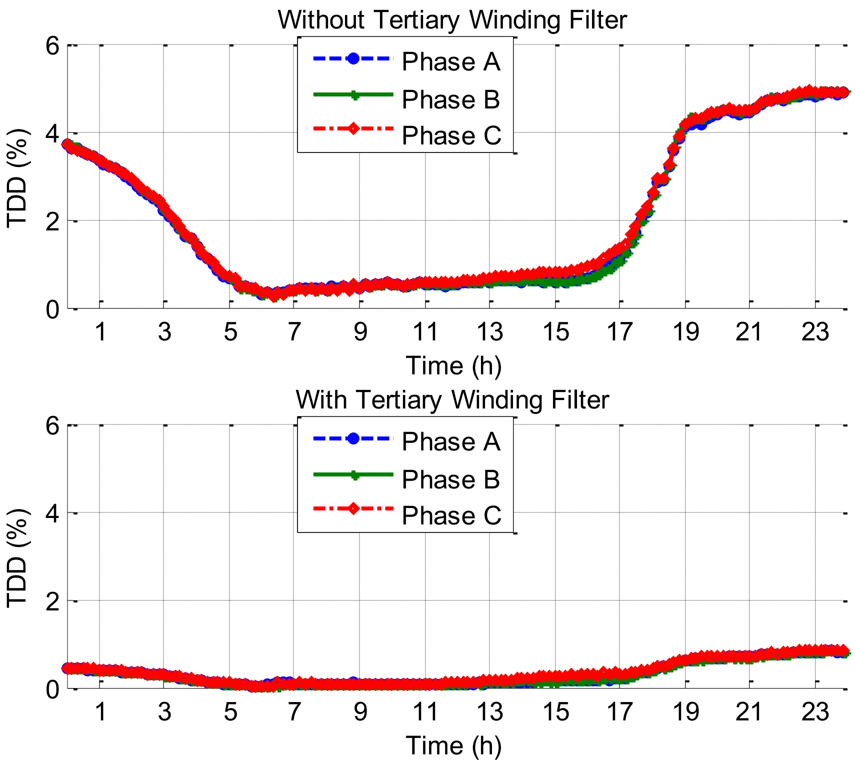

Figure 3.11: TDD variation of currents propagating into transmission system

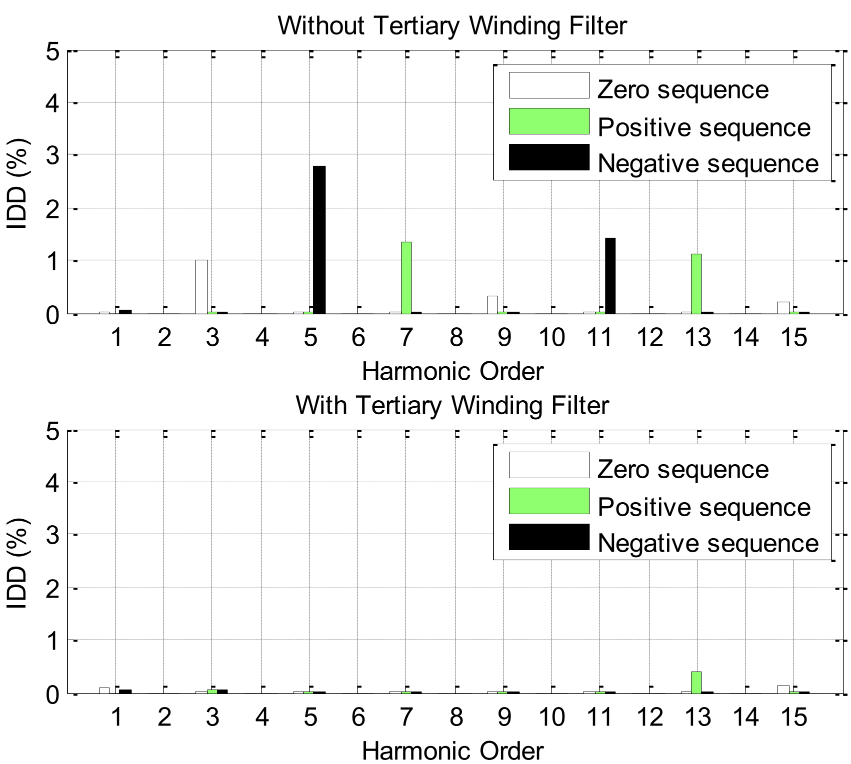

Figure 3.12: Typical IDD spectra of currents propagating into transmission system

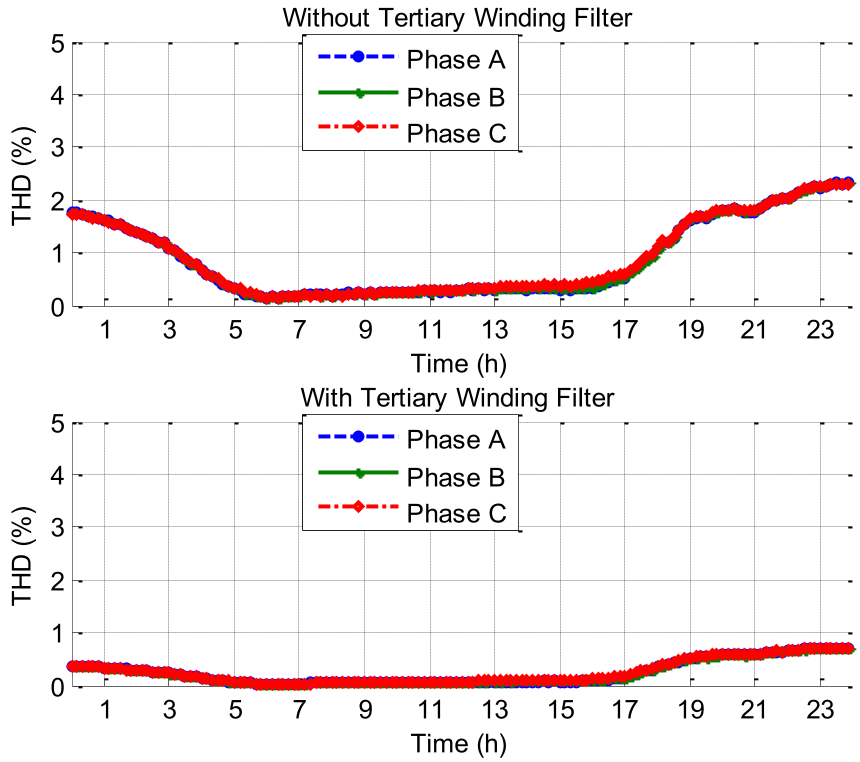

Figure 3.13: THD variation of voltages at primary side of substation transformer

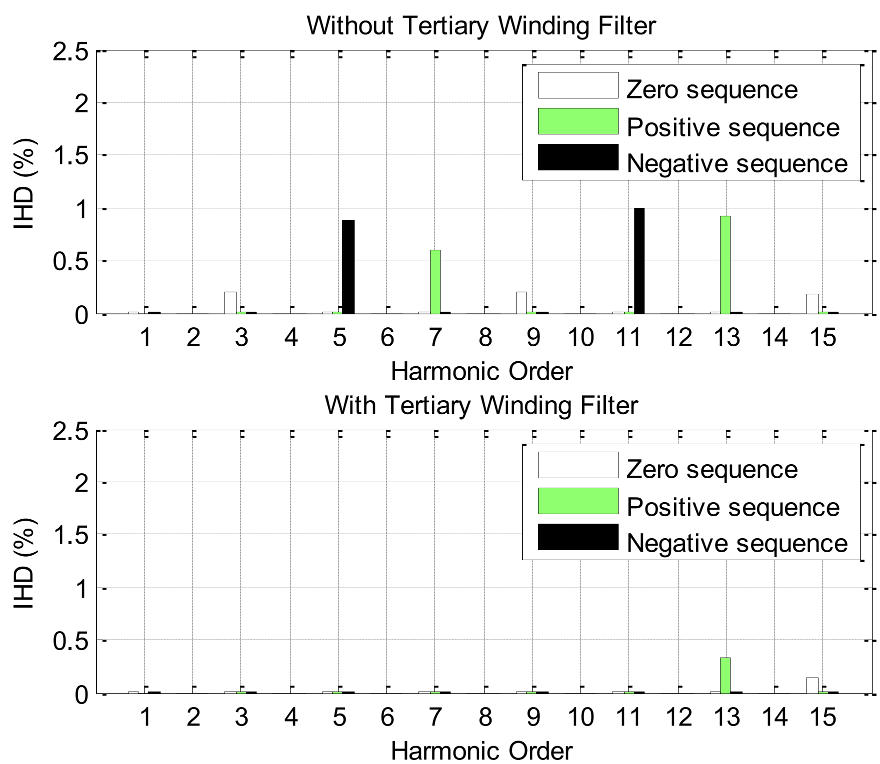

Figure 3.14: Typical IHD spectra of voltages at primary side of substation transformer

As can be seen from these four figures, both the harmonic currents propagating into the transmission system and the harmonic voltages at the primary side of the substation transformer have been greatly reduced when the tertiary winding filter is installed, which demonstrates the effectiveness of the tertiary winding filter.

3.4.2 Robustness Studies

As discussed in Subsection 3.3.1, the sharp tuned filter is not able to function when either the system frequency deviates from its rated value or the filter component parameters differ from their designed values. This subsection shows that the tertiary winding filter designed by the proposed method is not sharp tuned. It is done by investigating the filter's filtering performance with respect to the variations of the system frequency and component parameters (including the LC component parameters and the substation transformer parameters). Based on [95] and the data specification collected from manufactures, the ranges of the variations are as follows:

- Frequency: -1% to 1%;
- Capacitance: 0 to 10%;
- Inductance: -3% to 3%;
- Resistance: -10% to 10%.

For comparison, both the tertiary winding filter designed by the method proposed in this thesis, which minimizes the tuning sharpness at the tuned frequencies, and the tertiary winding filter designed by the method in [96], which does not consider the sharp tuned issue, are investigated. The method of investigation is as follows. The selected base case is the tertiary winding filter with the parameters shown in Table 3.2 and Table 3.3 and those obtained from [96]. The component parameters and the system frequency are then assumed to vary randomly around the design parameters in the above given range. A normal distribution is assumed for the variations. This will result in tens of thousands of possible combinations or scenarios of component parameters and the system frequency. The harmonic trapped ratio is then calculated for all the studied scenarios.

In this study, 100,000 combinations are calculated by using the MCS method. The results are shown as Figure 3.15 and Figure 3.16, which show that the filter designed by this thesis's new design method and the filter designed in [96] have comparable harmonic trapped ratio variation histograms for the 3rd, 9th, 5th and 11th harmonic. This indicates the filters designed by using these two methods have similar robustness at these harmonics.

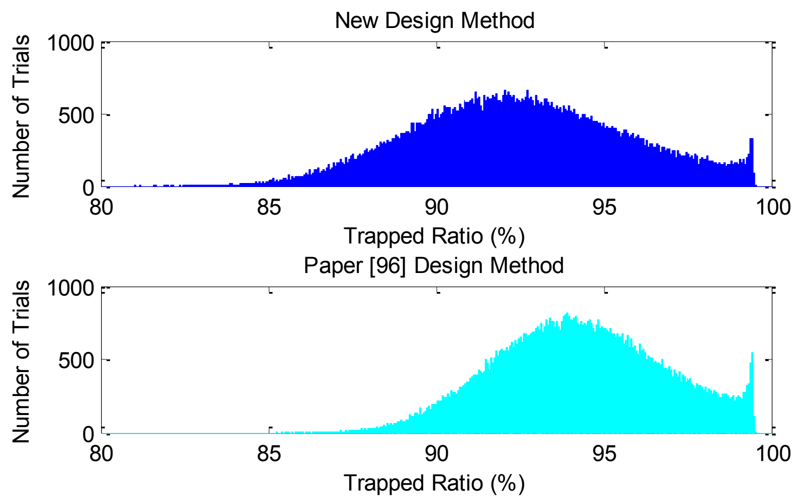

(a) 3rd harmonic

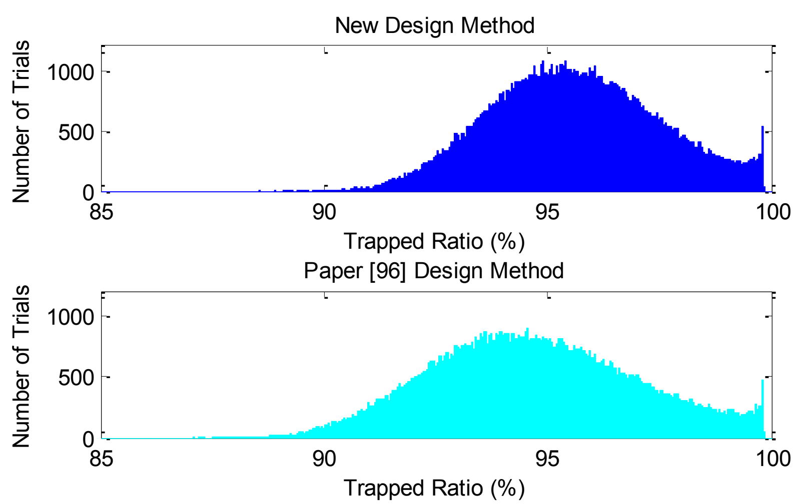

(b) 9th harmonic

Figure 3.15: ZS harmonic trapped ratio variation histogram

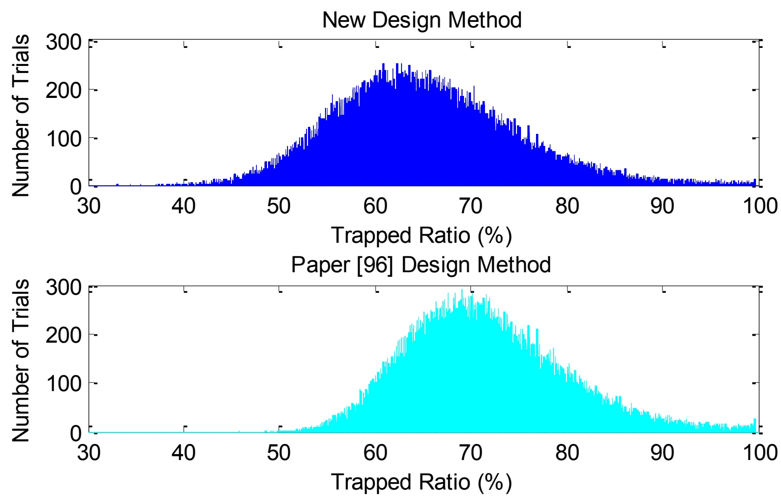

(a) 5th harmonic

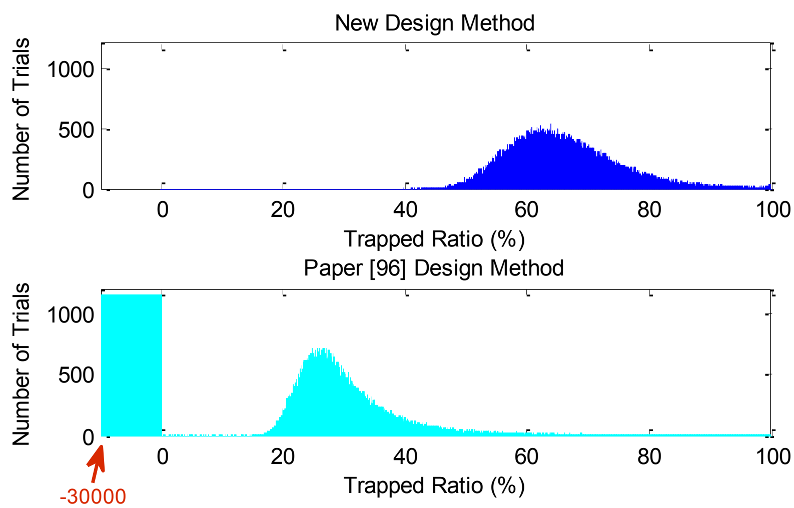

(b) 7th harmonic

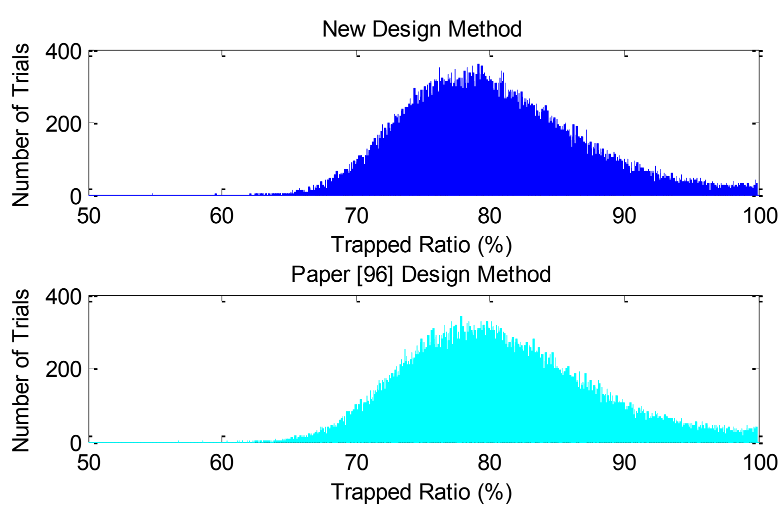

(c) 11th harmonic

Figure 3.16: NZS harmonic trapped ratio variation histogram

However, for the 7th harmonic, the harmonic trapped ratio of the filter designed by using the new design method varies around 40% to 100%, while the harmonic trapped ratio of the filter designed in [96] can have negative values for 1146 trials. The negative harmonic trapped ratio indicates that for these trials, the filter designed in [96] will not trap the 7th harmonic, but will cause 7th harmonic amplification because the filter is sharp tuned at the 7th harmonic, and the system frequency change and the LC parameter variation make the filter parallel resonant with the system impedance. The sharp tuning at the 7th harmonic is also confirmed by the calculated quality factor given in Table 3.4.

Therefore, the above studies show that, in terms of the harmonic trapped ratio variation with respect to the system frequency change and component parameter uncertainty, the tertiary winding filter designed by using the new design method in this thesis is more robust than the filter designed in [96].

Table 3.4: Quality Factor of Tertiary Winding Filter Designed by Different Methods

		Quality Factor	
		New Design Method	Paper [96] Design Method
ZS	3	315.99	236.99
	9	568.77	710.97
NZS	5	3322.63	2617.65
	7	5166.06	30694.28
	11	3973.09	3760.22

3.4.3 System Performance Studies

This subsection conducts several simulation studies on the test system #2 (see Figure 3.17) an extension of the IEEE 14 bus transmission system proposed in [97] aiming to further examine:

- Will the distribution harmonic loads at other bus lead to the tertiary winding filter overloading?

- Is it essential to equip all the buses with distribution harmonic loads with the tertiary winding filter?

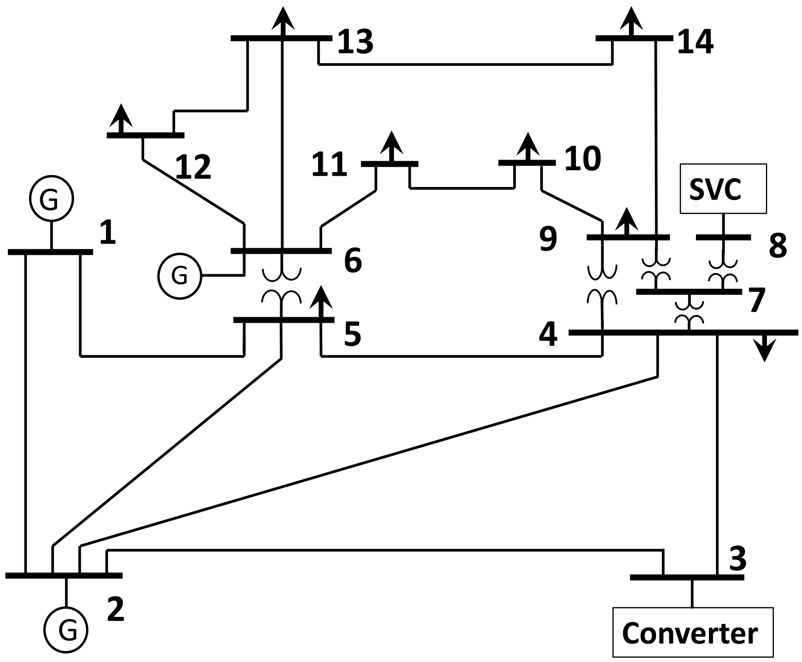

Figure 3.17: Network configuration of the test system #2

The major difference of the test system #2 from the IEEE 14 bus transmission system includes:

- All components in the system are modeled in phase domain.
- The loads at Bus 4, Bus 5, Bus 9, Bus 10, Bus 11, Bus 12, Bus 13 and Bus 14 are selected to be modified as distribution system loads as the test system #1. To reduce the complexity, the aggregate distribution system load model (see Figure 3.18) is adopted. It should be noted that the total fundamental frequency loads at Bus 4, Bus 5, Bus 9, Bus 10, Bus 11, Bus 12, Bus 13 and Bus 14 keep the same with that in the IEEE 14 bus transmission system, while their harmonic characteristic parameters which include the harmonic current spectrum of each phase and harmonic impedance matrix are derived from the test system #1 at peak load instant.

- To simplify the analysis, the harmonic currents injected by HVDC and SVC are neglected.

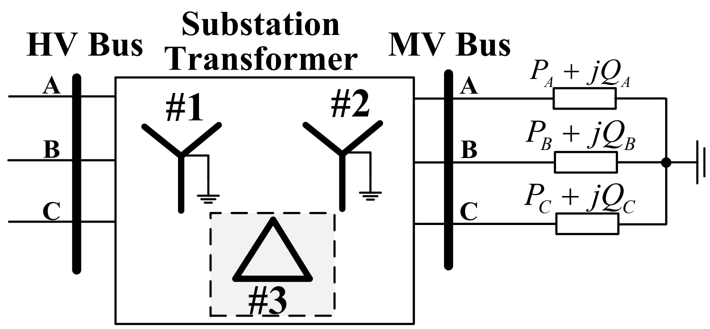

(a) Fundamental frequency model

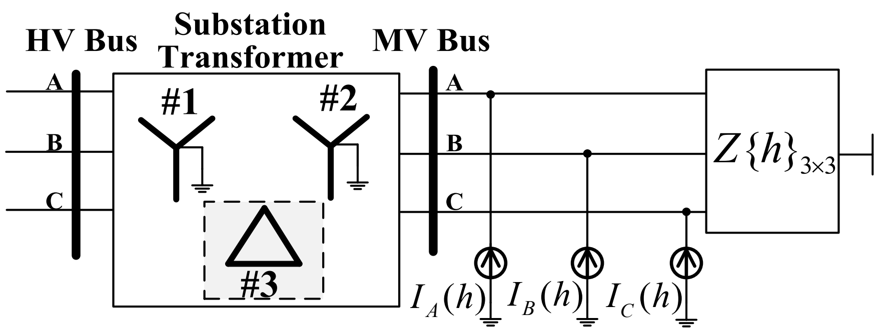

(b) Harmonic frequency model

Figure 3.18: Aggregate distribution system load model

A. Influence of Distribution Harmonic Loads at Other Buses

In the previous subsections, the tertiary winding filter was thoroughly examined in the distribution system. However in the tertiary winding filter design, loading assessment was conducted without considering the influence of distribution harmonic loads at other buses. Will this be an issue for the tertiary winding filter if there are multiple distribution harmonic loads at other buses in the transmission system? To answer this question, eight sets of cases are studied. Each set of cases consists of two cases:

i. There is no distribution harmonic loads at other buses except where the tertiary winding filter is installed;

ii. All the load buses (Bus 4, Bus 5, Bus 9, Bus 10, Bus 11, Bus 12, Bus 13, and Bus 14) are modified as distribution harmonic loads. The detailed description of these case sets and overloaded components for different cases are given in Table 3.5.

Table 3.5: Loading Assessment Result

Case Set	Case	Filter Placement	Distribution Harmonic Loads Location	Overloaded Components
1	i	Bus 4	Bus 4	None
	ii	Bus 4	All load buses	None
2	i	Bus 5	Bus 5	None
	ii	Bus 5	All load buses	None
3	i	Bus 9	Bus 9	None
	ii	Bus 9	All load buses	None
4	i	Bus 10	Bus 10	None
	ii	Bus 10	All load buses	C_4
5	i	Bus 11	Bus 11	None
	ii	Bus 11	All load buses	C_4
6	i	Bus 12	Bus 12	None
	ii	Bus 12	All load buses	C_4
7	i	Bus 13	Bus 13	None
	ii	Bus 13	All load buses	None
8	i	Bus 14	Bus 14	None
	ii	Bus 14	All load buses	None

Loading assessment for all eight case sets show that the distribution harmonic loads at other buses have influence on the loading level of the tertiary winding filter. The influence is different for the tertiary winding filter at different locations. According to Table 3.5, indicated by Case Set 4, 5 and 6, the tertiary winding filter designed based on the distribution harmonic load information at its own bus will be overloaded by distribution harmonic loads at other buses. Thus if multiple distribution harmonic loads exist, the transmission system harmonic power flow should be incorporated into the filter loading assessment and components of larger sizes should be adopted when overloading issues are identified.

B. Installation Density Study

This subsection presents the sensitivity study to assess the influence of the installation density of the tertiary winding filter on the overall transmission system harmonic distortion level. Simulation results for the following case sets are compared in Figure 3.19.

i. The test system # 2 with the loads at bus 4, bus 5, bus 9, bus 10, bus 11, bus 12, bus 13 and bus 14 all modified as distribution harmonic loads.

ii~ix, based on i, install one tertiary winding filter at any one, any two,…, all of the buses with distribution harmonic loads.

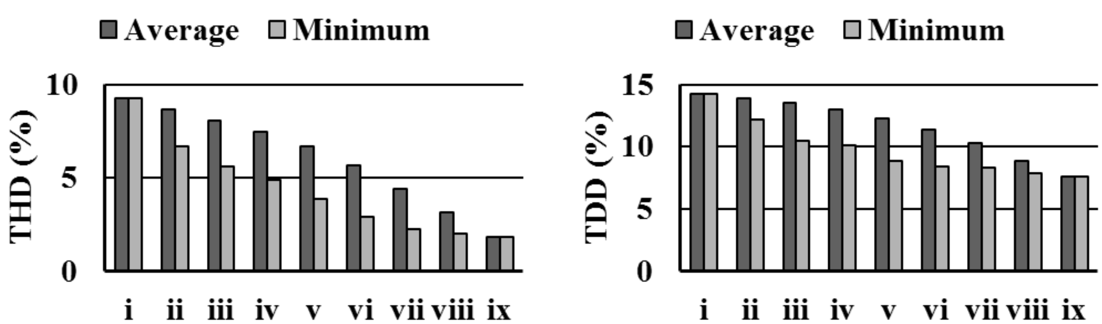

Figure 3.19: Average minimum harmonic distortion level for different case sets

In Figure 3.19, the average voltage THD is the voltage THD average over all buses in each case for each case set and the average current TDD is the current TDD average over all transmission lines and transmission transformers in each case for each case set, while the minimum voltage THD is the minimum voltage THD average over all buses for each case set and the minimum current TDD is the minimum current TDD average over all transmission lines and transmission transformers for each case set. As shown in Figure 3.19, the more the tertiary winding filter installed the lower the overall transmission system harmonic distortion level is in terms of both the bus voltage THD and transmission equipment TDD.

Table 3.6 further gives the filter placement which results the minimum harmonic distortion level for Case Set ii ~ viii and the corresponding overall system voltage distortion level and current distortion level with such placement.

Table 3.6: Optimum Filter Placement for Different Case Sets

Case Set	Optimum Filter Placement	Overall System Harmonic Distortion	
		Voltage THD* (%)	Current TDD* (%)
ii	Bus 9	6.70 (8.63)	12.14 (13.92)
iii	Bus 9, Bus 14	5.61 (8.07)	10.49 (13.50)
iv	Bus 9, Bus 10, Bus 14	4.92 (7.48)	10.09 (12.98)
v	Bus 9, Bus 10, Bus 14, Bus 4	3.86 (6.70)	8.83 (12.30)
vi	Bus 9, Bus 10, Bus 14, Bus 4, Bus 5	2.93 (5.65)	8.37 (11.39)
vii	Bus 9, Bus 10, Bus 14, Bus 4, Bus 5, Bus 13	2.25 (4.41)	8.31 (10.26)
viii	Bus 9, Bus 10, Bus 14, Bus 4, Bus 5, Bus13, Bus 12	2.01 (3.15)	7.87 (8.88)

*Figure in the bracket is the average value for each case set.

As indicated by Figure 3.19 and Table 3.6, with the optimum filter placement, better harmonic mitigation effects can be achieved. Another useful information could be extracted from Table 3.6 is that the distribution harmonic load at Bus 9 has the largest impacts on the overall system distortion level, since for all the optimum filter placement one tertiary winding filter should be placed at Bus 9.

3.5 Application Considerations

Most substation transformers are custom made and have tertiary windings. It is relatively easy to make the six terminals of the tertiary windings available for the proposed application. Therefore, utility companies could order such a transformer for new substations. The tertiary winding filter can then be implemented by connecting corresponding LC components. The same applies to the existing substations where six terminals of the tertiary windings are accessible.

For existing substations where only three terminals of the tertiary windings are accessible, the delta connection cannot be achieved. As a result, ZS filtering is not doable. But the NZS filtering can still be achieved by connecting shunt LC filters to the tertiary windings. This configuration is similar to what is proposed in [98]. Since the tertiary winding has lower rated voltages than the secondary winding, this scheme still costs less than the traditional MV passive filter connected to the secondary bus.

3.6 Summary

This chapter presented a novel and effective scheme to prevent harmonic currents from propagating into the transmission systems. The basic idea is to utilize the low-voltage tertiary winding of a substation transformer to create a tuned low impedance path for the harmonics. A new filter topology was proposed for the purpose of trapping five harmonics. The design issues of the proposed filters were investigated and solved. The main findings and contributions of this chapter can be summarized as follows.

- The proposed tertiary winding filter is a novel scheme to create a low-cost filter through utilizing the low-voltage tertiary winding of a substation transformer. The scheme further consists of a new filter topology that can trap two ZS harmonics and three NZS harmonics simultaneously.
- The filter and its design method were tested through extensive case studies. The results demonstrated the effectiveness of the filter and the robustness of the proposed design method. In addition, system performance studies also revealed

that proper placement could achieve the same reduction of the overall system harmonic distortion level by using fewer filters.

- Compared to other applicable schemes, the main benefit of the proposed tertiary winding filter is its utilization of the low-voltage tertiary winding of an existing substation transformer to construct a low impedance path with low-voltage LC components, which can lead to a significant cost reduction.

Chapter 4

Design Method for 3rd Order High Pass Filter

The 3rdHP filter is widely used in industry and is a good candidate for mitigating harmonic distortions caused by mass-distributed harmonic sources. However, a technically sound design method has not been well established for this filter. In response to this situation, a complete design method along with simple design formulas for the 3rdHP filter is proposed in this chapter.

This chapter is organized as follows. First, a review of the 3rdHP filter is given in Section 4.1. Next, the two accepted design equations are described in Section 4.2. Then Section 4.3 presents the loss minimization based design condition. The design condition based on the harmonic reduction ratio is established in Section 4.4. Section 4.5 provides a case study to validate the proposed design method, while Section 4.6 summarizes this chapter.

4.1 Review on 3rd Order High Pass Filter

The 3rdHP filter was first applied into the France-England cross channel HVDC link 1 project [32]. From then on, it has been widely used for high order harmonics' filtering in both HVDC links and industrial systems [1, 31-33]. The filter is shown in Figure 4.1 along with its frequency response. For low order harmonics that is less than the tuned frequency, the filter's L branch dominates so it behaves as a single-tuned filter. For high order harmonics, the C_2+R branch dominates so it behaves as a first order high pass filter. The purpose of C_2 is to reduce the filter loss at the fundamental frequency [1, 33].

Although the topology and the basic characteristics of 3rdHP are introduced in several periodicals [28, 99] and other concerned publications [1, 31], but a technically sound design method for the 3rdHP filter has not been established. For example, several literatures use the condition of $C_2 = C_1$ for the filter design and yet no justification has been given [1, 31, 33]. Reference [32] showed filter component parameters of $C_2 \neq C_1$ without explaining how C_2 was determined. Moreover, the filter consists of four elements. Four design conditions or equations are therefore needed to determine their parameters. So far, only two conditions (the reactive power output requirement and the tuned frequency requirement) are generally agreed upon by designers and users. These two conditions are not sufficient to determine all four parameters.

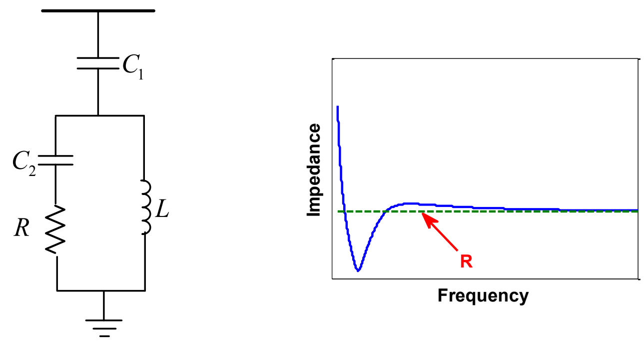

Figure 4.1: 3rdHP filter configuration and its frequency response

4.2 Accepted Design Equations

As explained earlier, the 3rdHP filter has four components. Therefore, four equations (or conditions) are required to determine four component parameters (C_1, C_2, L and R). Two conditions are well understood and accepted by industry and research community:

- Condition 1: The reactive power output of the filter shall be equal to the required amount Q_F. This condition yields the following design equation:

$$C_1 = \frac{Q_F}{\omega_1 V^2}, \tag{4.1}$$

  where ω_1 is the power frequency and V is the rated voltage.

- Condition 2: The filter is tuned to frequency ω_H. This means that L is resonant with C_1, which leads to:

$$L = \frac{1}{\omega_H^2 C_1}. \tag{4.2}$$

  Equation (4.2) establishes the 2nd design equation.

4.3 Design Condition Based on Loss Minimization

The objective of C_2 is to reduce the filter loss at the fundamental frequency. It is, therefore, logical to use loss minimization to establish the 3rd design equation.

According to Figure 4.1, the filter impedance is given by

$$Z_F(\omega) = \frac{1}{j\omega C_1} + \left(\frac{1}{j\omega C_2} + R \right) // j\omega L \,, \tag{4.3}$$

where ω is the angular frequency.

Accordingly, the reactive component $X_F(\omega)$ and resistive component $R_F(\omega)$ of the filter impedance can be derived as

$$\begin{cases} X_F(\omega) = \mathrm{Im}(Z_F(\omega)) = \dfrac{a\omega^4 + b\omega^2 - 1}{\left(\omega^2 (RC_2)^2 + (\omega^2 LC_2 - 1)^2\right)\omega C_1} \\ R_F(\omega) = \mathrm{Re}(Z_F(\omega)) = \dfrac{RL^2 C_2{}^2 \omega^4}{\omega^2 (RC_2)^2 + (\omega^2 LC_2 - 1)^2} \end{cases}, \tag{4.4}$$

where

$$\begin{cases} a = R^2 LC_2{}^2 C_1 - L^2 C_2 C_1 - L^2 C_2^2 \\ b = LC_1 - R^2 C_2^2 + 2LC_2 \end{cases}. \tag{4.5}$$

The fundamental frequency loss of the filter is as follows

$$P_{Floss} = \mathrm{Re}\left(\frac{V^2}{Z_F(\omega_1)} \right) = \frac{V^2 R_F(\omega_1)}{R_F^2(\omega_1) + X_F^2(\omega_1)} \,, \tag{4.6}$$

where ω_1 is the fundamental angular frequency.

Take equation (4.4) into equation (4.6), and rearrange both the numerator and the denominator in the descending powers with respect to ω_1. The fundamental frequency loss of the filter can be further represented by

$$P_{Floss} = \frac{V^2 A\omega_1^6}{AR\omega_1^6 + B\omega_1^4 + C\omega_1^2 + 1}, \tag{4.7}$$

where

$$\begin{cases} A = C_1^2 C_2^2 L^2 R \\ B = C_1^2 L^2 - 2C_1 C_2^2 L R^2 + 2C_1 C_2 L^2 + C_2^2 L^2 \\ C = C_2^2 R^2 - 2LC_2 - 2LC_1 \end{cases}. \tag{4.8}$$

Since C_1 and L can be found by using equation (4.1) and equation (4.2), only C_2 and R are to be determined. The problem can be formulated as finding an optimal solution for both R and C_2:

$$\begin{aligned} &\min P_{Floss} = f(R, C_2) \\ &s.t. \begin{cases} g_1(R, C_2) = C_2 - C_1 \le 0 \\ g_2(R, C_2) = \dfrac{C_1 L}{R^2 C_1 - L} - C_2 \le 0 \\ g_3(R, C_2) = L - R^2 C_1 < 0 \end{cases} \end{aligned}. \tag{4.9}$$

The constraints g_1, g_2 and g_3 of the above formulation are established based on the requirement that the filter impedance must be inductive for frequencies higher than the tuned frequency. The following subsections first give the details of these constraints and then present the solution of the optimization problem.

4.3.1 Inductive Impedance Constraint

Resonance only happens when the system is inductive and the filter is capacitive or when the system is capacitive and the filter is inductive. The system impedance is more likely to be inductive over a wide frequency range. This is especially true for the industrial system, where the system impedance is dominated by the service transformer short circuit impedance. Therefore, if the filter is all inductive after the tuned harmonic order, the likelihood of the filter to be resonant with system is then greatly reduced. This reasoning has led us to propose the following design constraint: the filter's impedance should be all inductive above the tuned frequency, that is,

$$X_F(\omega) \geq 0, \quad \omega \geq \omega_H \ . \tag{4.10}$$

Moreover, since at fundamental frequency the filter provides reactive power compensation, the impedance of the filter at the fundamental frequency is capacitive, which means

$$X_F(\omega_1) < 0 . \tag{4.11}$$

Let $x = \omega^2$. Then the numerator polynomial of $X_F(\omega)$ (as shown in equation (4.4)) can be represented by $ax^2 + bx - 1$. According to inequalities (4.10) and (4.11), as well as that the denominator of $X_F(\omega)$ is always positive, the numerator polynomial of $X_F(\omega)$ only has one positive root that is no larger than ω_H. Accordingly, $ax^2 + bx - 1 = 0$ only has one positive root that is no larger than ω_H^2. By Vieta's formulas, we have $x_1 x_2 = -1/a < 0$ or $a = 0$ which leads to

$$R^2 L C_2{}^2 C_1 - L^2 C_2 C_1 - L^2 C_2^2 \geq 0 , \tag{4.12}$$

By inequality (4.10), we have

$$X_F(\omega_H) \geq 0 . \tag{4.13}$$

Taking equation (4.2) into inequality (4.13), the following inequality can be obtained:

$$0 < C_2 \leq C_1 . \tag{4.14}$$

By inequality (4.12) and inequality (4.14), we have

$$0 < \frac{C_1 L}{R^2 C_1 - L} \leq C_2 \leq C_1 , \tag{4.15}$$

which can be also represented in the form of constraints g_1, g_2 and g_3.

4.3.2 Analytical Solution to the Optimization Problem

The optimization problem (shown as formulation (4.9)) can be solved by using the KKT optimality conditions as follows.

Let $\left(R^*, C_2^*\right)$ be the optimal point of the above optimization problem. Then according to the KKT optimality conditions [100], we have

$$\nabla f(R^*, C_2^*) + \mu_1 \nabla g_1(R^*, C_2^*) + \mu_2 \nabla g_2(R^*, C_2^*) + \mu_3 \nabla g_3(R^*, C_2^*) = 0\,, \tag{4.16}$$

$$g_1(R^*, C_2^*) \le 0\,, \tag{4.17}$$

$$\mu_1 \ge 0\,, \tag{4.18}$$

$$\mu_1 g_1(R^*, C_2^*) = 0\,, \tag{4.19}$$

$$g_2(R^*, C_2^*) \le 0\,, \tag{4.20}$$

$$\mu_2 \ge 0\,, \tag{4.21}$$

$$\mu_2 g_2(R^*, C_2^*) = 0\,, \tag{4.22}$$

$$g_3(R^*, C_2^*) < 0\,, \tag{4.23}$$

$$\mu_3 \ge 0\,, \tag{4.24}$$

$$\mu_3 g_3(R^*, C_2^*) = 0\,. \tag{4.25}$$

The partial derivative of $f(R, C_2)$ with respect to C_2 is given by

$$\frac{\partial f(R, C_2)}{\partial C_2} = \frac{2C_1^2 C_2 L^2 R \omega_1^6 \left(C_1 L \omega_1^2 - 1\right)\left(C_1 L \omega_1^2 + C_2 L \omega_1^2 - 1\right)}{\left(A\omega_1^6 + B\omega_1^4 + C\omega_1^2 + 1\right)^2}\,. \tag{4.26}$$

$n_H \ge 2$, according to equation (4.2),

$$C_1 L\omega_1^2 - 1 = \frac{1}{n_H^2} - 1 < 0 \,. \tag{4.27}$$

According to equation (4.2) and inequality (4.15),

$$C_1 L\omega_1^2 + C_2 L\omega_1^2 - 1 \le 2C_1 L\omega_1^2 - 1 = \frac{2}{n_H^2} - 1 < 0 \,. \tag{4.28}$$

By inequality (4.27) and inequality (4.28),

$$\frac{\partial f(R, C_2)}{\partial C_2} > 0 \,. \tag{4.29}$$

The partial derivative of $g_1(R, C_2)$ with respect to C_2 is

$$\frac{\partial g_1(R, C_2)}{\partial C_2} = 1 \,. \tag{4.30}$$

The partial derivative of $g_2(R, C_2)$ with respect to C_2 is

$$\frac{\partial g_2(R, C_2)}{\partial C_2} = -1 \,. \tag{4.31}$$

The partial derivative of $g_3(R, C_2)$ with respect to C_2 is

$$\frac{\partial g_3(R, C_2)}{\partial C_2} = 0 \,. \tag{4.32}$$

According to inequality (4.23), inequality (4.24) and equation (4.25), $\mu_3 = 0$.

Further, according to inequality (4.20), inequality (4.21), and equation (4.22), either $\mu_2 = 0$ or $g_2(R^*, C_2^*) = 0$.

However, when $\mu_2 = 0$, according to equation (4.16)

$$\left.\frac{\partial f(R,C_2)}{\partial C_2}\right|_{(R^*,C_2^*)} + \mu_1 \left.\frac{\partial g_1(R,C_2)}{\partial C_2}\right|_{(R^*,C_2^*)} = 0$$
$$\Rightarrow \left.\frac{\partial f(R,C_2)}{\partial C_2}\right|_{(R^*,C_2^*)} + \mu_1 = 0 \quad , \tag{4.33}$$

which means

$$\mu_1 = -\left.\frac{\partial f(R,C_2)}{\partial C_2}\right|_{(R^*,C_2^*)} < 0 . \tag{4.34}$$

This is in contradiction with the KKT condition dual feasibility (4.18). Hence $\mu_2 \neq 0$.

Similar investigation for $g_2(R^*, C_2^*) = 0$ does not indicate any contradiction or inconsistency in KKT conditions (4.16) to (4.25). Therefore, the equation defines the relationship between C_2 and R to achieve the minimum fundamental frequency loss is obtained as:

$$g_2(R,C_2) = 0 \Rightarrow C_2 = \frac{C_1 L}{R^2 C_1 - L} . \tag{4.35}$$

4.4 Design Condition Based on Harmonic Reduction

To finalize the 3rdHP filter components' parameters, one more design equation is needed. Here, the common scenarios for harmonic filter application are first introduced. Based on the analysis, the harmonic reduction ratio is then chosen to establish a generic design equation. Thereafter, an explicit fourth design equation for the case where the system impedance can be approximated as a linear reactance is derived.

Harmonic filters are most commonly used either to reduce the harmonic voltage at the installation bus (Figure 4.2 (a)) or to reduce the harmonic current flowing through a branch connected to the installation bus (Figure 4.2 (b)). These scenarios can be illustrated by the Thevenin's equivalent circuit (as shown in Figure 4.3) and Norton's equivalent circuit (as shown in Figure 4.4), respectively. In Figure 4.3, $V_{\mathrm{Th}}(h)$ is the open circuit harmonic voltage at bus i; $Z_{\mathrm{Th}}(h)$ is the self harmonic impedance at bus i; and $Z_F(h)$ is the harmonic impedance of the installed filter. In Figure 4.4, $z_{ii}(h)$ and $z_{jj}(h)$ are the self harmonic impedance at bus i and bus j when branch ij is disconnected, and $I_{ii}(h)$ is the equivalent harmonic source current seen from bus i.

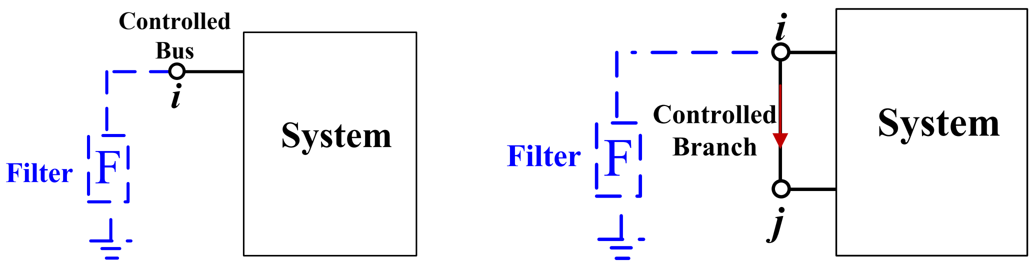

(a) Harmonic voltage reduction (b) Harmonic current reduction

Figure 4.2: Common scenarios for the harmonic filter application

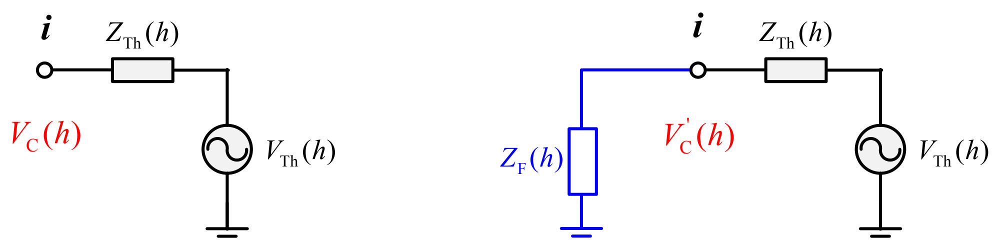

(a) Before the installation of the filter (b) After the installation of the filter

Figure 4.3: Equivalent circuits for the harmonic voltage reduction scenario

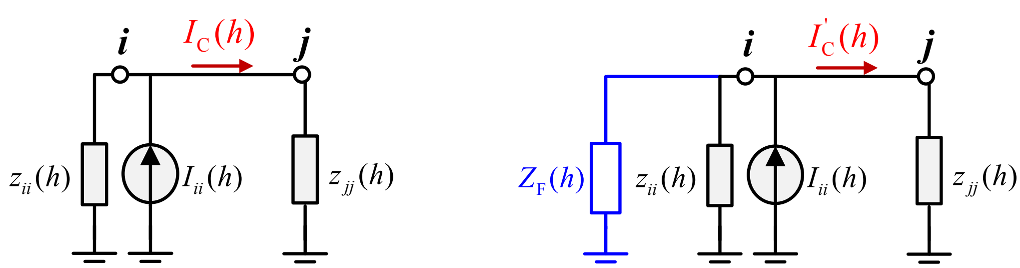

(a) Before the installation of the filter (b) After the installation of the filter

Figure 4.4: Equivalent circuits for the harmonic current reduction scenario

According to Figure 4.3, the harmonic voltages at the controlled bus i, before and after the installation of the filter, are given by

$$\begin{cases} V_{\mathrm{C}}(h) = V_{\mathrm{Th}}(h) \\ V_{\mathrm{C}}^{'}(h) = \dfrac{Z_{\mathrm{F}}(h)}{Z_{\mathrm{Th}}(h) + Z_{\mathrm{F}}(h)} V_{\mathrm{Th}}(h) \end{cases}. \tag{4.36}$$

Therefore, the harmonic voltage reduction ratio of the filter for the harmonic voltage reduction scenario is

$$a_{\mathrm{V}}(h) = 1 - \left| \frac{V_{\mathrm{C}}^{'}(h)}{V_{\mathrm{C}}(h)} \right| = 1 - \left| \frac{Z_{\mathrm{F}}(h)}{Z_{\mathrm{Th}}(h) + Z_{\mathrm{F}}(h)} \right|. \tag{4.37}$$

According to Figure 4.4, the harmonic currents on the controlled branch *ij* before and after the installation of the filter, are given by

$$\begin{cases} I_{\mathrm{C}}(h) = \dfrac{z_{ii}(h)}{z_{ii}(h) + z_{jj}(h)} I_{ii}(h) \\ I_{\mathrm{C}}^{'}(h) = \dfrac{z_{ii}(h) / / Z_{\mathrm{F}}(h)}{z_{ii}(h) / / Z_{\mathrm{F}}(h) + z_{jj}(h)} I_{ii}(h) \end{cases}. \tag{4.38}$$

Therefore, the harmonic current reduction ratio of the filter for the harmonic current reduction scenario is

$$\begin{aligned} a_{\mathrm{I}}(h) &= 1 - \left| \frac{I_{\mathrm{C}}^{'}(h)}{I_{\mathrm{C}}(h)} \right| = 1 - \left| \left(\frac{z_{ii}(h) / / Z_{\mathrm{F}}(h)}{z_{ii}(h) / / Z_{\mathrm{F}}(h) + z_{jj}(h)} \right) / \left(\frac{z_{ii}(h)}{z_{ii}(h) + z_{jj}(h)} \right) \right| \\ &= 1 - \left| \frac{Z_{\mathrm{F}}(h)}{z_{ii}(h) / / z_{jj}(h) + Z_{\mathrm{F}}(h)} \right| \end{aligned}. \tag{4.39}$$

By comparing equation (4.37) and equation (4.39), we can see both the harmonic voltage reduction ratio and the harmonic current reduction ratio have a similar form and are also unrelated to the harmonic source. Such good features are utilized to establish a generic design condition for both the harmonic voltage reduction scenario and the harmonic current reduction scenario.

The goal of the generic design condition is, therefore, chosen to reduce the harmonic voltage or the harmonic current at the tuned harmonic order (i.e., $V_{\mathrm{C}}^{'}(n_H)$ or $I_{\mathrm{C}}^{'}(n_H)$) by

$a\%$ in comparison with that before the filter is installed (i.e., $V_{\mathrm{C}}(n_H)$ or $I_{\mathrm{C}}(n_H)$). This choice results in the 4th design equation:

$$a_{\mathrm{V}}(h) = a\% \text{ or } a_{\mathrm{I}}(h) = a\% . \tag{4.40}$$

The above design equation can be solved analytically for the case where the system impedance can be approximated as a reactance in the form of $Z_{\mathrm{Th}}(\omega_H) = jn_H X_S$ for the harmonic voltage reduction scenario or $z_{ii}(h)//z_{jj}(h) = jn_H X_S$ for the harmonic current reduction scenario, where X_{S} is the short-circuit reactance of the system, and $n_H = \omega_H / \omega_1$. This condition can be met for many industrial facilities which are supplied by a service transformer. The reactance of the service transformer dominates the system's impedance. For such systems, the resulting design equation is

$$R = \sqrt{\frac{3}{2}R_0^2 - \frac{R_0^3}{n_H X_s} + \frac{R_0^2\sqrt{4R_0^2 + \left(4n_H X_S R_0 - 7n_H^2 X_S^2\right)\left(1-a\%\right)^2}}{2n_H X_s\left(1-a\%\right)}} , \tag{4.41}$$

where $R_0 = \sqrt{L/C_1}$.

The derivation of equation (4.41) is as follows.

Substitute equation (4.37) with $Z_{\mathrm{Th}}(\omega_H) = jn_H X_S$ or equation (4.39) with $z_{ii}(h)//z_{jj}(h) = jn_H X_S$ into equation (4.40) and rearrange; then the following equation can be obtained:

$$a\% = \left(1 - \sqrt{\frac{R_F^2(\omega_H) + X_F^2(\omega_H)}{R_F^2(\omega_H) + \left(X_F(\omega_H) + n_H X_s\right)^2}}\right) \times 100\% . \tag{4.42}$$

Substitute equation (4.2) and equation (4.35) into equation (4.4). Then we can obtain

$$\begin{cases} R_F(\omega_H) = \dfrac{RL^2}{C_1^2 R^4 - 3C_1 R^2 L + 4L^2} \\ X_F(\omega_H) = -\dfrac{L^{\frac{3}{2}}\left(2L - C_1 R^2\right)}{\sqrt{C_1}\left(C_1^2 R^4 - 3C_1 R^2 L + 4L^2\right)} \end{cases}. \tag{4.43}$$

Substitute equation (4.43) into equation (4.42), then the following equation can be obtained:

$$\alpha R^4 + \beta R^2 + \gamma = 0, \tag{4.44}$$

where

$$\begin{cases} \alpha = n_H^2 X_S^2 C_1^3 \left(1 - a\%\right)^2 \\ \beta = \left(-3n_H^2 X_S^2 C_1^2 L + 2n_H X_s C_1^{\frac{3}{2}} L^{\frac{3}{2}}\right)\left(1 - a\%\right)^2 \\ \gamma = \left(L^3 + 4n_H^2 X_S^2 C_1 L^2 - 4n_H X_s C_1^{\frac{1}{2}} L^{\frac{5}{2}}\right)\left(1 - a\%\right)^2 - L^3 \end{cases}. \tag{4.45}$$

Rearrange γ as follows:

$$\begin{aligned} \gamma &= L^3\left[\left(1 - a\%\right)^2 - 1\right] + 4n_H X_s C_1^{\frac{1}{2}} L^{\frac{5}{2}}\left(\frac{n_H X_S}{\sqrt{L / C_1}} - 1\right) \\ &= L^3\left[\left(1 - a\%\right)^2 - 1\right] + 4n_H X_s C_1^{\frac{1}{2}} L^{\frac{5}{2}}\left(\frac{n_H^2 X_S}{X_{C_1}} - 1\right) \\ &= L^3\left[\left(1 - a\%\right)^2 - 1\right] + 4n_H X_s C_1^{\frac{1}{2}} L^{\frac{5}{2}}\left(\frac{n_H^2}{n_S^2} - 1\right) \end{aligned}, \tag{4.46}$$

where $n_S = \sqrt{X_{C_1} / X_S}$ is the resonant harmonic order of the capacitor bank with the system, which is larger than n_H.

Therefore, $n_H^2 / n_S^2 - 1 < 0$. Moreover, $\left(1 - a\%\right)^2 - 1 < 0$. Hence,

$$\gamma = L^3\left[\left(1-a\%\right)^2 - 1\right] + 4n_H X_s C_1^{\frac{1}{2}} L^{\frac{5}{2}}\left(\frac{n_H^2}{n_S^2} - 1\right) < 0\,. \tag{4.47}$$

In addition,

$$\Delta = \beta^2 - 4\alpha\gamma > \beta^2 > 0\,. \tag{4.48}$$

Further, according to the Vieta's formulas, since

$$\frac{\gamma}{\alpha} < 0\,, \tag{4.49}$$

equation (4.44) with respect to $x = R^2$ has and only has one positive root. According to the physical meaning, this positive root is the desired one. Accordingly, the root of equation (4.44) is given by

$$x_1 = \frac{-\beta + \sqrt{\beta^2 - 4\alpha\gamma}}{2\alpha}, x_2 = \frac{-\beta - \sqrt{\beta^2 - 4\alpha\gamma}}{2\alpha}\,. \tag{4.50}$$

According to equation (4.48),

$$\begin{cases} -\beta + \sqrt{\beta^2 - 4\alpha\gamma} > -\beta + |\beta| \geq 0 \\ -\beta - \sqrt{\beta^2 - 4\alpha\gamma} < -\beta - |\beta| \leq 0 \end{cases}. \tag{4.51}$$

Therefore, $x_1 > 0, x_2 < 0$. Hence, $R = \sqrt{x_1}$, and replace $\sqrt{L / C_1}$ by R_0, Equation (4.41) is obtained.

4.5 Case Studies

The proposed design method can be summarized as follows: determine C_1 by using equation (4.1), L by using equation (4.2), R by using equation (4.40) or equation (4.41), and finally C_2 by using equation (4.35). It can be seen that the design procedure is very simple.

The 3rdHP filter designed by the proposed method has been compared with that designed by using the condition of $C_2 = C_1$ and with the actual filter installation documented in [32] for a HVDC link (Corisca tapping substation).

The same design input data as follows are used for the comparison.

- System rated voltage: V = 90 kV;
- System short circuit level at the filter installation location: 360 MVA (The system short circuit impedance is pure inductive);
- System voltage distortion: contains 1.5% background voltage harmonics for the 3rd to 13rd harmonics;
- Required reactive power support: Q_F = 10 MVAr;
- Harmonic reduction ratio for 7th harmonic: $a\%$ = 53.5%.

The results are shown in Figure 4.5 and Table 4.1. It can be seen that the proposed design method results in a 3rdHP filter with much less fundamental frequency loss.

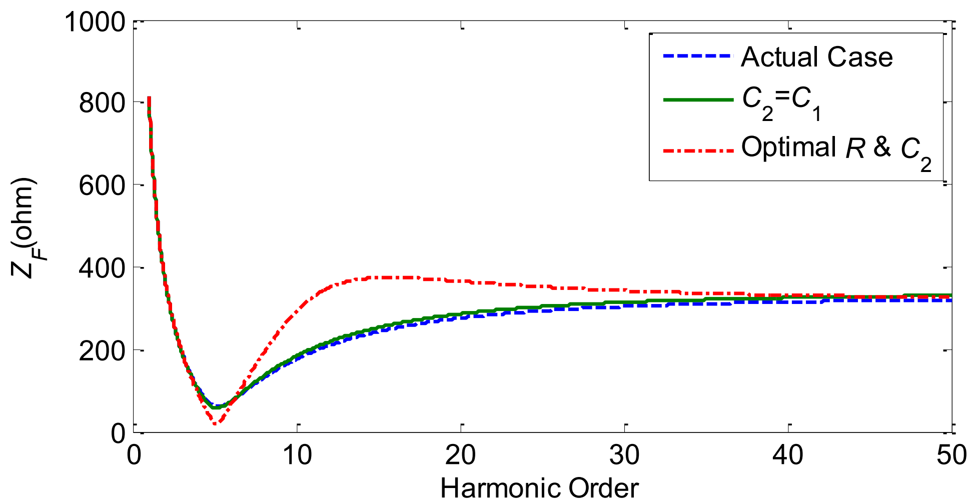

Figure 4.5: Comparison of the filter impedance characteristic

Cost estimation has been conducted to compare the costs of the 3rdHP filters designed by different methods. The results are shown as Table 4.2. The estimation method and the component cost data are provided in Appendix B. It can be seen from Table 4.2, the 3rdHP filter designed by the proposed method is slightly cheaper than that designed by the other two methods. This is mainly due to that the proposed design method utilizes the fundamental frequency loss minimization as a design condition which leads to a smaller resistor in terms of kW capacity.

Table 4.1: Design Results for Different Design Methods

		Actual Case [32]	$C_2 = C_1$	Optimal R & C_2
C_1	Value (μF)	3.79	3.79	3.79
	Rating V_{rms} (kV)	93.04	93.02	92.96
C_2	Value (μF)	4.73	3.79	1.06
	Rating V_{rms} (kV)	5.08	5.89	13.99
L	Value (mH)	82.40	82.40	82.40
	Rating I_{rms} (A)	67.01	66.71	65.52
R	Value (ohm)	330.00	340.10	315.77
	Rating I_{rms} (A)	5.35	4.96	3.29
Tuned Harmonic Order		5.7	5.7	5.7
7th Harmonic Voltage Reduction Ratio (%)		53.47	53.47	53.47
Power Loss (kW)	Fundamental Frequency	5.12	3.57	0.29
	Harmonic Frequency	23.22	21.53	9.99
	Total	28.34	25.09	10.27

Table 4.2: Estimated Cost for 3rdHP Filter Designed by Different Methods

		Actual Case [32]	$C_1 = C_2$	Optimal R & C_2
Individual RLC Component Cost	C_1	$48,479	$48,479	$48,479
	C_2	$1,077	$5,387	$4,848
	L	$24,589	$24,369	$23,506
	R	$4,485	$3,972	$1,626
Total RLC Component Cost		$78,630	$82,206	$78,458

It should be noted that the estimated cost for the capacitors are based on the assumption they are all constructed using basic capacitor units with a rated terminal to terminal rms voltage as 4.16 kV and a rated kVAr as 50 kVAr. This type of the basic capacitor unit is chosen based on the basic insulation level requirement for power equipment in a 90 kV system, industry practice and IEEE Std 18-2012 [94]. The required number of parallel branches and the number of the basic capacitor units in each branch to construct the main capacitor C_1 and the auxiliary capacitor C_2 for the 3rdHP filter designed by different methods are given in Table 4.3. The method to determine these numbers are given in Chapter 6.

Table 4.3: Required Number of Basic Capacitor Units

		Actual Case [32]	$C_1 = C_2$	Optimal R & C_2
C_1	Number of parallel branches	6	6	6
	Number of basic capacitor units in one branch	15	15	15
C_2	Number of parallel branches	1	2	1
	Number of basic capacitor units in one branch	2	5	9
Total number required to construct the capacitors in the 3rdHP filter		276	300	297

4.6 Summary

This chapter proposed a new design concept for the 3rdHP filter. A complete and simple design method in terms of four design formulas was established accordingly. The case study results showed that the proposed method can result in a 3rdHP filter with much less fundamental frequency loss compared to that designed by using other methods.

Chapter 5

Resonance-Free Shunt Capacitors

Due to the mass-distributed harmonic sources in today's power systems, harmonic resonance has recently become an important concern for the application of shunt capacitors. A potential solution to address this challenge is to convert a shunt capacitor into a passive filter.

This chapter presents design methods to configure a shunt capacitor as a C-type filter or a 3rdHP filter with guaranteed resonance-free performance. It is organized as follows. The current practice to address the shunt capacitor related harmonic resonance is first reviewed in Section 5.1. Next, the concept of the resonance-free condition is introduced in Section 5.2. Based on this concept, Section 5.3 provides the system-independent design methods for both the C-type filter configured capacitor and the 3rdHP filter configured capacitor. Then the performance of the two filter configured capacitors designed by the system-independent methods is compared in Section 5.4. As the filter component parameters determined by the system-independent methods are independent of system conditions, Section 5.5 creates a lookup table to facilitate the immediate use by industry. The usefulness of the system impedance information and the impact of the shunt capacitor device in a large system are investigated in Section 5.6 and Section 5.7, respectively. Section 5.8 summarizes this chapter.

5.1 Review on Current Practice

In response to shunt capacitor related harmonic resonance concerns, the idea of configuring a shunt capacitor as a single-tuned filter has been proposed. This is done by inserting a series inductor to the shunt branch [101-103]. The tuned frequency is normally the harmonic frequency closest to the capacitor-system resonance frequency, such as the 5th harmonic frequency. This approach does not always work since the newly configured capacitor may resonate at other frequencies due to the complex frequency response of the power system. Adding a damping resistor is not an option since it can significantly increase fundamental frequency loss of the shunt device.

As a result, some utilities have started to configure transmission voltage shunt capacitors as C-type filters [104, 105]. The C-type filter configuration possesses good damping characteristics at frequencies higher than its tuned frequency and has almost zero loss at the fundamental frequency. However, the design method to configure a shunt capacitor as a C-type filter that guarantees a resonance-free performance has not been developed.

The C-type filter is just one of the modified versions of the 2nd order high-pass (2ndHP) filter. Another version is 3rdHP filter [106]. Both the C-type filter and 3rdHP filter have the same number of RLC components. The main difference is on the mechanisms of reducing the fundamental frequency loss. In view of this situation, one would naturally wonder if the 3rdHP filter can also be used to construct a resonance-free shunt capacitor and which filter configuration has more advantages.

5.2 Resonance-Free Condition

Resonance involves the interaction of components with different impedance characteristics. A power system to which a shunt capacitor is connected can have different impedance characteristics at various frequencies such as those illustrated in Figure 5.1. The impedance characteristics may also change as a function of the number and type of network components in service. As a result, it is very difficult for a shunt capacitor not to resonate with the system impedance at some frequencies.

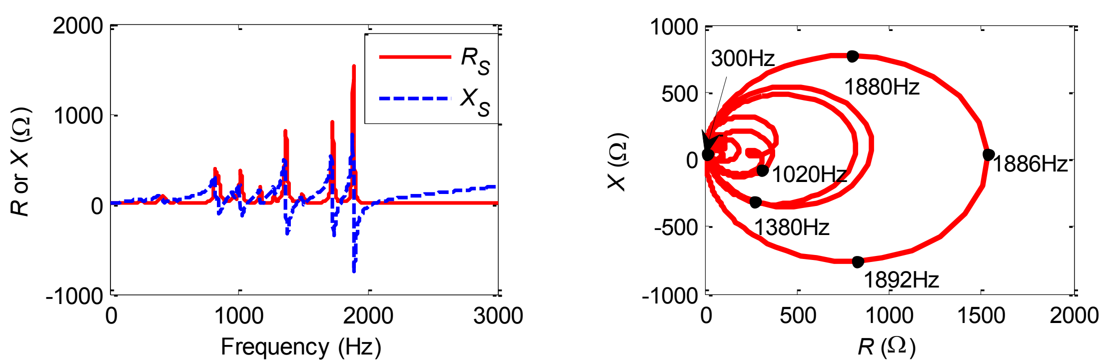

(a) Separate R and X plot (b) Spiral R-X plot

Figure 5.1: A sample power system frequency response obtained at a 144kV bus in Alberta transmission system

Figure 5.2 shows the equivalent circuit of the system and a passive shunt capacitor device. For simplicity, this device is called filter as the capacitor will take the form of either C-type or 3rdHP filter. Before the filter is connected, the harmonic voltage at the interconnection point is $V_F^0(\omega)$, where ω is the angular frequency. After connecting the filter, the voltage becomes $V_F(\omega)$. The ratio of these two voltages is defined as the harmonic amplification ratio (*HAR*):

$$HAR(\omega) = \left| \frac{V_F(\omega)}{V_F^0(\omega)} \right| \tag{5.1}$$

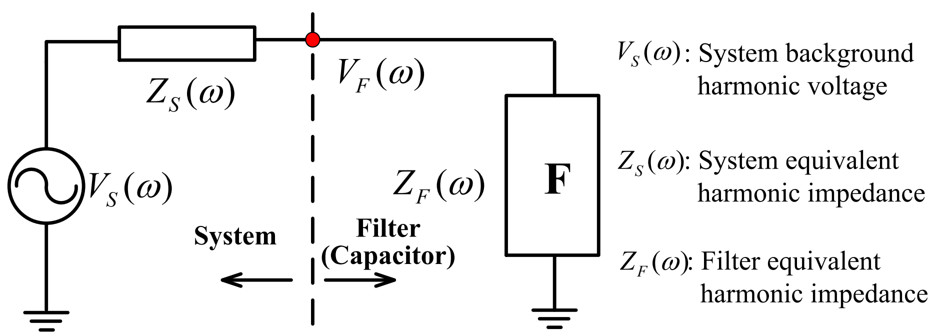

Figure 5.2: Equivalent circuit of the system and filter (capacitor)

According to Figure 5.2, $V_F^0(\omega)$ is equal to the system background harmonic voltage $V_S(\omega)$. Substituting it into equation (5.1) yields

$$HAR(\omega) = \left| \frac{V_F(\omega)}{V_F^0(\omega)} \right| = \left| \frac{Z_F(\omega)}{Z_F(\omega) + Z_S(\omega)} \right| \tag{5.2}$$

which can be further represented as

$$HAR(\omega) = \sqrt{\frac{R_F^2(\omega) + X_F^2(\omega)}{\left(R_F(\omega) + R_S(\omega)\right)^2 + \left(X_F(\omega) + X_S(\omega)\right)^2}} \tag{5.3}$$

where $X_S(\omega)$, $R_S(\omega)$ and $X_F(\omega)$, $R_F(\omega)$ are the imaginary and real component of $Z_S(\omega)$ and $Z_F(\omega)$, respectively.

In this thesis, the harmonic resonance is defined by using $HAR(\omega)$ index. If $HAR(\omega_h)$ is larger than a user defined threshold such as 2 at frequency ω_h, one can declare there is a harmonic resonance at ω_h. The severity of resonance depends on the bus harmonic voltage prior to the capacitor connection ($V_F^0(\omega)$). $HAR(\omega_h)=2$ means that the harmonic voltage will be amplified by a factor of 2.

As can be seen from equation (5.3), for a given frequency, the most serious voltage amplification occurs when the system impedance is purely reactive and is equal to the negative equivalent filter reactance, that is,

$$R_S(\omega)=0,\ X_S(\omega)=-X_F(\omega)\,. \tag{5.4}$$

Under such a condition, the denominator in equation (5.3) is minimum, which results in the largest (i.e., worst-case) amplification ratio of

$$HAR_{\text{worst}}(\omega)=\sqrt{1+\left(\frac{X_F(\omega)}{R_F(\omega)}\right)^2}\ . \tag{5.5}$$

Equation (5.5) suggests that the worst or the largest amplification ratio is different for different harmonic frequencies and it is only affected by the filter's reactance to resistance ratio at the harmonic frequencies.

<u>A resonance-free condition is defined as</u>

$$HAR_{\text{worst}}(\omega)\le HAR_{\text{limit}},\quad \text{for } \omega\ge\omega_H \tag{5.6}$$

where HAR_{limit} is a user specified threshold. Definition (5.6) quantifies a shunt capacitor as a resonance-free capacitor if the worst-case amplification of harmonic voltage caused by the capacitor is less than a user specified limit HAR_{limit}, for any harmonic frequencies higher than ω_H. This condition also guarantees that the voltage THD (VTHD) for the frequency range of interest will not be increased more than a factor of HAR_{limit}.

For example, field measurements conducted prior to capacitor connection may reveal the bus voltage $V_F^0(\omega)$ has 1.1% 5th harmonic voltage and 2.1% VTHD. A limit value of $HAR_{\text{limit}} = 1.2$ means the harmonic voltages after a shunt capacitor device connection are guaranteed to be no larger than 1.2 times of the pre-connection values, i.e., $VIHD_5 \leq 1.2*1.1\%$ and $VTHD \leq 1.2*2.1\%$. These values can then be compared with the IEEE Std 519 harmonic voltage limits to determine if they are acceptable. Since HAR_{limit} is applied to the worst-case system impedance condition of HAR_{worst}, the actual HAR value can be significantly less than HAR_{limit}. This will be further discussed in the case study of Section 5.4. The IEEE Std 519 harmonic current limits do not apply in this case since the shunt capacitor device is not a harmonic-producing customer.

Since the 5th harmonic is the lowest order characteristic harmonic in power systems, ω_H can be selected as the frequency of the 5th harmonic. As a result, a capacitor satisfying these conditions is guaranteed not to resonate with the system at any frequencies above and equal to the 5th harmonic.

Based on the above considerations, system-independent design methods for the C-type filter and 3rdHP filter configured resonance-free shunt capacitor are developed next.

5.3 System-Independent Design Methods

This section presents the system-independent design methods for the C-type filter and 3rdHP filter configured resonance-free capacitor, which are based on the resonance-free concept introduced in Section 5.2.

5.3.1 System-Independent Design Method for C-type Filter Configuration

The C-type filter (Figure 5.3 (b)) was first introduced in [107] to replace multiple single-tuned filters for a HVDC application. It is a modified version of the 2ndHP filter (Figure 5.3(a)) [105]. The objective of modification is to eliminate the fundamental frequency loss. It is achieved through the C_2+L branch which is tuned to series resonance at the fundamental frequency. This condition leads to the bypass of the R branch and, thereby, the elimination of loss at the fundamental frequency. At low order harmonics, the $C_2 + L$ branch dominates so the filter behaves like a single tuned filter (Figure 5.3 (c)). At high order harmonics, the R branch dominates and the filter behaves as a resister R in series with C_1 (Figure 5.3 (d)).

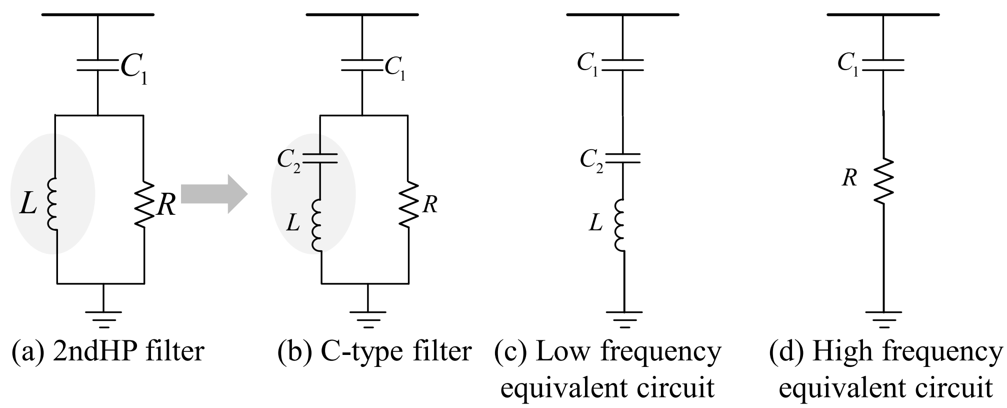

Figure 5.3: C-type filter and its equivalent circuits at different frequency ranges

A C-type filter has four components. Four design conditions or equations are therefore needed to determine its components' parameters.

A. Basic Design Equations

For the C-type filter, two design conditions are well understood and accepted by industry and research community:

- Condition 1: The reactive power output of the filter shall be equal to the required amount Q_F. This condition yields a design equation that is shown as equation (4.1).
- Condition 2: C_2 and L are tuned to the fundamental frequency to eliminate the fundamental frequency loss, which leads to

$$L = \frac{1}{\omega_1^2 C_2} . \tag{5.7}$$

B. Condition of Inductive Impedance

Depending on the combination of component parameters, a C-type filter can exhibit a capacitive or inductive impedance characteristic at any harmonic frequencies. Here we propose the following design condition: the impedance of C-type is always inductive above its tuned frequency, i.e.,

$$X_F(\omega) \geq 0,\ \omega \geq \omega_H. \tag{5.8}$$

This condition is based on the following consideration: If a system has an inductive impedance characteristic at frequency ω and the C-type also has an inductive impedance, the actual amplification ratio will be much less than HAR_{worst} because the term $X_F(\omega)+X_S(\omega)$ in equation (5.3) is additive. Since the system impedance is more likely to be inductive than capacitive at various frequencies, it is advantageous to have a C-type filter that exhibits inductive impedance above its tuned frequencies.

It has been proven mathematically in Appendix A.2 that condition (5.8) will always be satisfied if

$$C_2 \geq (n_H^2-1)/n_H^2 C_1, \tag{5.9}$$

and

$$X_F(\omega_H)=0, \tag{5.10}$$

where $n_H=\omega_H/\omega_1$.

Equation (5.10) leads to the third design equation:

$$R=\frac{n_H^2-1}{\omega_H\sqrt{(n_H^2-1)C_1C_2-C_2^2}}. \tag{5.11}$$

The derivation is given in Appendix A.1.

C. Resonance-Free Condition

The C-type filter configured shunt capacitor must be resonance-free. Thus, the fourth design equation is the resonance-free condition established by inequality (5.6). It is important to note that inequality (5.6) is for the worst-case condition of the supply system impedance. In reality, this design condition can result in a significant less harmonic voltage at the tuned frequency, i.e. the actual *HAR* value can be less than 0.75 (see Section 5.4).

Through extensive mathematical operations given in Appendix A.3, the frequency at which a C-type filter reaches its maximal HAR_{worst} has been found as follows:

1) when $C_2 = \dfrac{n_H^2 - 1}{n_H^2} C_1$,

$$\omega_{\max} = \omega_1 \sqrt{(\sqrt{25 n_H^4 - 22 n_H^2 + 1} + 5 n_H^2 - 1)/6}\,; \tag{5.12}$$

2) when $C_2 > \dfrac{n_H^2 - 1}{n_H^2} C_1$,

$$\omega_{\max} = \omega_1 \sqrt{(A+B)^{1/3} + D(A+B)^{-1/3} + (\beta - 1)/(\alpha - 1)}\,, \tag{5.13}$$

where

$$\begin{cases} \alpha = R^2/(L/C_1), \beta = R^2/(L/C_2) \\ A = \dfrac{\sqrt{324\beta^2(4-\beta) - 3(4(\alpha+8)(\alpha+\beta) + 9\beta^2)(\alpha+\beta)^2}}{18(\alpha-1)^2} \\ B = \dfrac{\alpha^2\beta - 2\alpha^2 + \alpha\beta^2 + \alpha\beta + 2\beta^3 - 7\beta^2 + 4\beta}{2(\alpha-1)^3} \\ D = (\alpha^2 + \alpha\beta + 2\alpha + 3\beta^2 - 7\beta)/(3(\alpha-1)^2) \end{cases}. \tag{5.14}$$

Resonance-free condition means this maximal HAR_{worst} must be less than or equal to HAR_{limit}. Substituting equation (5.12) or equation (5.13) according to the value of C_2 into inequality (5.6) yields the fourth design equation:

$$\sqrt{1 + \frac{\left((1-\alpha)h_{\max}^4 + (\alpha + \beta - 2)h_{\max}^2 + 1\right)^2}{C_1^2 R^2 \omega_1^2 h_{\max}^2 (h_{\max}^2 - 1)^4}} = HAR_{\text{limit}}\,, \tag{5.15}$$

where $h_{\max} = \omega_{\max}/\omega_1$.

D. Design Method Summary

To summarize, parameters of a C-type filter configured capacitor can be determined by using the following procedure:

1) Determine C_1 by using equation (4.1).
2) Set $C_2 = (n_H^2 - 1) / n_H^2 C_1$.
3) Calculate L and R by using equation (5.7) and equation (5.11), respectively.
4) Substitute the values of C_1, C_2, L and R into equation (5.15) to check if the fourth design equation is satisfied. If it is satisfied, then the C_2, L and R values are the solutions. Otherwise go to Step 5).
5) Try another value of C_2 by using the Bisection Method [108] and go to Step 3).

5.3.2 System-Independent Design Method for 3rdHP Filter Configuration

As discussed in the introduction and Chapter 4, the 3rdHP filter (Figure 5.4 (b)) is one most widely used filter to filter high order harmonics such as 11th, 13th etc., for both industrial systems and HVDC links [31, 106]. It is also a modified version of the 2ndHP filter. The objective of modification is again to reduce the fundamental frequency loss. It is achieved by inserting C_2 into R branch, which increases the impedance of that branch at fundamental frequency and thus reduces fundamental frequency loss of component R. At low frequencies below the tuned frequency, the filter's L branch dominates so it behaves as a single-tuned filter (Figure 5.4 (c)), while at high frequencies, the $C_2 + R$ branch dominates hence it behaves as a first order high pass filter (Figure 5.4 (d)).

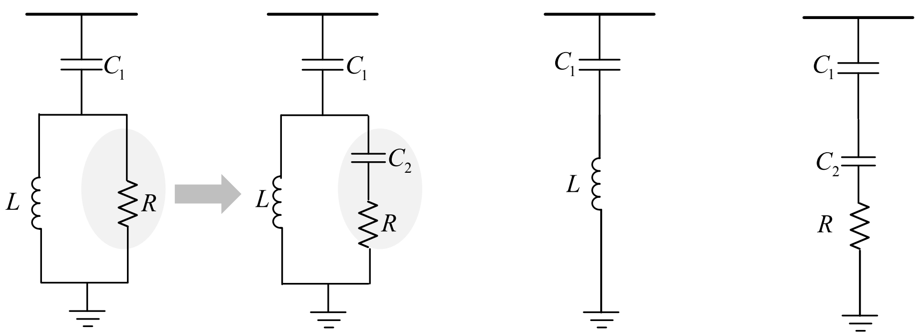

(a) 2ndHP filter (b) 3rdHP filter (c) Low frequency equivalent circuit (d) High frequency equivalent circuit

Figure 5.4: 3rdHP filter and its equivalent circuits at different frequency ranges

Similar to the C-type filter, a 3rdHP filter also has four components. Thus, it also needs four design equations.

A. Basic Design Equations

The two design requirements well accepted by industry and research community [39, 109] are given in Section 4.1. They are repeated here for the ease of illustration.

- Condition 1: The reactive power output of the filter shall be equal to the required amount Q_F. This condition yields a design equation that is shown as equation (4.1).
- Condition 2: The filter is tuned to have a low non-capacitive impedance at frequency ω_H. This can be achieved by selecting L that is resonate with C_1 at frequency ω_H, which establishes the second design equation shown as (4.2)

B. Condition of Loss Minimization

The main purpose of the auxiliary capacitor in the 3rdHP filter is to reduce the filter loss at the fundamental frequency. It is, therefore, logical to use loss minimization to establish the third design equation. Chapter 4 has shown that the corresponding design equation is equation (4.35).

It should be noted that this design equation is obtained based on the requirement that the filter impedance must be inductive for frequencies higher than the tuned frequency, which requires the damping resistor must satisfy the condition $R \geq \sqrt{2L/C_1}$ [109]. Detailed derivations can refer to Chapter 4.

C. Resonance-Free Condition

It is also evident that this filter configuration must be resonance-free, i.e., its maximal HAR_{worst} must be less than or equal to HAR_{limit}. Through extensive mathematical operations shown in Appendix A.4, the frequency at which 3rdHP filter reaches its maximal HAR_{worst} has been found as follows:

$$\omega_{\max} = \frac{\sqrt{5}(R^2 - \gamma^2)}{\sqrt{3(R^4 - R^2\gamma^2 - \gamma^4)}}\omega_H , \tag{5.16}$$

where $\gamma = \sqrt{L/C_1}$.

Accordingly, substitute equation (5.16) into inequality(5.6). Then the fourth design equation for the 3rdHP filter can be derived as follows:

$$\sqrt{1 + \frac{108(R^4 - R^2\gamma^2 - \gamma^4)^5}{3125R^2\gamma^6(R^2 - \gamma^2)^6}} = HAR_{\text{limit}} . \tag{5.17}$$

D. Design Method Summary

To summarize, parameters of a 3rdHP filter configured capacitor can be determined by using the following procedure:

1) Determine C_1 by using equation (4.1) and L by using equation (4.2).
2) Set $R = \sqrt{2L/C_1}$ and $\gamma = \sqrt{L/C_1}$.
3) Substitute the values R and γ into equation (5.17) to check if the fourth design equation is satisfied. If it is satisfied, then the R value is the solution. Calculate C_2 by using equation (4.35). Otherwise, go to Step 4).
4) Try another value of R by using the Bisection Method [108] and go to Step 3.

5.4 Comparison of Characteristics of Different Filter Configurations

This section compares the performance of the two filter configured capacitors designed by the proposed system-independent methods through a case study.

5.4.1 Case Description

Figure 5.5 shows the simplified single line diagram of a part of 240/144 kV transmission system in Alberta, Canada. The system has over 1000 transmission voltage buses and a number of shunt capacitors. This study involves a 30 MVAr reactive power to be added to substation SX.

The system frequency response as seen from this substation is shown as Figure 5.1. The response shows multiple series and parallel resonance points. The background voltage distortion spectra at 144 kV bus in substation SX is shown as Figure 5.6.

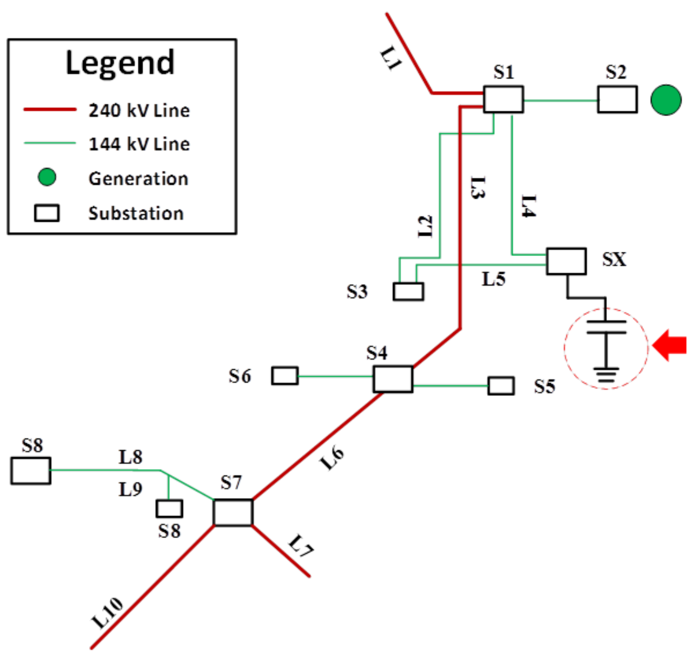

Figure 5.5: Single line diagram

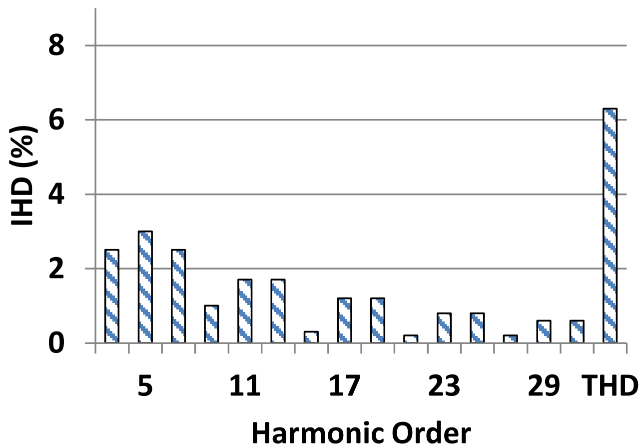

Figure 5.6: Background voltage spectra at substation SX

5.4.2 Design Results

The proposed methods are applied to determine the parameters for the C-type and 3rdHP filters. The resonance free condition is selected as HAR_{limit}=1.2 and the tuned frequency is $f_H = 300\text{Hz}$ (i.e., 5th harmonic).

The design results are shown in Figure 5.7 to Figure 5.9. Figure 5.7 shows the frequency response of the filters. It can be seen that both filters have a large equivalent resistance above the tuned frequency. This resistance is the source of damping that brings down the amplification ratio. Both filters have similar frequency response characteristics.

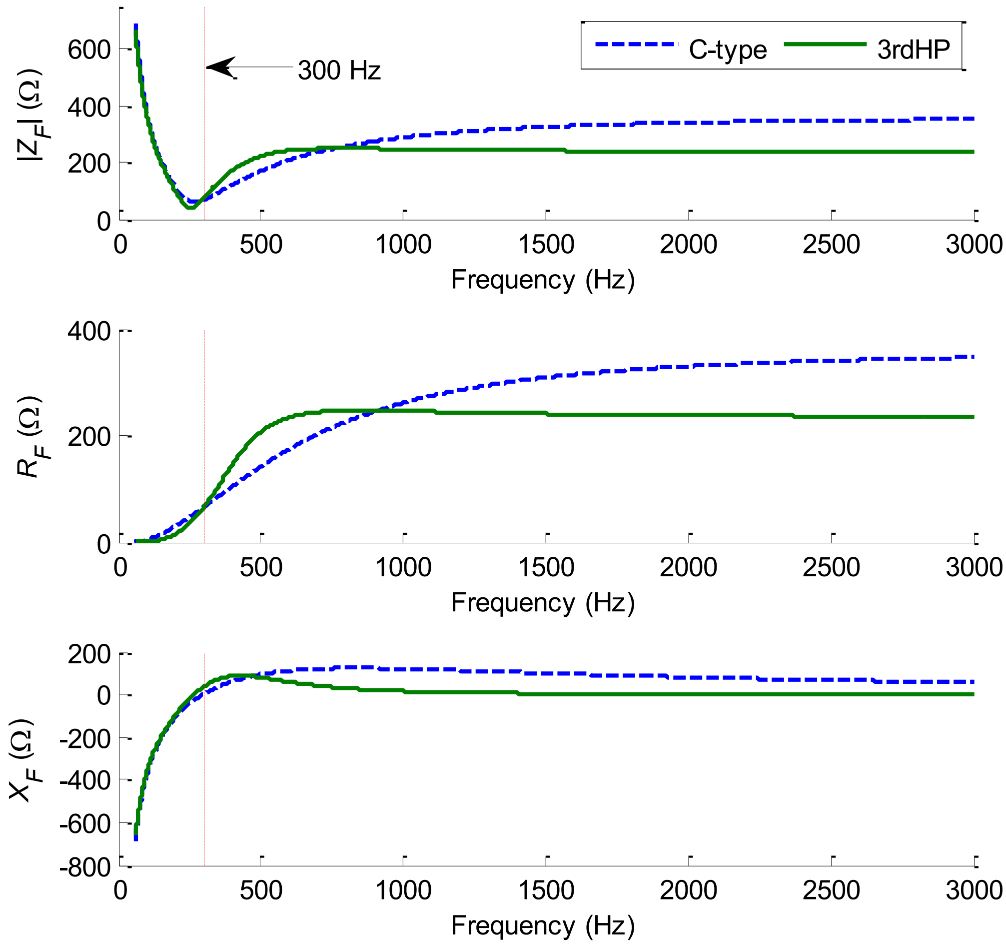

Figure 5.7: Frequency response of filters designed by the system-independent methods

The theoretical worst-case and the actual (system-dependent) harmonic amplification ratios are shown in Figure 5.8. The worst-case ratio is determined according to equation (5.5), which assumes that the system impedance has no resistance and is in perfect resonance with the filter. The actual amplification ratio is calculated considering the system impedance (i.e., using equation (5.3)). The amplification ratio associated with pure capacitor installation is also calculated. The ratio is close to 2 around the 5th harmonic and is as high as 14 around the 11th harmonic. The results reveal the following:

- If not configured as a filter, the shunt capacitor will result in excessive harmonic amplification at several harmonic frequencies. On the other hand, either C-type or 3rdHP filter configured capacitor will not increase harmonic voltages since the actual amplification ratio is always less than 1 for all harmonics.

- The actual harmonic voltage reduction performance is much better than the worst-case design limit. For example, the actual *HAR* at the tuned frequency (5th harmonic) is less than 0.75 even though the design limit is 1.2. This also suggests that the resonance-free capacitor so designed can actually reduce harmonic voltages at its tuned frequency.
- The C-type and 3rdHP filters have similar resonance mitigation performance.

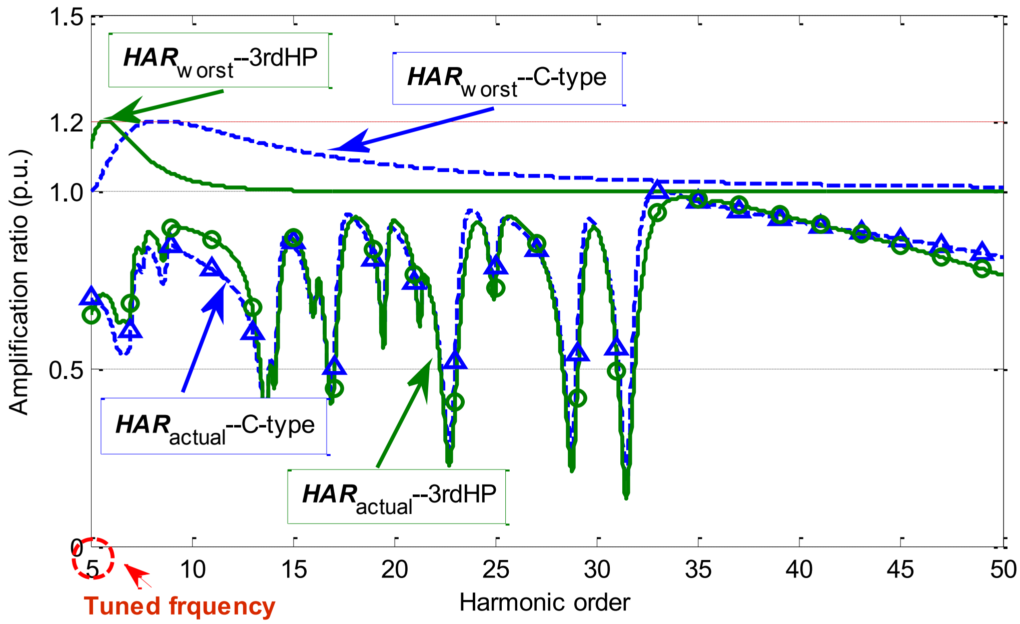

Figure 5.8: Harmonic amplification ratio of filter configured capacitors designed by the system-independent methods

Figure 5.9 gives the voltage spectra at substation SX for installation scenarios:

1) No capacitor;
2) Pure capacitor;
3) C-type filter configured capacitor designed by the system-independent method;
4) 3rdHP filter configured capacitor designed by the system-independent method.

As can be seen from Figure 5.9, a pure capacitor will cause a significant voltage distortion increase at this substation, while either a C-type or a 3rdHP configured capacitor can lead to a slight decrease of the harmonic voltages.

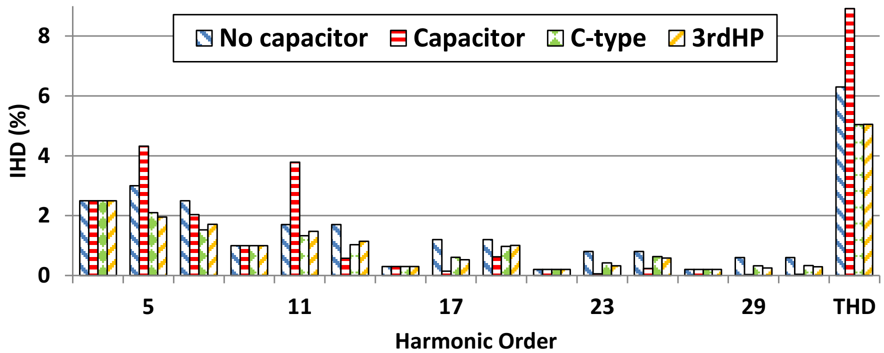

Figure 5.9: Voltage spectra at SX for different installation scenarios

Table 5.1 shows filter component parameters and performance indices. It can be seen that the two filter configurations have similar parameters and performance indices. Both the C-type filter and the 3rdHP filter require a C_1 with the same capacitance, while the voltage rating of C_1 for 3rdHP filter is 3% higher than that for C-type filter. The C-type filter requires a C_2 with a larger capacitance while the 3rdHP filter requires a C_2 with a larger voltage rating. By converting the rated voltage into the rated capacity, the C-type filter requires a 1.55 MVAr C_2, while the 3rdHP filter requires a 0.77 MVAr C_2. Therefore, in the sense of rated capacity, C-type filter requires a much larger C_2. The inductance of L and the resistance of R for 3rdHP filter are around 20% and 35% less than that for C-type filter, respectively, while the rated current of L and the rated current of R for 3rdHP filter are around 8% and 16% higher than that for C-type filter, respectively. The harmonic amplification ratio and the losses for the two filters are comparable.

Table 5.1: Filter component parameters and Performance Indices

			C-type	3rdHP
Specification	C_1	Value (uF)	3.84	3.84
		Rating V_{rms} (kV)	147.42	152.73
	C_2	Value (uF)	75.66	2.06
		Rating V_{rms} (kV)	7.38	31.59
	L	Value (mH)	92.99	73.34
		Rating I_{rms} (A)	123.76	133.42
	R	Value (Ω)	361.02	233.84
		Rating I_{rms} (A)	14.89	17.40
Performance	Reactive power (MVAr)		30.00	31.28
	HAR_{actual} (p.u.)	Maximum	1.00	0.98
		Average (among harmonics)	0.80	0.80
	Power loss (kW)	Fundamental frequency	0.00	5.14
		Harmonic frequencies	240.25	207.21
		Total	240.25	212.35
		% loss (of filter MVAr)	0.80	0.68

5.4.3 Cost Analysis

Figure 5.10 shows the total filter RLC component cost (excluding switchgears but including CTs) for the studied case. In this plot, the costs are normalized values with respect to the reference case of HAR_{limit}=1.05 and 3rdHP filter configuration (~$390,000) for easier comparison. The cost data is estimated from those of installed C-type filters and capacitor as given in Appendix B. It is worthwhile to note that the component costs are mainly determined by their KVArms values which are case dependent. As a result, the cost plot is only applicable for the studied case. The results show that the 3rdHP is about 5% cheaper for the HAR_{limit}=1.05 case. The reason that the cost increases with HAR_{limit} is as follows: An increased HAR_{limit} implies that the bus voltage has higher harmonic voltages. This in turn leads higher KVArms values for the components. So the total cost can rise as in the case of 3rdHP configuration.

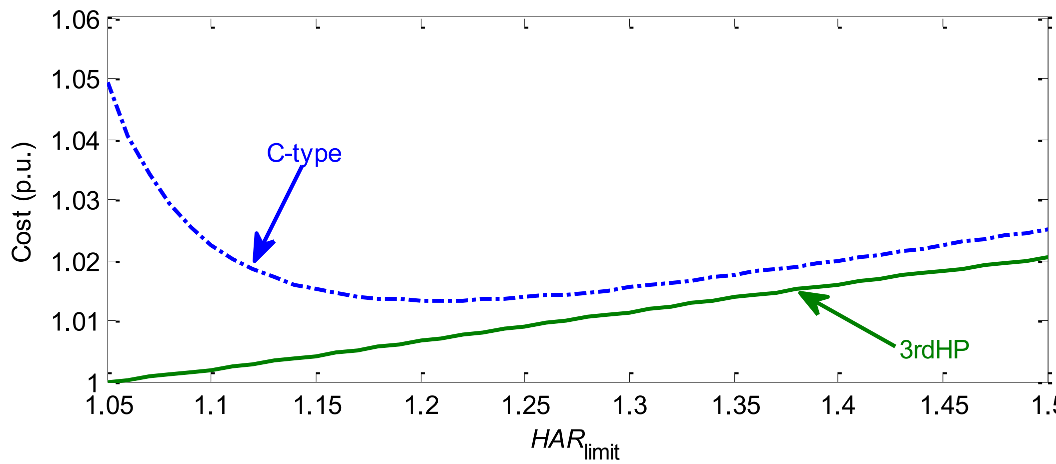

Figure 5.10: Filter cost as a function of HAR_{limit}

The costs as affected by the tuned frequency are also investigated. It is found that the cost is about 1.4 to 1.7 times of those shown in Figure 5.10, if the capacitor is tuned to the 3rd harmonic instead of the 5th harmonic. This finding suggests it may be beneficial to tune the capacitor to the 5th harmonic coupled with an undergrounded connection. This is because the 3rd harmonic is dominated in ZS and the capacitor so configured is unlikely to amplify the 3rd harmonic voltage.

5.4.4 Robustness Study

In practice, parameters of the filter components are not exact due to aging or manufacturing variations, and the system frequency always varies. This subsection investigates the impact of this issue on filter performance and loading condition. Based on [95] and the data specification collected from manufactures, the range of variations for the system frequency and RLC component parameters are as follows:

- Frequency: -1% to 1%;
- Capacitance: 0 to 10%;
- Inductance: -3% to 3%;
- Resistance: -10% to 10%.

The method of investigation is as follows. The base case is selected as the design parameters and the associated performance indices of Subsection 5.4.2. The system frequency and component parameters are then assumed varying randomly around the design parameters based on the above given range. A normal distribution is assumed for the variations. This will result in tens of thousands of possible combinations or scenarios of the system frequency and component parameters. Each filter performance index is then calculated for all studied scenarios and a pair of statistical values representing the 95% variation interval are then determined from the tens of thousands scenarios.

In this study, 100,000 combinations are calculated by using the MCS method. The results (the variation from the base case in percentage) are shown in Table 5.2.

Table 5.2: Filter Loading and Performance Index Variation

<table>
<tr><th colspan="3"></th><th>C-type</th><th>3rdHP</th></tr>
<tr><td rowspan="4" colspan="2">Loading (%)</td><td>C_1</td><td>-0.85 to 0.26</td><td>-0.94 to 0.06</td></tr>
<tr><td>C_2</td><td>-6.49 to 6.12</td><td>-11.57 to 0.54</td></tr>
<tr><td>L</td><td>0.09 to 9.62</td><td>-0.13 to 9.32</td></tr>
<tr><td>R</td><td>-9.38 to 5.77</td><td>-6.13 to 4.48</td></tr>
<tr><td rowspan="7">Performance</td><td colspan="2">Reactive Power Support (%)</td><td>0.10 to 10.43</td><td>-0.13 to 10.59</td></tr>
<tr><td rowspan="2">HAR_{worst} (%)</td><td>Maximum</td><td>-4.22 to 6.91</td><td>-3.31 to 3.90</td></tr>
<tr><td>Average (among harmonics)</td><td>-1.61 to 2.35</td><td>-0.54 to 0.77</td></tr>
<tr><td rowspan="2">HAR_{actual} (%)</td><td>Maximum</td><td>-0.56 to 0.65</td><td>-0.09 to 0.06</td></tr>
<tr><td>Average (among harmonics)</td><td>-1.03 to 0.97</td><td>-0.89 to 0.20</td></tr>
<tr><td rowspan="2">Power loss (%)</td><td>Harmonic frequency</td><td>-10.53 to 2.52</td><td>-8.09 to 3.31</td></tr>
<tr><td>Total</td><td>-10.28 to 2.70</td><td>-7.19 to 3.60</td></tr>
</table>

The observations from Table 5.2 suggest that

- Both the component loading and filter's performance indices all vary around the base case value within a small range (below 12%). It should be noted that the reactive power support is approximately in a linear relation with C_1. So its variation range is similar with the capacitance manufacturing error tolerance.

- The performance of both filters as designed by the proposed system-independent methods is quite robust. Both filter types have comparable robustness.
- The 3rdHP filter configuration is slightly more attractive from the harmonic amplification perspective since the variation ranges of its HAR_{worst} and HAR_{actual} are all smaller.

5.4.5 Switching Transient Study

The switching of a shunt capacitor device can cause transient overvoltage. Which filter configured shunt capacitor will induce a lower switching transient is investigated in this subsection.

The tool used in the investigation is an add-on subroutine to PSS/E, which is developed in PDS lab. It utilizes the short-circuit solution engine of the PSS/E to determine the frequency response of the studied network and performs the transient simulation in the frequency domain. It also deploys a 2-stage searching scheme, which facilities the determination of the "worst-case" switching. Details about this tool can be referred to [110].

The switching transient of the pure shunt capacitor, the C-type filter configured shunt capacitor, and the 3rdHP filter configured shunt capacitor designed in Subsection 5.4.2 is studied. For each configuration, 1000 simulations with different switching instants are performed. The results are shown in Figure 5.11 to Figure 5.13. The results include two types of plot:

- Distribution of the voltage peak, which includes probability distribution and cumulative distribution.
- Power-quality indices of all switching on the ITIC power-quality envelop [111]. On this plot, the horizontal and vertical axes are the duration and magnitude of the transient. The acceptable and prohibited regions are defined on the curve. Each switching transient is represented by a dot on the figure. The magnitude and duration of the worst-case transient can be identified on the curve by finding the upper-most dot on the plot.

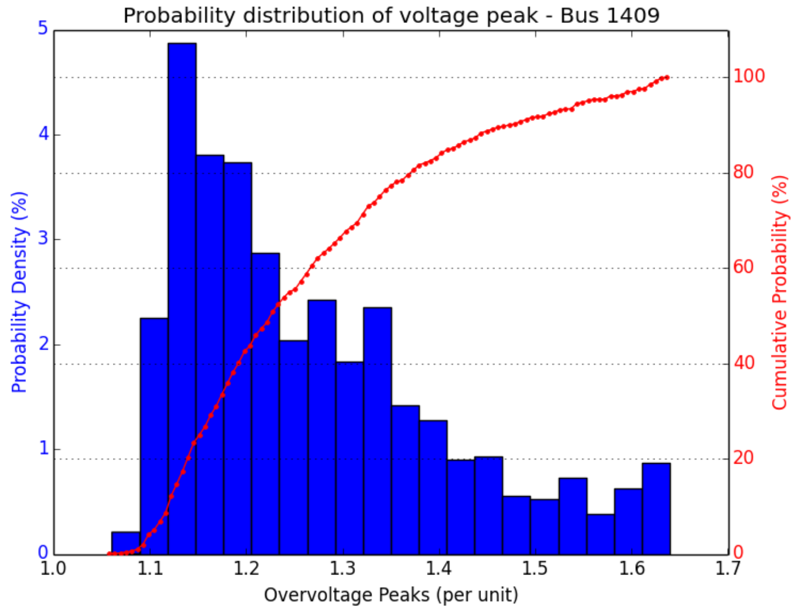

(a) Probability distribution

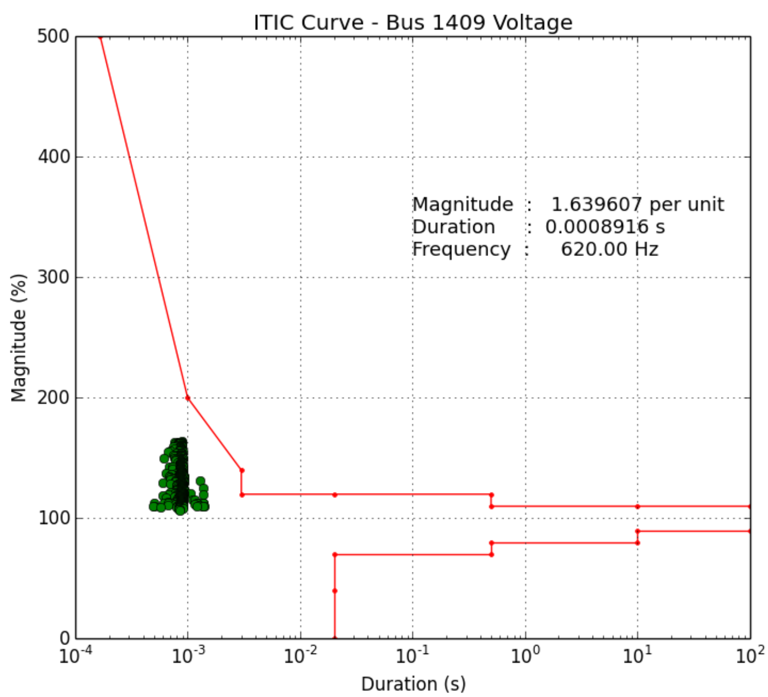

(b) Transient overvoltage on ITIC curve

Figure 5.11: Transient voltage results for a pure shunt capacitor

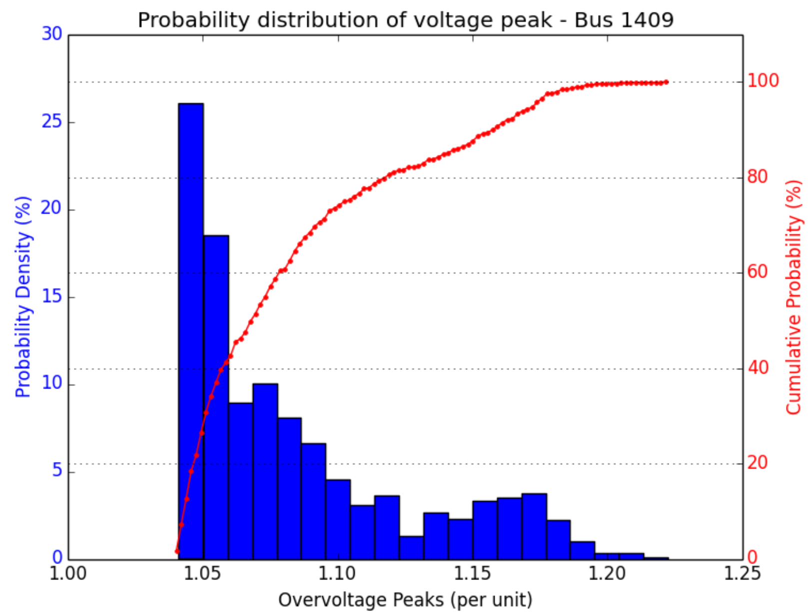

(a) Probability distribution

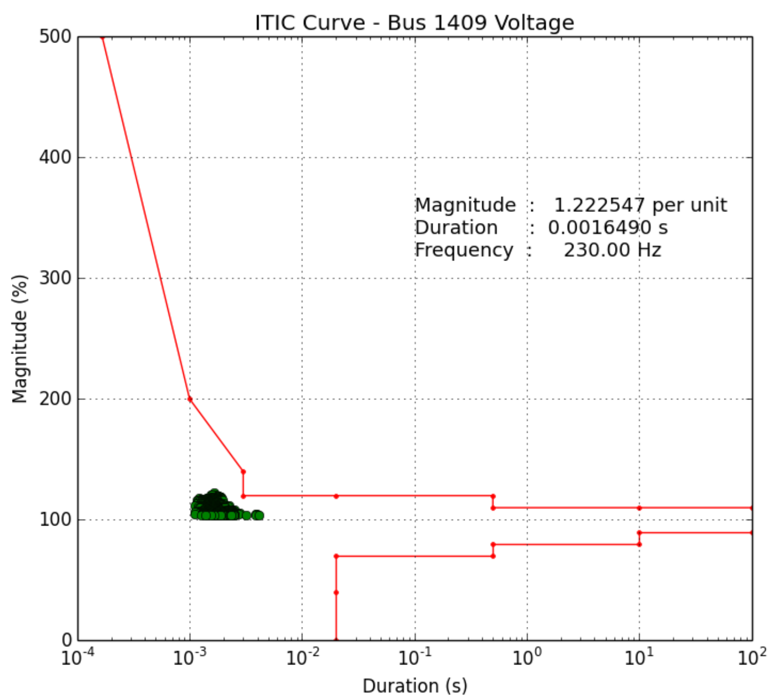

(b) Transient overvoltage on ITIC curve

Figure 5.12: Transient voltage results for the C-type filter configured shunt capacitor

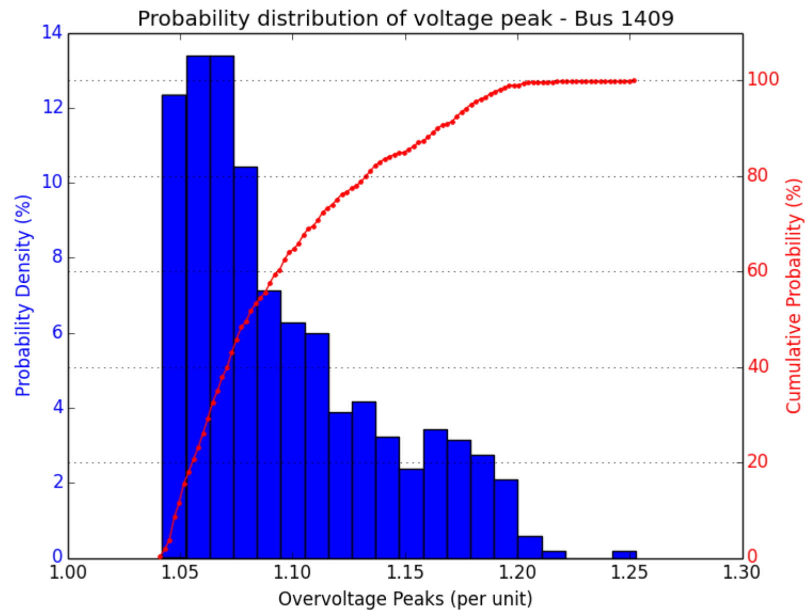

(a) Probability distribution

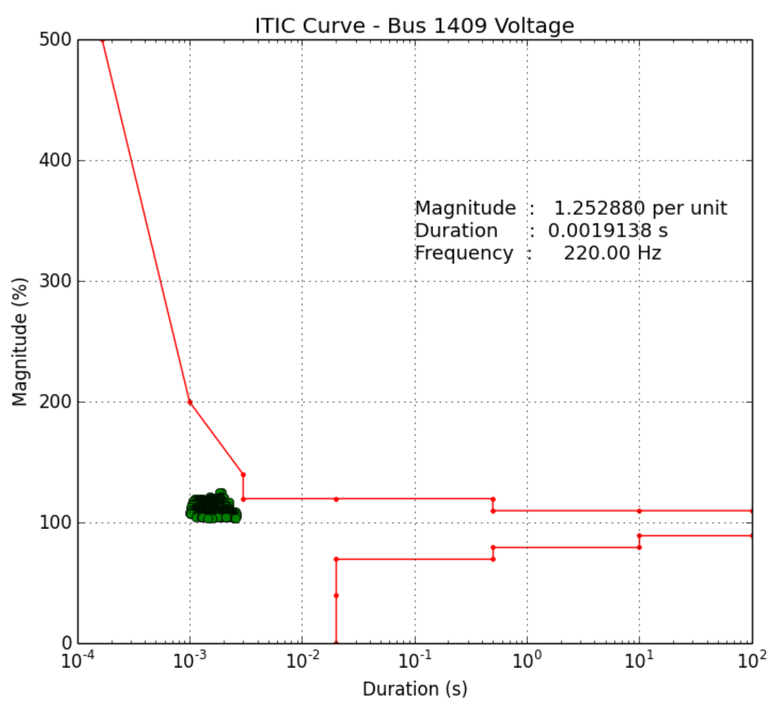

(b) Transient overvoltage on ITIC curve

Figure 5.13: Transient voltage results for the 3rdHP filter configured shunt capacitor

To facilitate the ease of comparison, the worst-case transient voltage for the different configurations is further summarized in Table 5.3. The following observations can be obtained from Figure 5.11 to Figure 5.13 and Table 5.3.

- Both the C-type filter and 3rdHP filter configurations have a lower worst-case transient overvoltage magnitude than that of the pure capacitor.
- The C-type filter configuration is slightly more advantageous in terms of the lower magnitude and shorter duration of the worst-case transient overvoltage.

Table 5.3: Worst-Case Transient Overvoltage

		Capacitor	C-type	3rdHP
Worst-Case Transient Overvoltage	Magnitude	1.640 p.u.	1.222 p.u.	1.253 p.u.
	Duration	0.816 ms	1.649 ms	1.914 ms
	Frequency	620 Hz	230 Hz	220 Hz

5.5 Lookup Table for Filter Component Parameters

A very interesting outcome of the proposed system-independent filter design method is that the filter component parameters are independent of the system impedances. This is because the parameters are determined for the worst-case system condition. As a result, a standard set of filter component parameters can be calculated and achieved for direct use by industry. For this purpose, a lookup table of per-unit filter component parameters has been created and is shown in Table 5.4. The table lists the parameters for two tuned frequencies (n_H=3 and n_H=5) under eleven HAR_{limit} values. Since the filter is resonance-free regardless the value of the system impedance, the n_H=3 case also works for ZS impedance condition.

Table 5.4: Lookup Table for Per-Unit Filter Component Parameters

			$n_H = 3$		$n_H = 5$	
			C-type	3rdHP	C-type	3rdHP
HAR_{limit}	1.008603	C_1	1.0000	1.0000	1.0000	1.0000
		C_2	3.6344	1.0000	10.2163	1.0000
		L	0.2752	0.1111	0.0979	0.0400
		R	0.6695	0.4714	0.4045	0.2828
	1.05	C_1	1.0000	1.0000	1.0000	1.0000
		C_2	5.2833	0.7613	15.4307	0.7613
		L	0.1893	0.1111	0.0648	0.0400
		R	0.7039	0.5070	0.4174	0.3042
	1.10	C_1	1.0000	1.0000	1.0000	1.0000
		C_2	5.9845	0.6519	17.6440	0.6519
		L	0.1671	0.1111	0.0567	0.0400
		R	0.7678	0.5306	0.4533	0.3184
	1.15	C_1	1.0000	1.0000	1.0000	1.0000
		C_2	6.3782	0.5852	18.8862	0.5852
		L	0.1568	0.1111	0.0529	0.0400
		R	0.8291	0.5486	0.4884	0.3292
	1.20	C_1	1.0000	1.0000	1.0000	1.0000
		C_2	6.6414	0.5372	19.7164	0.5372
		L	0.1506	0.1111	0.0507	0.0400
		R	0.8878	0.5639	0.5223	0.3383
	1.25	C_1	1.0000	1.0000	1.0000	1.0000
		C_2	6.8330	0.5000	20.3207	0.5000
		L	0.1463	0.1111	0.0492	0.0400
		R	0.9443	0.5774	0.5551	0.3464
	1.30	C_1	1.0000	1.0000	1.0000	1.0000
		C_2	6.9799	0.4697	20.7838	0.4697
		L	0.1433	0.1111	0.0481	0.0400
		R	0.9993	0.5896	0.5871	0.3538

Table 5.4: Lookup Table for Per-Unit Filter Component Parameters (continued)

			$n_H = 3$		$n_H = 5$	
			C-type	3rdHP	C-type	3rdHP
HAR_{limit}	1.35	C_1	1.0000	1.0000	1.0000	1.0000
		C_2	7.0964	0.4443	21.1514	0.4443
		L	0.1409	0.1111	0.0473	0.0400
		R	1.0531	0.6010	0.6184	0.3606
	1.40	C_1	1.0000	1.0000	1.0000	1.0000
		C_2	7.1914	0.4225	21.4509	0.4225
		L	0.1391	0.1111	0.0466	0.0400
		R	1.1059	0.6117	0.6491	0.3670
	1.45	C_1	1.0000	1.0000	1.0000	1.0000
		C_2	7.2704	0.4034	21.6998	0.4034
		L	0.1375	0.1111	0.0461	0.0400
		R	1.1578	0.6217	0.6794	0.3730
	1.50	C_1	1.0000	1.0000	1.0000	1.0000
		C_2	7.3370	0.3866	21.9099	0.3866
		L	0.1363	0.1111	0.0456	0.0400
		R	1.2091	0.6313	0.7093	0.3788

The base set of Table 5.4 is:

- Rated voltage of the system where the capacitor is to be installed (V_r);
- Rated reactive power of the main capacitor C_1 under rated voltage condition (Q_r);
- System fundamental frequency f_1.

Thus base value for capacitance C_b, inductance L_b and resistance R_b is determined as

$$\begin{cases} C_b = \dfrac{Q_r}{2\pi f_1 V_r^2} \\ L_b = \dfrac{V_r^2}{2\pi f_1 Q_r} \\ R_b = \dfrac{V_r^2}{Q_r} \end{cases} . \tag{5.18}$$

Whenever a shunt capacitor needs to be configured into a resonance-free filter, parameters of the filter components can be determined by using Table 5.4 as follows:

- Determine the base values (V_r, Q_r, f_1) to be used;
- Calculate the base values of the capacitance C_b, inductance L_b and resistance R_b;
- Decide on the harmonic voltage amplification limit HAR_{limit}, tuned harmonic order n_H , and the filter topology to be used;
- Locate the p.u. values of the component parameters in Table 5.4;
- Multiply the p.u. values by the corresponding base values to get the physical values.

Take the case in Section 5.4 as an example. For this case, V_r =144 kV, Q_r =30 MVAr , f_1=60 Hz. Therefore, the base value C_b=30/(2*π*60*144^2)=3.838e-6 F, R_b=144^2/30=691.2 ohm, L_b=144^2/(2*π*60*30)=1.835 H. The required HAR_{limit} = 1.2, the tuned harmonic order $n_H = 5$, here we choose to configure the shunt capacitor into 3rdHP filter. Per this requirement, the shaded values in Table 5.4 are located. Multiply these values by the C_b, R_b, L_b, then the physical values for the component parameters are obtained. It can be easily verified, these physical values for the component parameters are the same as shown in Table 5.1.

It is worthwhile to point out that although the filter component parameters are independent of the system conditions, the component loading levels and costs are affected by the system impedance and background harmonic voltages. The component loading level can be determined through harmonic power flow studies. Such a study is also needed to determine the actual *HAR* values and harmonic voltage levels. The actual values are guaranteed to be less than HAR_{limit} so the harmonic voltage levels can be significantly less than those prior to capacitor connection. Finally, one may want to check if there is acceptable amplification of harmonic voltages at other buses. The HAR_{limit} condition works for the capacitor installation bus. It is not possible to guarantee that other buses meet this condition as well, which is illustrated in Section 5.7.

To further facilitate the selection of proper HAR_{limit} value in terms of the parameters of components, the variations of filter component parameters as functions of the HAR_{limit} is shown in Figure 5.14 and Figure 5.15 for the case of n_H=3 and the case of n_H=5 , respectively. In these two figures, all component parameters are normalized values with respect to the case of HAR_{limit}=1.008603 for easier comparison.

It should be also noted that HAR_{limit} cannot be less than 1.0. A value less than 1.0 implies a guaranteed reduction of all harmonic voltages regardless of the system conditions. This is clearly not achievable. It can be proven that the minimum value of HAR_{limit} is 1.008603 for the 3rdHP filter configuration. The minimum value for the C-type filter configuration cannot be established analytically. Numerical study shows that the value is close to 1.0 and it decreases with the tuned frequency.

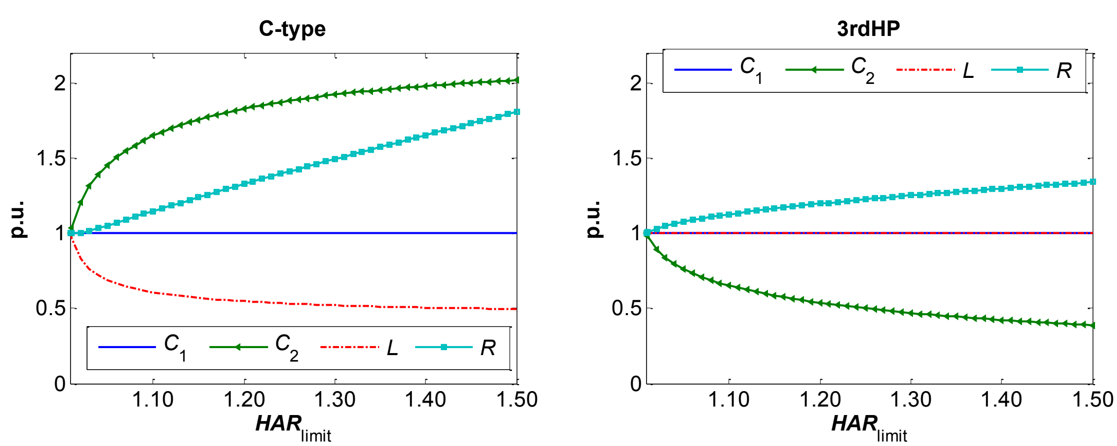

Figure 5.14: Filter component parameter variations as functions of user selected HAR_{limit} (n_H=3)

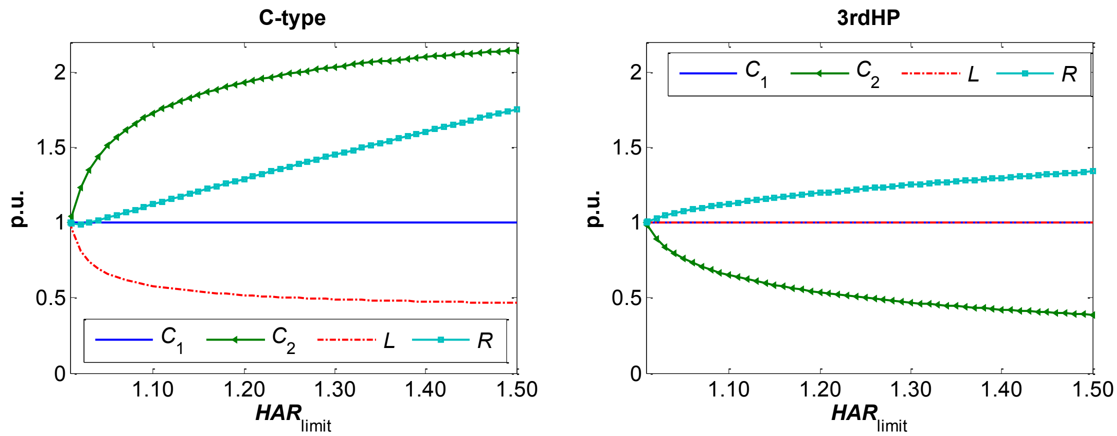

Figure 5.15: Filter component parameter variations as functions of user selected HAR_{limit} (n_H=5)

5.6 System-Dependent Design Methods

Unlike the system-independent design method, which assumes an unknown system impedance, the system-dependent design methods proposed here incorporate the system impedance information into the determination of the filter component parameters.

5.6.1 System-Dependent Design Method for C-type Filter Configuration

The system-dependent design method for the C-type filter configured shunt capacitor also has four design equations.

A. Basic Design Equations

The first two design equations are the same as those given in the system-independent design method in Subsection 5.3.1, i.e., equation (4.1) and equation (5.7).

B. Condition of Pure Resistive Impedance

The filter is tuned to have a pure resistive impedance at its tuned frequency, thus to guarantee a definite harmonic reduction at the tuned frequency. This leads to the same third design equation as that given in Subsection 5.3.1, i.e., equation (5.11).

It should be further noted that for the system-dependent design method, as the system impedance is known, the filter-system resonance can be directly avoided in the filter component parameter determination. Hence, there is no need to confine the filter's impedance to be inductive above its tuned frequency to reduce the likelihood of the filter-system resonance. Thus, for the system-dependent method, the third design condition does not involve the limit on C_2 (equation (5.9)).

C. General Anti-Resonance Performance Optimization Condition

The fourth design equation is established based on the following considerations. First, the filter configuration must be resonance-free, i.e., its *HAR* among the concerned harmonics in different operating conditions must be less than or equal to HAR_{limit}. As the system impedance is known, this requirement leads to the constraint as follows:

$$HAR_{i,h}(C_1,\ C_2,\ R,\ L) \le HAR_{\text{limit}} \quad \text{for } i \in S_I,\ h \in S_H\,, \tag{5.19}$$

where S_I represents the operating condition set, and S_H represents the concerned harmonics set,

$$HAR_{i,h}(C_1,\ C_2,\ R,\ L) = \left| \frac{Z_F(\omega_h)}{Z_F(\omega_h) + Z_{Si}(\omega_h)} \right|. \tag{5.20}$$

According to Figure 5.3 (b), the impedance of the C-type filter $Z_F(\omega)$ is given by

$$Z_F(\omega) = \frac{1}{j\omega C_1} + \left(\frac{1}{j\omega C_2} + j\omega L \right) // R\,. \tag{5.21}$$

Furthermore, thousands of different sets of RLC parameters can satisfy equation (5.19). The average *HAR* among concerned harmonics in different operating conditions (HAR_{ave}) well reflects the general anti-resonance performance of the filter. It is, therefore, reasonable to choose the parameters that will lead to the minimum HAR_{ave} for the system with the specific harmonic impedance. Therefore, the fourth design equation is established as follows:

$$\min HAR_{ave}(C_1,\ C_2,\ R,\ L) = \frac{1}{IH}\sum_{i\in S_I}\sum_{h\in S_H} HAR_{i,h}(C_1,\ C_2,\ R,\ L) \quad , \qquad (5.22)$$
$$s.t.\ HAR_{i,h}(C_1,\ C_2,\ R,\ L) \le HAR_{\text{limit}} \quad \text{for } i \in S_I,\ h \in S_H$$

where I is the total number of system operating condition, and H is the total number of concerned harmonics in each system operating condition.

D. Design Method Summary

To summarize, by the system-dependent design method, the parameters of a C-type filter configured capacitor can be determined by using the following procedure:

1) Determine C_1 by using equation (4.1);
2) Substitute C_1, equation (5.7) and equation (5.11) into optimization problem (5.22) and solve it to obtain the value of C_2;
3) Determine L by using equation (5.7) and R by using equation (5.11).

5.6.2 System-Dependent Design Method for 3rdHP Filter Configuration

The system-dependent design method for the 3rdHP filter configured shunt capacitor also has four design equations.

A. Basic Design Equations

The first two design equations are the same as those given in the system-independent design method in subsection 5.3.2, i.e., equation (4.1) and equation (4.2).

B. Constraint on Fundamental Frequency Loss

For the system-dependent design method, as the system impedance is known, the filter-system resonance can be directly avoided in the filter component parameter determination. Hence, the filter's impedance does not need to be limited to being inductive above its tuned frequency to reduce the likelihood of the filter-system resonance. Thus, for the system-dependent method, the loss minimization equation (4.35) is no longer valid. Without the inductive impedance constraint, the parameters which lead to the minimum fundamental frequency power loss are the sets of RLC parameters with either $C_2 = 0$ or $R = \infty$. With these sets of RLC parameters, the 3rdHP filter degrades into a single tuned filter, which has no anti-resonance ability. Therefore, here the fundamental frequency loss minimization is not adopted as a design condition. However, to reduce the operating cost, the fundamental frequency loss of the filter should be limited under a certain level, that is,

$$P_{Floss}(C_1, C_2, R, L) \le P_{\text{limit}}, \tag{5.23}$$

where

$$P_{Floss}(C_1, C_2, R, L) = \text{Re}\left(\frac{V^2}{Z_F(\omega_1)}\right). \tag{5.24}$$

According to Figure 5.4, the impedance of the 3rdHP filter $Z_F(\omega)$ is given by

$$Z_F(\omega) = \frac{1}{j\omega C_1} + \left(\frac{1}{j\omega C_2} + R\right) // j\omega L. \tag{5.25}$$

C. General Anti-resonance Performance Optimization Condition

Similar to the design method for a C-type filter, the system-dependent design method for a 3rdHP filter also adopts the general anti-resonance performance optimization as one of its design conditions. The fourth design equation of the system-dependent design method for a 3rdHP filter is also established by the optimization problem (5.22) .

D. Design Method Summary

To summarize, by the system-dependent design method, the parameters of a 3rdHP filter configured capacitor can be determined by using the following procedure:

1) Determine C_1 by using equation (4.1), and L by using equation (4.2);
2) Substitute the constraint (5.23) into the optimization problem (5.22), and solve it to obtain the value of C_2 and the value of R.

5.6.3 Comparison of the System-Independent Design Method and the System-Dependent Design Method

Both the system-independent design method and the system-dependent design method are applied to the case introduced in Section 5.4 for varying HAR_{limit} from 1.1 to 1.5. The design results are provided in Table 5.5 to Table 5.8.

Table 5.5: System-Independent Design Results for C-type Filter Configuration

	HAR_{limit} (p.u.)		1.1	1.2	1.3	1.4	1.5
Specification	C_1	Value (uF)	3.84	3.84	3.84	3.84	3.84
		Rating V_{rms} (kV)	145.97	147.42	148.41	149.16	149.78
	C_2	Value (uF)	67.71	75.66	79.76	82.32	84.08
		Rating V_{rms} (kV)	8.17	7.38	7.07	6.89	6.78
	L	Value (mH)	103.91	92.99	88.22	85.47	83.68
		Rating I_{rms} (A)	122.59	123.76	124.67	125.43	126.08
	R	Value (Ω)	313.30	361.02	405.80	448.68	490.28
		Rating I_{rms} (A)	15.81	14.89	14.02	13.25	12.55
Performance	Reactive power (MVAr)		30.00	30.00	30.00	30.00	30.00
	HAR_{actual} (p.u.)	Maximum	0.99	1.00	1.01	1.02	1.03
		Average (among harmonics)	0.80	0.80	0.81	0.81	0.81
	Power loss (kW)	Fundamental frequency	0.00	0.00	0.00	0.00	0.00
		Harmonic frequencies	234.93	240.25	239.42	236.16	231.75
		Total	234.93	240.25	239.42	236.16	231.75
		% loss (of filter MVAr)	0.78	0.80	0.80	0.79	0.77

Table 5.6: System-Dependent Design Results for C-type Filter Configuration

		HAR_{limit} (p.u.)	1.1	1.2	1.3	1.4	1.5
Specification	C_1	Value (uF)	3.84	3.84	3.84	3.84	3.84
		Rating V_{rms} (kV)	145.74	145.74	145.74	145.74	145.74
	C_2	Value (uF)	66.17	66.17	66.17	66.17	66.17
		Rating V_{rms} (kV)	8.36	8.36	8.36	8.36	8.36
	L	Value (mH)	106.34	106.34	106.34	106.34	106.34
		Rating I_{rms} (A)	122.42	122.42	122.42	122.42	122.42
	R	Value (Ω)	307.34	307.34	307.34	307.34	307.34
		Rating I_{rms} (A)	15.91	15.91	15.91	15.91	15.91
Performance	Reactive power (MVAr)		30.00	30.00	30.00	30.00	30.00
	HAR_{actual} (p.u.)	Maximum	0.98	0.98	0.98	0.98	0.98
		Average (among harmonics)	0.61	0.61	0.61	0.61	0.61
	Power loss (kW)	Fundamental frequency	0.00	0.00	0.00	0.00	0.00
		Harmonic frequencies	233.36	233.36	233.36	233.36	233.36
		Total	233.36	233.36	233.36	233.36	233.36
		% loss (of filter MVAr)	0.78	0.78	0.78	0.78	0.78

Table 5.7: System-Independent Design Results for 3rdHP Filter Configuration

		HAR_{limit} (p.u.)	1.1	1.2	1.3	1.4	1.5
Specification	C_1	Value (uF)	3.84	3.84	3.84	3.84	3.84
		Rating V_{rms} (kV)	152.16	152.73	153.27	153.75	154.20
	C_2	Value (uF)	2.50	2.06	1.80	1.62	1.48
		Rating V_{rms} (kV)	27.81	31.59	34.37	36.64	38.57
	L	Value (mH)	73.34	73.34	73.34	73.34	73.34
		Rating I_{rms} (A)	133.29	133.42	133.65	133.90	134.14
	R	Value (Ω)	220.06	233.84	244.53	253.67	261.80
		Rating I_{rms} (A)	18.58	17.40	16.55	15.87	15.28

Table 5.7: System-Independent Design Results for 3rdHP Filter Configuration (continued)

		HAR_{limit} (p.u.)	1.1	1.2	1.3	1.4	1.5
Performance	Reactive power (MVAr)		30.00	30.00	31.28	31.28	31.27
	HAR_{actual} (p.u.)	Maximum	0.98	0.98	0.98	0.99	0.99
		Average (among harmonics)	0.79	0.80	0.80	0.81	0.81
	Power loss (kW)	Fundamental frequency	7.12	5.14	4.11	3.45	2.98
		Harmonic frequencies	220.87	207.21	196.82	188.11	180.51
		Total	227.99	212.35	200.93	191.56	183.49
		% loss (of filter MVAr)	0.73	0.68	0.64	0.61	0.59

Table 5.8: System-Dependent Design Results for 3rdHP Filter Configuration

		HAR_{limit} (p.u.)	1.1	1.2	1.3	1.4	1.5
Specification	C_1	Value (uF)	3.84	3.84	3.84	3.84	3.84
		Rating V_{rms} (kV)	150.31	150.29	150.28	150.58	151.04
	C_2	Value (uF)	3.28	2.92	2.72	2.47	2.23
		Rating V_{rms} (kV)	28.64	32.84	36.05	38.60	40.73
	L	Value (mH)	73.34	73.34	73.34	73.34	73.34
		Rating I_{rms} (A)	132.89	132.69	132.64	132.70	132.86
	R	Value (Ω)	123.62	112.29	103.39	105.98	112.44
		Rating I_{rms} (A)	25.07	25.62	26.21	25.44	24.28
Performance	Reactive power (MVAr)		30.00	30.00	31.29	31.29	31.29
	HAR_{actual} (p.u.)	Maximum	1.10	1.20	1.30	1.28	1.22
		Average (among harmonics)	0.56	0.57	0.59	0.60	0.61
	Power loss (kW)	Fundamental frequency	7.12	5.14	4.11	3.45	2.98
		Harmonic frequencies	225.92	216.02	208.95	202.26	195.80
		Total	233.05	221.16	213.06	205.71	198.78
		% loss (of filter MVAr)	0.74	0.71	0.68	0.66	0.64

Figure 5.16 and Figure 5.17 further compare the average *HAR* among harmonics of the filter obtained by using different design methods.

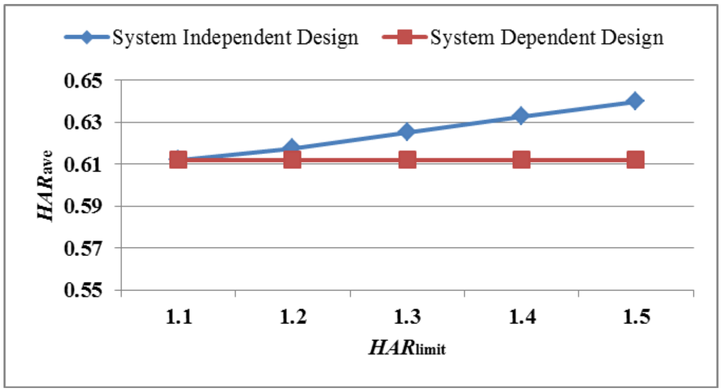

Figure 5.16: Average *HAR* among harmonics for designed C-type filter with different HAR_{limit}

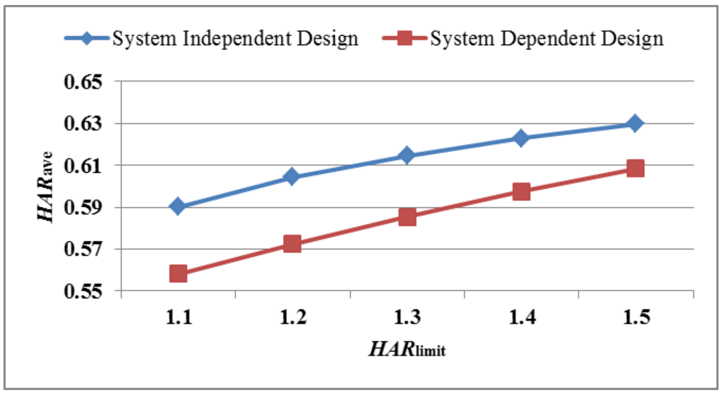

Figure 5.17: Average *HAR* among harmonics for designed 3rdHP filter with different HAR_{limit}

Table 5.9 and Table 5.10 give the cost estimation of the filter obtained by using different design methods.

Table 5.9: Cost Estimation for C-type Filter

HAR_{limit} (p.u.)	1.1	1.2	1.3	1.4	1.5
System-Independent Design ($1000)	396.08	392.49	393.31	395.06	396.99
System-Dependent Design ($1000)	397.47	397.47	397.47	397.47	397.47
Relative cost saving of system-dependent design method (%)	-0.35	-1.25	-1.05	-0.61	-0.12

Table 5.10: Cost Estimation for 3rdHP Filter

HAR_{limit} (p.u.)	1.1	1.2	1.3	1.4	1.5
System-Independent Design ($1000)	388.07	389.91	391.77	393.55	395.21
System-Dependent Design ($1000)	378.53	377.87	377.78	379.19	381.20
Relative cost saving of system-dependent design method (%)	2.52	3.18	3.70	3.79	3.68

The comparisons reveal that

- For the same HAR_{limit}, both design methods give similar design RLC parameters.
- For the same HAR_{limit}, the rating of the RLC components designed by using the two methods are comparable.
- For the same HAR_{limit}, the filter designed by using the system-dependent method may have a lower average *HAR* among harmonics.
- For the same HAR_{limit}, the C-type filter designed by using the system-dependent method costs a little more (around 1%), while the 3rdHP filter designed by using the system-dependent method costs a little less (around 3%) (see the last row of Table 5.9 and Table 5.10).

The above observations show that when the system harmonic impedance is known by using the proposed system-dependent method, the both C-type filter and 3rdHP filter can be designed to have a better performance (in terms of a lower average *HAR* among harmonics). However, the performance improvement is relatively insignificant, and for the C-type filter there is also a slight cost increase. For these reasons, the system impedance information is not of great importance for the design process.

Furthermore, the difficulty and cost of obtaining the system harmonic impedance cannot be ignored. The system-dependent design, therefore, has no obvious advantage over the system-independent design.

5.7 Impact of the Shunt Capacitor Device in Large System

In the application of the shunt capacitor device, the following questions are also of interest.

- Will the adding of the shunt capacitor device cause harmonic amplification at other buses in a large system?
- If the answer is yes, what factors determine the harmonic amplification ratio?

This section aims to answer the above two questions. It is organized as follows. The problem to be investigated is first formulated mathematically by using a generic system model. Theoretical analysis is then conducted, which is followed by a numerical case study.

5.7.1 Problem Formulation

For a system with *n* buses, the nodal voltage equation at a certain harmonic *h* is given by

$$[\mathbf{Y}(h)]_{n\times n}\mathbf{V}(h) = \mathbf{I}_S(h), \tag{5.26}$$

where $[\mathbf{Y}(h)]_{n\times n}$ is the node admittance matrix; $\mathbf{V}(h) = \begin{bmatrix} V_1(h) & \ldots & V_i(h) & \ldots & V_j(h) & \ldots & V_n(h) \end{bmatrix}^T$ is the node voltage vector; and $\mathbf{I}_S(h) = \begin{bmatrix} I_{1s}(h) & \ldots & I_{is}(h) & \ldots & I_{js}(h) & \ldots & I_{ns}(h) \end{bmatrix}^T$ is the current source vector.

The problem to be investigated is how, after installing a shunt capacitor device at local bus *i*, the harmonic voltage at local bus *i* and remote bus *j* change, or, in other words, the problem is whether $\left|V_i^{'}(h)\right|$ and $\left|V_j^{'}(h)\right|$ (see Figure 5.18 (b)) are larger than $\left|V_i(h)\right|$ and $\left|V_j(h)\right|$ (see Figure 5.18 (a)).

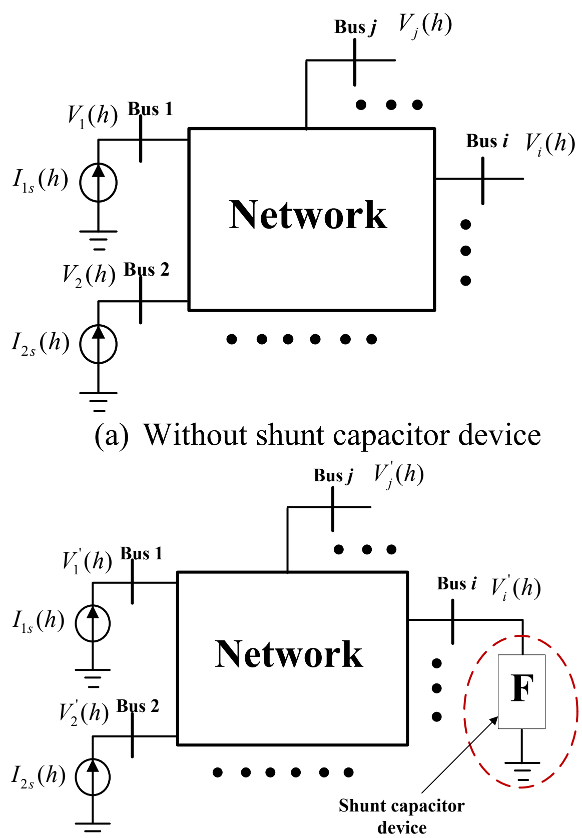

(a) Without shunt capacitor device

(b) With shunt capacitor device

Figure 5.18: System schematic diagram for the impact study of the shunt capacitor device

5.7.2 Theoretical Analysis

As only the local bus *i* and remote bus *j* are of concern, all other buses in the system can be seen as internal buses. By eliminating them in the nodal voltage equation (5.26), the following two-bus nodal voltage equation for the system without a shunt capacitor device can be obtained as:

$$\left[\mathbf{Y}_{ij}^{eq}\right]\mathbf{V}_{ij} = \mathbf{I}_{ij}^{eq} \Leftrightarrow \begin{bmatrix} Y_{ii}^{eq} & Y_{ij}^{eq} \\ Y_{ij}^{eq} & Y_{jj}^{eq} \end{bmatrix} \begin{bmatrix} V_i \\ V_j \end{bmatrix} = \begin{bmatrix} I_i^{eq} \\ I_j^{eq} \end{bmatrix}, \tag{5.27}$$

in which, for the sake of simplicity, the harmonic order *h* is omitted.

The installation of the shunt capacitor device affects only the self-admittance at the local bus *i*. With a shunt capacitor device at local bus ***i***, the two-bus nodal voltage equation for the system becomes

$$
\begin{aligned}
&\left(\left[\mathbf{Y}_{ij}^{eq}\right]+\left[\Delta\mathbf{Y}_{ij}^{eq}\right]\right)\mathbf{V}_{ij}^{'}=\mathbf{I}_{ij}^{eq} \\
&\Leftrightarrow \pm\left(\begin{bmatrix} Y_{ii}^{eq} & Y_{ij}^{eq} \\ Y_{ij}^{eq} & Y_{jj}^{eq} \end{bmatrix}+\begin{bmatrix} \dfrac{1}{Z_F} & 0 \\ 0 & 0 \end{bmatrix}\right)\begin{bmatrix} V_i^{'} \\ V_j^{'} \end{bmatrix}=\begin{bmatrix} I_i^{eq} \\ I_j^{eq} \end{bmatrix}, \\
&\Leftrightarrow \begin{bmatrix} Y_{ii}^{eq}+\dfrac{1}{Z_F} & Y_{ij}^{eq} \\ Y_{ij}^{eq} & Y_{jj}^{eq} \end{bmatrix}\begin{bmatrix} V_i^{'} \\ V_j^{'} \end{bmatrix}=\begin{bmatrix} I_i^{eq} \\ I_j^{eq} \end{bmatrix}
\end{aligned}
\tag{5.28}
$$

in which Z_F is the impedance of the resonance-free capacitor.

Put equation (5.27) into equation (5.28) and subtract I_i^{eq} and I_j^{eq}. Then rearrange. The following equation is obtained:

$$
\begin{cases} V_i^{'}=\dfrac{Z_F}{Z_F+Z_{ii}^{eq}}V_i \\ V_j^{'}=V_j+\dfrac{-Z_{ij}^{eq}}{Z_F+Z_{ii}^{eq}}V_i \end{cases},
\tag{5.29}
$$

where Z_{ii}^{eq} is the self-impedance of bus *i*, and Z_{ij}^{eq} is the mutual impedance between the local bus *i* and remote bus *j*, which are given as below:

$$
\begin{cases} Z_{ii}^{eq}=\dfrac{Y_{jj}^{eq}}{Y_{ii}^{eq}Y_{jj}^{eq}-\left(Y_{ij}^{eq}\right)^2} \\ Z_{ij}^{eq}=\dfrac{-Y_{ij}^{eq}}{Y_{ii}^{eq}Y_{jj}^{eq}-\left(Y_{ij}^{eq}\right)^2} \end{cases}.
\tag{5.30}
$$

A. Impact on Local Bus *i*

By equation (5.29), we can obtain

$$\frac{|V_i^{'}|}{|V_i|} = \left|\frac{Z_F}{Z_F + Z_{ii}^{eq}}\right| = \sqrt{\frac{R_F^2 + X_F^2}{\left(R_F + R_{ii}^{eq}\right)^2 + \left(X_F + X_{ii}^{eq}\right)^2}}, \tag{5.31}$$

where

$$R_F = real(Z_F),\ X_F = imag(Z_F),\ R_{ii}^{eq} = real(Z_{ii}^{eq}),\ X_{ii}^{eq} = imag(Z_{ii}^{eq}). \tag{5.32}$$

In the worst-case scenario, i.e., when $R_{ii}^{eq} = 0,\ X_{ii}^{eq} = -X_F$,

$$\frac{|V_i^{'}|}{|V_i|} = \sqrt{1 + \frac{X_F^2}{R_F^2}}. \tag{5.33}$$

For the resonance-free capacitor, $\sqrt{1 + \frac{X_F^2}{R_F^2}} \leq HAR_{\text{limit}}$, so $\frac{|V_i^{'}|}{|V_i|} \leq HAR_{\text{limit}}$. The installation of the resonance-free capacitor at the local bus *i* will not cause a harmonic voltage amplification larger than HAR_{limit} at the local bus *i*.

B. Impact on Remote Bus *j*

By equation (5.29), we can obtain

$$\frac{|V_j^{'}|}{|V_j|} = \left|1 + \frac{-Z_{ij}^{eq}}{Z_F + Z_{ii}^{eq}} \frac{V_i}{V_j}\right|. \tag{5.34}$$

As V_i , V_j, Z_{ij}^{eq} , Z_{ii}^{eq} are all independent complex variables, $\frac{-Z_{ij}^{eq}}{Z_F + Z_{ii}^{eq}} \frac{V_i}{V_j}$ can be any value. So $\frac{|V_j^{'}|}{|V_j|}$ may be larger than 1 or smaller than 1 depending on the different values of V_i, V_j, Z_{ij}^{eq}, Z_{ii}^{eq}. The impact of installing the resonance-free capacitor at local bus *i* on remote bus *j* is system-dependent.

5.7.3 Numerical Case Study

In this subsection, the impact of the shunt capacitor device is numerically investigated by using the case presented in Section 5.4. The impact of the shunt capacitor device on the local bus has been revealed numerically by Figure 5.8. Therefore, this subsection presents mainly the numerical case study results for the impact on the remote buses.

In the case study, the self impedance Z_{ii}^{eq} at the shunt capacitor device installation bus *i*, and the mutual impedance Z_{ij}^{eq} between the bus *i* and selected remote bus *j* are obtained using the add-on subroutine of PSS/E mentioned in Subsection 5.4.5. The study has investigated the harmonic amplification ratio for three remote buses with different physical distances to the shunt capacitor device installation bus. The phase angle difference of the harmonic voltages at the shunt capacitor device installation bus *i* and the remote bus *j* are assumed to vary from 0 to π, while the magnitude ratio of these two voltages are assumed to vary from 0.5 to 2.

Figure 5.19 to Figure 5.21 show some sample results for the case in which a 3rdHP filter is installed at bus *i*. The results for the C-type filter case are similar.

The observations comply with the analytical analysis and further suggest that

- Installing the shunt capacitor device does affect the harmonic voltage at other buses.
- The phase angle difference between V_i and V_j affects the harmonic voltage amplification ratio.
- The magnitude ratio of the harmonic voltages at the local bus *i* and the remote bus *j* affects the harmonic voltage amplification ratio at the remote bus *j*. The larger this ratio, the larger the harmonic voltage amplification ratio at bus *j*.
- The impact of the shunt capacitor device decreases with the physical distance.

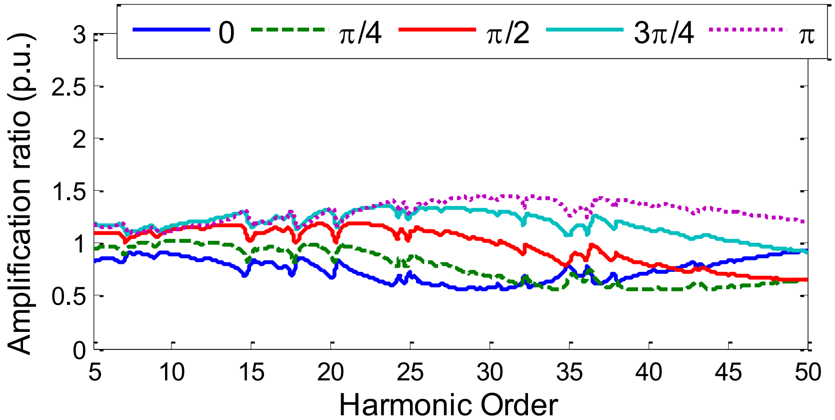

(a) $\left|\frac{V_i}{V_j}\right| = 0.5$

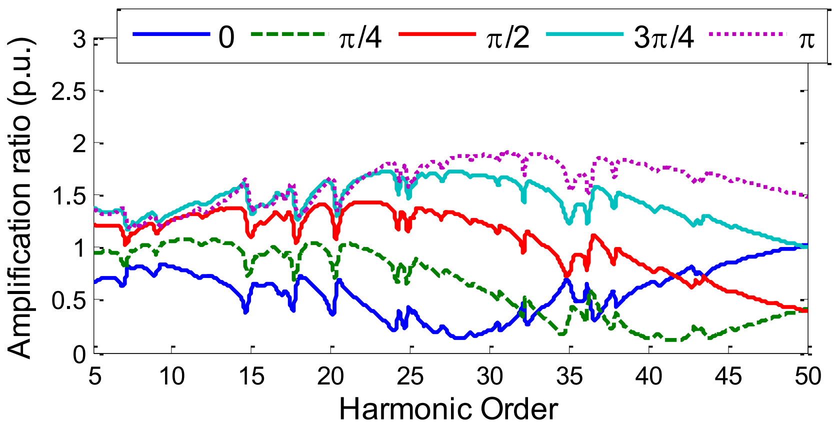

(b) $\left|\frac{V_i}{V_j}\right| = 1$

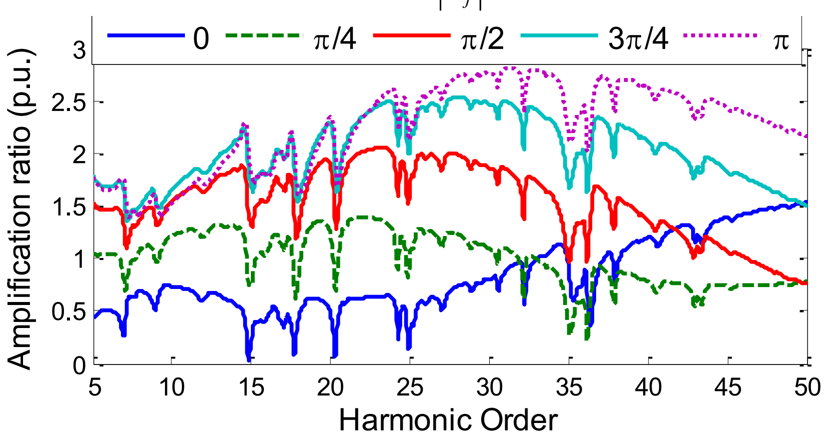

(c) $\left|\frac{V_i}{V_j}\right| = 2$

Figure 5.19: HAR_{actual} at a remote bus indirectly connected to the 3rdHP filter installation bus with physical distance around 30km

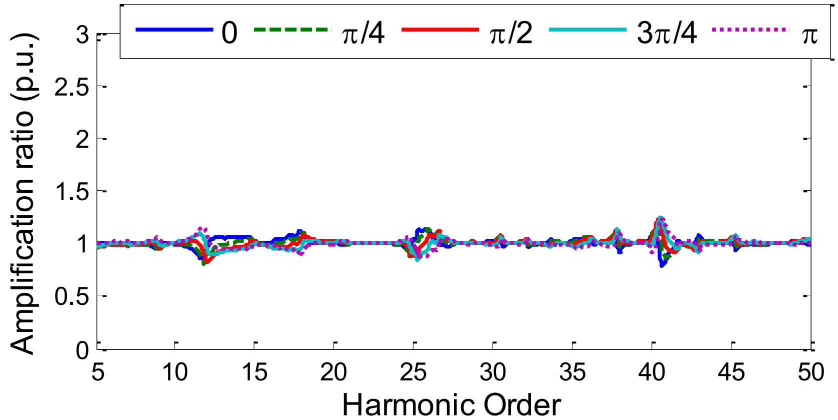

(a) $\left|\frac{V_i}{V_j}\right| = 0.5$

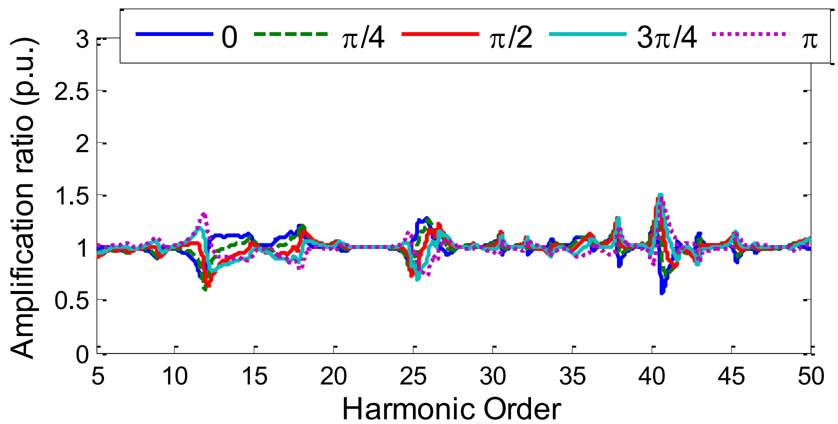

(b) $\left|\frac{V_i}{V_j}\right| = 1$

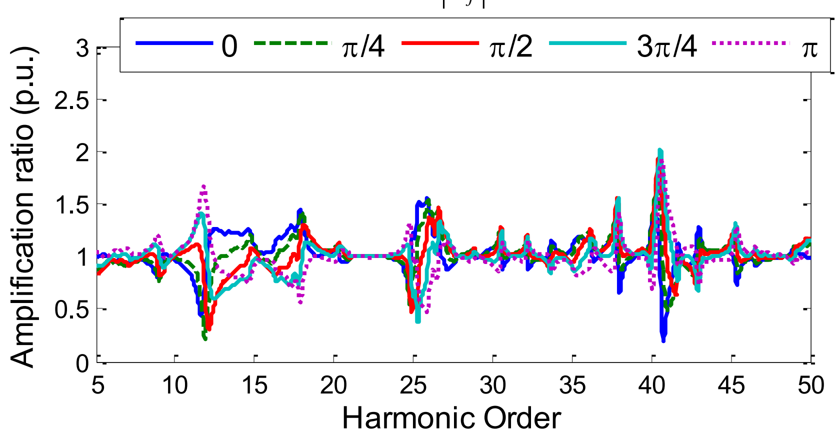

(c) $\left|\frac{V_i}{V_j}\right| = 2$

Figure 5.20: HAR_{actual} at a remote bus indirectly connected to the 3rdHP filter installation bus with physical distance around 70km

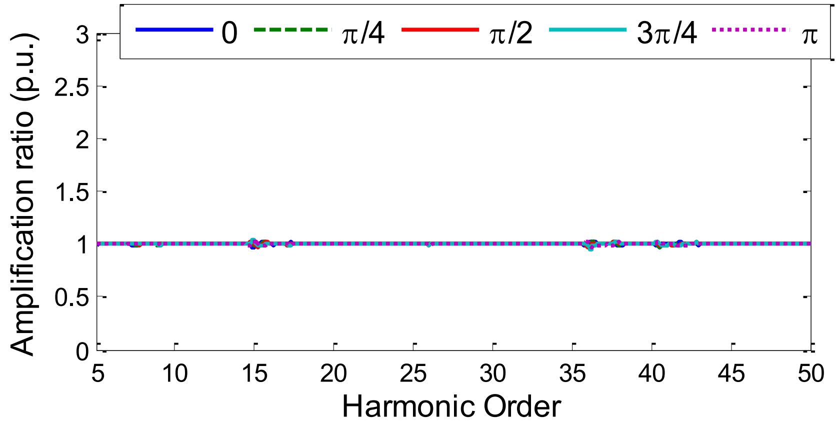

(a) $\left|\frac{V_i}{V_j}\right| = 0.5$

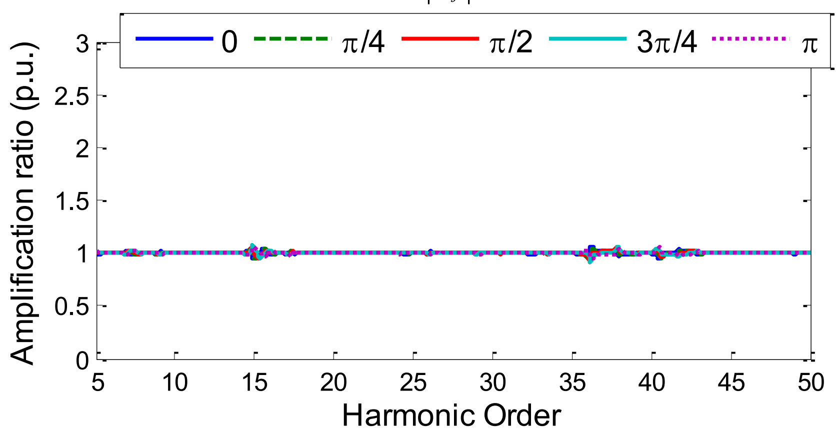

(b) $\left|\frac{V_i}{V_j}\right| = 1$

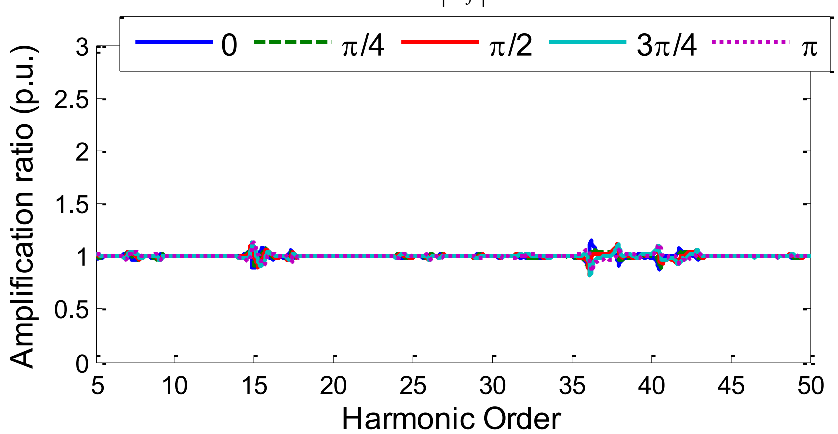

(c) $\left|\frac{V_i}{V_j}\right| = 2$

Figure 5.21: HAR_{actual} at a remote bus indirectly connected to the 3rdHP filter installation bus with physical distance around 400km

5.8 Summary

This chapter presented research findings on how to make a shunt capacitor resonance-free. The concept of resonance-free was introduced first and quantified mathematically. Based on this concept and rigorous mathematical derivations, system-independent design methods to configure a shunt capacitor as a resonance-free C-type filer or 3rdHP filer were developed. To facilitate the direct use by industry, a lookup table of per-unit filter component parameters determined by the proposed system-independent design methods was also created.

Comparative analysis was conducted on the two filter configurations. The results showed that they had comparable performance characteristics. The 3rdHP filter had more advantages in terms of higher resonance mitigation robustness against system frequency change and component parameter variations. The C-type filter had more advantages in term of the lower magnitude and shorter duration of the worst-case transient overvoltage.

In addition, the usefulness of the system impedance information was investigated. Optimization design methods based on system impedance information were also developed. Case studies revealed that the knowledge of the system impedance led to only limited performance improvement of the designed filters.

Moreover, the impact of the shunt capacitor device in a large system was investigated analytically and numerically. The results showed that the impact of installing a resonance-free shunt capacitor device at the local bus i on the remote bus j was system-dependent, and that this impact decreased with the physical distances between the two buses.

Chapter 6

Improvement of Filter Design

Traditional filter design methods consider the component loading in the design process [104, 112-115]. The loading of components impacts the component parameter selection. The design method used in this thesis breaks down the design process into two independent steps: RLC parameter determination and size (or rating) determination based on the component loading. This chapter first explains the motivation of the method used in this thesis and then details about how to determine the capacitor size (or rating) are given.

6.1 Motivation

A passive filter has three different types of components: inductors, resistors and capacitors. Inductors and resistors are typically made to order, and their ratings depend mainly on the rms current I_{rms} flowing through them. Therefore, the filter design has no loading constraints for inductors and resistors. The ratings or the sizes of the inductors and resistors can be determined by using the harmonic load flow study when the filter RLC parameters are finalized.

However, capacitors usually consist of standard units which are connected in series and/or parallel in order to obtain the desired overall voltage and kVAr rating [1]. According to IEEE Standard 1531 [95] and IEEE Standard 18-2012 [94], four loading constraints need to be considered to determine the rating of a capacitor. For a capacitor in a filter, these four loading constraints are complex functions of the filter RLC parameters and the system harmonic condition. Traditional filter design methods incorporate these constraints directly into the filter RLC parameter determination [104, 112-115]. The filter RLC parameter and component size (or rating) are determined in a coupled way, which involves solving a high-dimensional non-linear non-convex complex constraint programming problem.

To avoid the exceptional computational burden of the traditional design methods and motivated by how the ratings of inductors and resistors are determined, this thesis proposes to break down the filter design process into two decoupled steps. The first step is RLC parameter determination and the second step is component size (or rating) determination based on the component loading. Examples of how RLC parameter determination is done for different filters are provided in Chapter 3, Chapter 4 and Chapter 5. The sizes (or ratings) of inductors or resistors can be directly determined by using I_{rms}. The following section describes a way to determine the capacitor size (or rating) by merging the four loading constraints into one.

6.2 Capacitor Size Determination

This section first presents how to determine the size of the capacitor in terms of the minimum voltage rating based on the four loading constraints given in IEEE Standard 1531[95] and IEEE Standard 18-2012[94]. Then the method to obtain the number of basic capacitor units to assemble the capacitor of the required voltage rating is described. Finally, the proposed methods are illustrated by using a numerical example.

6.2.1 Minimum Voltage Rating

The loading of the capacitor is defined in terms of the following four indices:

1) rms voltage V_{rms}
2) peak voltage V_{peak}
3) rms current I_{rms}
4) kVAr Q

The above indices can be determined by using the harmonic load flow study once the parameters (i.e., capacitance, inductance and resistance) of all the components in a filter are determined.

According to IEEE Standard 1531[95] and IEEE Standard 18-2012[94], the loading of the utilized capacitors, which have to be capable of continuous operation under contingency system and bank conditions, should not exceed the following limitations:

1) 110% of rated rms voltage V_{rated}, i.e.,

$$V_{\text{rms}} \leq 1.1 \times V_{\text{rated}}; \tag{6.1}$$

2) 120% of rated peak voltage, i.e.,

$$V_{\text{peak}} \leq 1.2 \times \sqrt{2} V_{\text{rated}}; \tag{6.2}$$

3) 135% of nominal rms current I_{rated} based on rated kVAr Q_{rated} and rated rms voltage V_{rated}, i.e.,

$$I_{\text{rms}} \leq 1.35 \times I_{\text{rated}}, \tag{6.3}$$

where $I_{\text{rated}} = Q_{\text{rated}} / V_{\text{rated}}$;

4) 135% of rated kVAr, i.e.,

$$Q \leq 1.35 \times Q_{\text{rated}}. \tag{6.4}$$

Further, V_{rated}, I_{rated} and Q_{rated} correlate with each other through the following equations:

$$I_{\text{rated}} = \omega_1 C V_{\text{rated}}, \tag{6.5}$$

$$Q_{\text{rated}} = \omega_1 C V_{\text{rated}}^2, \tag{6.6}$$

where ω_1 is the fundamental angular frequency, C is the capacitance of the capacitor.

By using equations (6.1) to (6.6), the following inequality is obtained:

$$V_{\text{rated}} \geq \max\left\{\frac{V_{\text{rms}}}{1.1}, \frac{V_{\text{peak}}}{1.2\sqrt{2}}, \frac{I_{\text{rms}}}{1.35 \times \omega_1 C}, \sqrt{\frac{Q}{1.35 \times \omega_1 C}}\right\}. \tag{6.7}$$

As a result, the minimum rating of the capacitor with a 10% safe margin in terms of the rms voltage, $V_{\min}$ is given by

$$V_{\min} = 1.1 \times \max\left\{ \frac{V_{\text{rms}}}{1.1},\ \frac{V_{\text{peak}}}{1.2\sqrt{2}},\ \frac{I_{\text{rms}}}{1.35 \times \omega_1 C},\ \sqrt{\frac{Q}{1.35 \times \omega_1 C}} \right\}. \tag{6.8}$$

6.2.2 Basic Capacitor Unit Number Determination

The capacitor is an assembly of basic capacitor units. This subsection further gives the method for how to determine the number of the basic capacitor units in order to construct the capacitor, after its capacitance C and minimum rating (for example, the minimum rated rms voltage $V_{\min}$) are known.

The basic capacitor unit is characterized by its rated terminal to terminal rms voltage V_0 and rated kVAr Q_0. The capacitor is essentially composed of a certain number of parallel branches which consist of a certain number of series connected basic capacitor units. The number of parallel branches (*m*) and the number of the basic capacitor units (*n*) in each branch are determined by using an iterative process as follows:

1) Initially, the number of the basic capacitor units in each branch is set as

$$n = \left\lceil \frac{V_p}{V_0} \right\rceil, \tag{6.9}$$

   where $V_p = V_{\min}$, if the capacitor is a single phase capacitor or a three phase delta connected capacitor, $V_p = V_{\min} / \sqrt{3}$ if the capacitor is a three phase Y connected capacitor, and $\lceil\ \rceil$ represents the function that rounds its element to the nearest integer towards infinity.

2) Calculate the rated rms phase voltage of the capacitor V_{prated} by using

$$V_{prated} = nV_0. \tag{6.10}$$

3) Calculate the rated kVAr of the capacitor by using

$$Q_{rated} = p\omega_1 C V_{prated}^2 , \tag{6.11}$$

where $p = 1$ for a single phase capacitor and $p = 3$ for a three phase capacitor.

4) If the rated kVAr Q_{rated} is larger than a specified limit $Q_{\max}$, i.e., $Q_{rated} > Q_{\max}$, stop the process. There is no reasonable configuration for the basic capacitor unit of the given type to construct the required capacitor. Otherwise, go to step 5).
5) Calculate the number of branches m by using

$$m = \left\lceil \frac{Q_{rated}}{pnQ_0} \right\rceil . \tag{6.12}$$

6) Calculate the total capacitance of the assembled capacitor by using

$$C_{Total} = \frac{m}{n} \frac{Q_0}{\omega V_0^2} . \tag{6.13}$$

7) Check if the value of C_{Total} is in the acceptable range $[0.9C,\ C]$, which is established based on the capacitance manufacturing variance [95].
8) If the value of C_{Total} is in the acceptable range, then the configuration of the given type of basic capacitor to construct the required capacitor is to have m branches, which consist of n series connected basic capacitor units in each phase. Output these results. Otherwise, let n=n+1 and go to step 2).

The above process is also depicted as Figure 6.1.

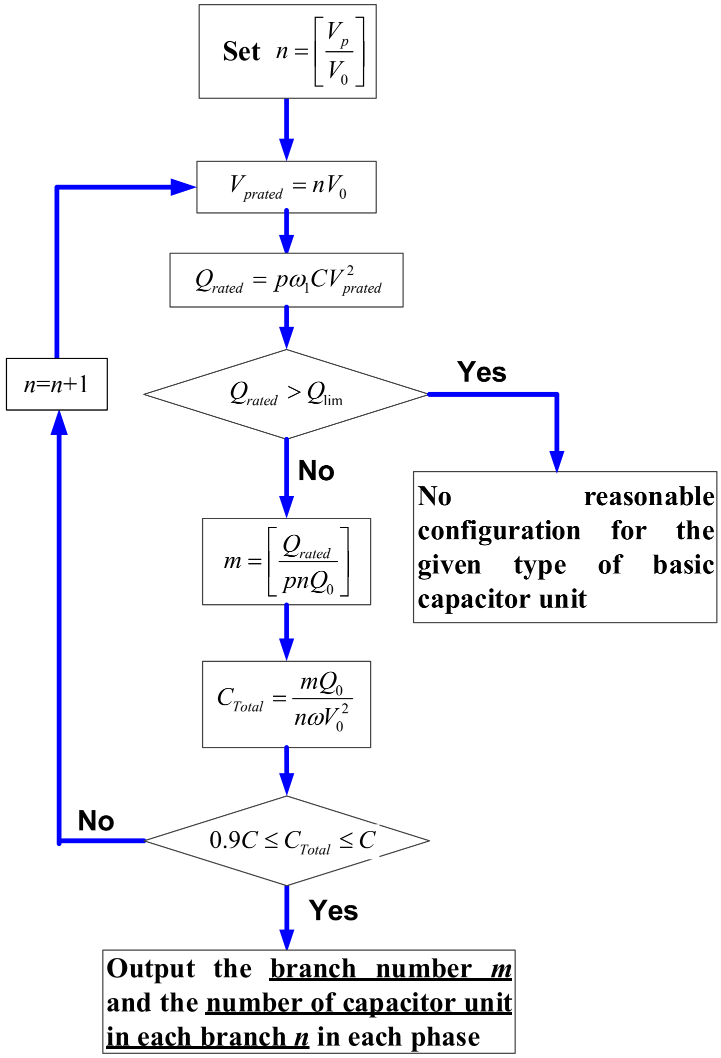

Figure 6.1: Basic capacitor unit number determination

6.2.3 Numerical Example

This subsection uses the determination of the size (in terms of the minimum voltage rating) of the auxiliary capacitor C_2 in the 3rdHP filter configured shunt capacitor designed in Section 5.4.2 as an example.

For the case studied in Section 5.4.2, the capacitance of C_2 of the designed 3rdHP filter configured shunt capacitor and its loading indices are as follows:

1) $C_2 = 2.06$ uF
2) $V_{rms} = 8.89$ kV
3) $V_{peak} = 30.06$ kV

4) I_{rms} = 17.40 A
5) Q = 0.21 MVAr

Take the above data into equation (6.8); then the minimum voltage rating $V_{\min}$ for the auxiliary capacitor is obtained as 31.59 kV.

Suppose the basic capacitor unit used to assemble the auxiliary capacitor C_2 has a rated terminal to terminal rms voltage V_0 of 11.4 kV and a rated kVAr Q_0 of 50 kVAr. By using the procedure given in subsection 6.2.2, the number of parallel branches and the number of the basic capacitor units in each branch used to construct the auxiliary capacitor C_2 are obtained as 4 and 2, respectively.

6.3 Summary

This chapter presented the motivation to decouple the loading constraints from the filter component parameter determination. The method to determine the capacitor size (or rating) based on the capacitor's loading indices was also given along with the procedure to calculate the number of basic capacitor units used to construct the capacitor with the required capacitance and rating. This chapter also included a numerical example to showcase the application of the proposed method and procedure.

Chapter 7

Conclusions and Future Work

7.1 Thesis Conclusions and Contributions

This thesis approached topics related to the modeling and mitigation of the harmonic distortions caused by mass-distributed harmonic sources. The existing measures are not always effective in managing the new harmonic situation of today's power systems, which consist of a large number of small and dispersed harmonic sources. An extensive set of studies was conducted to propose and assess different methods for effectively modeling and mitigating the harmonic distortions caused by mass-distributed harmonic sources. All the discussed modeling and mitigating methods were evaluated by performing simulation studies or theoretical analysis. The key conclusions and contributions of this thesis can be summarized as follows.

- An analytical method was proposed to establish a probabilistic harmonic model for the secondary residential system. This method derives the aggregate secondary system model based on the electrical model and the random usage pattern model of home appliances, to account for the technological advances and the behavior evolution of consumers. The resulting model is a time-varying steady-state probabilistic equivalent circuit model whose parameters are characterized bivariate normal distributions. The model can be easily implemented for primary system harmonic assessment. Extensive case studies based on the proposed analytical method and the MCS method confirmed the effectiveness and efficiency of the proposed method.
- A novel and effective scheme to prevent harmonic currents from propagating into the transmission systems was proposed. Its basic idea is to utilize the low-voltage tertiary winding of a substation transformer to create a tuned low-impedance path for the harmonics. The scheme further consists of a new filter topology that can trap two ZS harmonics and three NZS harmonics

simultaneously. The design issues of the proposed filters were investigated and solved. Extensive case studies validated both the proposed tertiary winding filter and its design method.

- A complete and simple design method in terms of four design formulas was established for the 3rdHP filter. Rigorous mathematical derivations provided a solid foundation for the proposed method. The case study results also confirmed that the proposed method resulted in a 3rdHP filter with a minimal fundamental frequency loss.
- The concept of resonance-free was introduced and quantified mathematically. Through rigorous mathematical derivations, system-independent design methods to configure a shunt capacitor as a resonance-free C-type filer or 3rdHP filer were developed. A lookup table of per-unit component parameters for both the C-type filter and the 3rdHP filter with guaranteed resonance-free performance was also created for the direct use by industry. The two filter configurations were compared thoroughly by case studies. The results showed that they have comparable performance characteristics. Moreover, the usefulness of the system impedance information was investigated. The case study results revealed that the optimized design based on the system impedance information yielded little performance improvement and cost reduction.
- This thesis also proposed to decouple the component size determination and the component parameter determination in the filter design and gave a practical method for determining the capacitor size according to the capacitor's loading conditions.

7.2 Suggestions for Future Work

The author’s suggestions for continuing the studies on modeling and mitigating of harmonic distortions caused by mass-distributed harmonic sources are as follows.

- In this thesis, an analytical method for building an aggregate harmonic model for a secondary residential system was developed. The extension of this work is to develop a method for building an aggregate harmonic model for a whole residential distribution system. The developed method should be able to merge all aggregate secondary system harmonic models in a residential distribution system into one model. It should be noted that the distribution of service transformers in the primary feeder is much more dispersed than that of the households in the secondary feeders. Besides, the service transformers are usually not evenly connected to the three phases of the primary feeder. Moreover, there may be capacitor banks in the primary feeder. All these features will significantly affect the harmonic current aggregation at the residential distribution substation. Therefore, the method to be developed should have the ability to quantify these impacts.

- As the proposed tertiary winding filter in Chapter 3 inserts multiple LC components into the delta connected tertiary winding of the substation transformer, its corresponding impact on the protection setting of the transformer should be investigated through theoretical analysis and simulation studies.
- A transmission system usually connects multiple residential distribution systems. As shown by the transmission system case studies in Chapter 3, due to the inherent characteristics of a transmission network, the harmonic currents injected from different residential distribution systems have different impacts on the transmission system. Therefore, when the filter resources are limited, it is necessary to find optimal locations to implement them either for the purpose of reducing the overall harmonic distortion level of the transmission system or to tackle a specific harmonic issue at a certain point in the transmission system (such as the overloading of the capacitors at a HVDC station).
- A rough cost estimation was made for the filter in Chapter 4 and Chapter 5, based on the limited cost data collected from utility companies. When more cost data are available, a more precise cost analysis on resonance-free capacitors of different filter configurations can be conducted.

References

[1] J. Arrillaga, D. A. Bradley, and P. S. Bodger, *Power System Harmonics*: John Wiley & Sons, 1985.

[2] V. E. Wagner, J. C. Balda, D. C. Griffith, A. McEachern, T. M. Barnes, D. P. Hartmann*, et al.*, "Effects of harmonics on equipment," *Power Delivery, IEEE Transactions on,* vol. 8, pp. 672-680, Apr. 1993.

[3] G. C. Montanari and D. Fabiani, "The effect of nonsinusoidal voltage on intrinsic aging of cable and capacitor insulating materials," *Dielectrics and Electrical Insulation, IEEE Transactions on,* vol. 6, pp. 798-802, Dec. 1999.

[4] S. B. Gin, J. H. Sawada, and T. R. Treasure, "BC Hydro harmonic resonance experience," in *2000 IEEE Power Engineering Society Summer Meeting*, Seattle, WA, USA, 2000, pp. 1088-1093 vol. 2.

[5] G. J. Wakileh, *Power Systems Hamronics: Fundamentals, Analysis and Filter Design*. Berlin: Springer-Verlag, 2001.

[6] "IEEE Recommended Practice and Requirements for Harmonic Control in Electric Power Systems," *IEEE Std 519-2014 (Revision of IEEE Std 519-1992),* pp. 1-29, 2014.

[7] A. Nassif, "Modeling, measurement and mitigation of power system harmonics," PhD thesis, Dept. Elect. Comput. Eng., Univ. Alberta, Edmonton, AB, Canada, 2009.

[8] Q. Shi, "Power quality impact of photovoltaic systems on residential distribution networks," M. Sc. dissertation, Dept. Elect. Comput. Eng., Univ. Alberta, Edmonton, AB, Canada, 2014.

[9] Y. Wang, J. Yong, Y. Sun, W. Xu, and D. Wong, "Characteristics of harmonic distortions in residential distribution systems," *Power Delivery, IEEE Transactions on,* vol. 32, pp. 1495-1504, Jun. 2017.

[10] G. Todeschini, D. R. Mueller, and G. Y. Morris, "Telephone interference caused by harmonics in distribution systems: Analysis and simulations," in *2013 IEEE Power & Energy Society General Meeting*, Vancouver, BC, Canada, 2013, pp. 1-5.

[11] J. Desmet, G. Vanalme, C. Debruyne, and L. Vandevelde, "Influence of harmonic currents on cable losses for different grid configurations," in *14th International Conference on Harmonics and Quality of Power (ICHQP)*, Bergamo, Lombardy, Italy, 2010, pp. 1-6.

[12] "Principles and Practices of Electrical Coordination between Pipelines and Electric Supply Lines," *CSA Standard C22.3 No.6-13,* 2013.

[13] C. Jiang, R. Torquato, D. Salles, and W. Xu, "Method to assess the power-quality impact of plug-in electric vehicles," *Power Delivery, IEEE Transactions on,* vol. 29, pp. 958-965, Apr. 2014.

[14] W. Xu, J. R. Marti, and H. W. Dommel, "A multiphase harmonic load flow solution technique," *Power Systems, IEEE Transactions on,* vol. 6, pp. 174-182, Feb. 1991.

[15] I. Richardson, M. Thomson, D. Infield, and C. Clifford, "Domestic electricity use: A high-resolution energy demand model," *Energy and Buildings,* vol. 42, pp. 1878-1887, Oct. 2010.

[16] D. Salles, C. Jiang, W. Xu, W. Freitas, and H. E. Mazin, "Assessing the collective harmonic impact of modern residential loads -- Part I: Methodology," *Power Delivery, IEEE Transactions on,* vol. 27, pp. 1937-1946, Oct. 2012.

[17] C. Jiang, D. Salles, W. Xu, and W. Freitas, "Assessing the collective harmonic impact of modern residential loads--Part II: Applications," *Power Delivery, IEEE Transactions on,* vol. 27, pp. 1947-1955, Oct. 2012.

[18] A. Mau Teng and J. V. Milanovic, "Development of stochastic aggregate harmonic load model based on field measurements," *Power Delivery, IEEE Transactions on* vol. 22, pp. 323-330, Jan. 2007.

[19] A. Mau Teng and J. V. Milanovic, "Establishing harmonic distortion level of distribution network based on stochastic aggregate harmonic load models," *Power Delivery, IEEE Transactions on,* vol. 22, pp. 1086-1092, Apr. 2007.

[20] A. Mansoor, W. M. Grady, P. T. Staats, R. S. Thallam, M. T. Doyle, and M. J. Samotyj, "Predicting the net harmonic currents produced by large numbers of distributed single-phase computer loads," *Power Delivery, IEEE Transactions on,* vol. 10, pp. 2001-2006, Oct. 1995.

[21] S. Bhattacharyya, S. Cobben, P. Ribeiro, and W. Kling, "Harmonic emission limits and responsibilities at a point of connection," *Generation, Transmission & Distribution, IET,* vol. 6, pp. 256-264, 2012.

[22] H. Sharma, M. Rylander, and D. Dorr, "Grid impacts due to increased penetration of newer harmonic sources," in *2013 IEEE Rural Electric Power Conference (REPC)*, Stone Mountain, GA, USA, 2013, pp. B5-1-B5-5.

[23] K. D. McBee and M. G. Simoes, "Evaluating the long-term impact of a continuously increasing harmonic demand on feeder-level voltage distortion," *Industry Applications, IEEE Transactions on,* vol. 50, pp. 2142-2149, May/Jun. 2014.

[24] "Power quality impact from mass penetration of energy efficient and consumer electronic devices," CEATI International Inc.Sept. 2011.

[25] Bonneville Power Administration (2013, Nov.). Technical Requirements for Interconnection to the BPA Transmission Grid [Online]. Available: http://www.bpa.gov/transmission/Doing%20Business/Interconnection/Documents/tech_requirements_interconnection.pdf

[26] NGET plc (2014, Aug.). The Grid Code [Online]. Available: http://www2.nationalgrid.com/uk/industry-information/electricity-codes/grid-code/the-grid-code/

[27] "Electromagnetic compatibility (EMC) Part 3-2: Limits for harmonic current emissions (equipment input current ≤16A per phase)," *IEC 61000-3-2,* 2009.

[28] A. B. Nassif, W. Xu, and W. Freitas, "An investigation on the selection of filter topologies for passive filter applications," *Power Delivery, IEEE Transactions on,* vol. 24, pp. 1710-1718, Jul. 2009.

[29] A. Mau Teng and J. V. Milanovic, "Planning approaches for the strategic placement of passive harmonic filters in fadial distribution networks," *Power Delivery, IEEE Transactions on,* vol. 22, pp. 347-353, Jan. 2007.

[30] Q. Shi, H. Liang, T. Hou, L. Bai, W. Xu, and F. Li, "Passive filter installation for harmonic mitigation of residential distribution systems," in *2017 IEEE Power Engineering Society General Meeting*, Chicago, IL, 2017, pp. 1-5.

[31] CIGRE WG 14.03, "AC harmonic filter and reactive compensation for HVDC: a general survey," *Electra,* no. 63, 1979.

[32] CIGRE WG 14.03, "AC harmonic filters and reactive compensation for HVDC with particular reference to non-characteristic hamonics," Tech. Rep. TB-065, Jun. 1990.

[33] Y. Xiao, "The method for designing the third order filter," in *8th International Conference On Harmonics and Quality of Power (ICHQP)*, Athens, Greece, 1998, pp. 139-142.

[34] P. Kundur, N. J. Balu, and M. G. Lauby, *Power System Stability and Control* vol. 7: McGraw-Hill New York, 1994.

[35] T. M. Blooming and D. J. Carnovale, "Capacitor application issues," *Industry Applications, IEEE Transactions on,* vol. 44, pp. 1013-1026, Jul./Aug. 2008.

[36] G. W. Chang, W. C. Chang, C. S. Chuang, and D. Y. Shih, "Fuzzy logic and immune-based algorithm for placement and sizing of shunt capacitor banks in a distorted power network," *Power Delivery, IEEE Transactions on,* vol. 26, pp. 2145-2153, Oct. 2011.

[37] M. De and S. K. Goswami, "Optimal reactive power procurement with voltage stability consideration in deregulated power system," *Power Systems, IEEE Transactions on,* vol. 29, pp. 2078-2086, Sept. 2014.

[38] H. Ahmadi and J. R. Marti, "Distribution system optimization based on a linear power-flow formulation," *Power Delivery, IEEE Transactions on,* vol. 30, pp. 25-33, Feb. 2015.

[39] J. C. Das, *Power System Harmonics and Passive Filter Designs*: John Wiley & Sons, Inc, 2015.

[40] N. Eghtedarpour, M. A. Karimi, and M. Tavakoli, "Harmonic resonance in power systems - a documented case," in *16th International Conference on Harmonics and Quality of Power (ICHQP)*, Bucharest, Romania, 2014, pp. 857-861.

[41] R. Koch and N. Gumede, "The impact of harmonic resonance conditions on the connection rules for large industrial installations," in *2005 IEEE Power Engineering Society Inaugural Conference and Exposition in Africa*, Durban, South Africa, 2005, pp. 320-325.

[42] C. H. Hu, C. J. Wu, S. S. Yen, Y. W. Chen, B. A. Wu, and J. S. Hwang, "Survey of harmonic voltage and current at distribution substation in Northern Taiwan," *Power Delivery, IEEE Transactions on,* vol. 12, pp. 1275-1284, Jul. 1997.

[43] G. T. Heydt, H. U. Patil, J. Loehr, and T. LaRose, "Harmonic resonance assessment for transmission class shunt capacitors," in *2016 IEEE/PES Transmission and Distribution Conference and Exposition (T&D)*, Dallas, TX, USA, 2016, pp. 1-5.

[44] R. R. A. Fortes, L. C. O. Oliveira, J. B. d. Souza, R. F. Buzo, and J. J. P. Álvarez, "Harmonic resonance in electrical grids with photovoltaic distributed generation," in *17th International Conference on Harmonics and Quality of Power (ICHQP)*, Belo Horizonte, Brazil, 2016, pp. 214-219.

[45] E. Ebrahimzadeh, F. Blaabjerg, X. Wang, and C. L. Bak, "Efficient approach for harmonic resonance identification of large wind power plants," in *2016 IEEE 7th International Symposium on Power Electronics for Distributed Generation Systems (PEDG)*, Vancouver, BC, Canada, 2016, pp. 1-7.

[46] C. Nie, W. Lei, H. Wang, K. Zhang, and Y. Wang, "Modeling and analysis of harmonic resonance in microgrid and research of active harmonic resistance method," in *9th International Conference on Power Electronics and ECCE Asia (ICPE-ECCE Asia)*, Seoul, South Korea, 2015, pp. 2489-2494.

[47] Y. Li, F. Liu, T. K. Saha, O. Krause, and Y. Cao, "Hybrid inductive and active filtering method for damping harmonic resonance in distribution network with non-linear loads," *IET Power Electronics,* vol. 8, pp. 1616-1624, 2015.

[48] Q. Shi, H. Hu, W. Xu, and J. Yong, "Low - order harmonic characteristics of photovoltaic inverters," *International Transactions on Electrical Energy Systems,* vol. 26, pp. 347-364, Feb. 2016.

[49] H. Hu, Q. Shi, Z. He, J. He, and S. Gao, "Potential harmonic resonance impacts of PV inverter filters on distribution systems," *IEEE Transactions on Sustainable Energy,* vol. 6, pp. 151-161, Jan. 2015.

[50] Z. Huang, W. Xu, and V. R. Dinavahi, "A practical harmonic resonance guideline for shunt capacitor applications," *Power Delivery, IEEE Transactions on,* vol. 18, pp. 1382-1387, Oct. 2003.

[51] C. Santos, L. Jorge, A. Blanco, F. Bastiao, L. Ferreira, P. Carvalho*, et al.*, "Voltage distortion in large-scale MV and HV distribution networks: Harmonic analysis and simulation," in *CIRED 20th International Conference and Exhibition on Electricity Distribution - Part 1*, Prague, Czech Republic, 2009, pp. 1-4.

[52] K. Yang, M. H. J. Bollen, and E. O. Anders Larsson, "Aggregation and amplification of wind-turbine harmonic emission in a wind park," *Power Delivery, IEEE Transactions on,* vol. 30, pp. 791-799, Apr. 2015.

[53] H. L. Santos, J. O. S. Paulino, W. C. Boaventura, L. M. R. Baccarini, and M. L. Murta, "Harmonic distortion influence on grounded wye shunt capacitor banks protection: experimental results," *Power Delivery, IEEE Transactions on,* vol. 28, pp. 1289-1296, Apr. 2013.

[54] A. Capasso, W. Grattieri, R. Lamedica, and A. Prudenzi, "A bottom-up approach to residential load modeling," *Power Systems, IEEE Transactions on,* vol. 9, pp. 957-964, May 1994.

[55] E. Carpaneto and G. Chicco, "Probabilistic characterisation of the aggregated residential load patterns," *Generation, Transmission & Distribution, IET,* vol. 2, pp. 373-382, 2008.

[56] R. Torquato, Q. Shi, W. Xu, and W. Freitas, "A Monte Carlo simulation platform for studying low voltage residential networks," *Smart Grid, IEEE Transactions on,* vol. 5, pp. 2766-2776, Nov. 2014.

[57] C. S. Chen, J. C. Hwang, and C. W. Huang, "Application of load survey systems to proper tariff design," *Power Systems, IEEE Transactions on,* vol. 12, pp. 1746-1751, Nov. 1997.

[58] J. A. Jardini, C. M. V. Tahan, M. R. Gouvea, A. Se Un, and F. M. Figueiredo, "Daily load profiles for residential, commercial and industrial low voltage consumers," *Power Delivery, IEEE Transactions on,* vol. 15, pp. 375-380, Jan. 2000.

[59] R. F. Chang, R. C. Leou, and C. N. Lu, "Distribution transformer load modeling using load research data," *Power Delivery, IEEE Transactions on,* vol. 17, pp. 655-661, Apr. 2002.

[60] Task Force on Harmonic Modeling and Simulation, "Modeling and simulation of the propagation of harmonics in electric power networks. I. Concepts, models, and simulation techniques," *Power Delivery, IEEE Transactions on,* vol. 11, pp. 452-465, Jan. 1996.

[61] J. Yong, L. Chen, and S. Chen, "Modeling of home appliances for power distribution system harmonic analysis," *IEEE Transactions on Power Delivery,* vol. 25, pp. 3147-3155, Oct. 2010.

[62] J. Molina and L. Sainz, "Model of electronic ballast compact fluorescent lamps," *Power Delivery, IEEE Transactions on,* vol. 29, pp. 1363-1371, Jun. 2014.

[63] W. G. Sherman, "Summation of harmonics with random phase angles," *Electrical Engineers, Proceedings of the Institution of,* vol. 119, pp. 1643-1648, Nov. 1972.

[64] S. R. Kaprielian, A. E. Emanuel, R. V. Dwyer, and H. Mehta, "Predicting voltage distortion in a system with multiple random harmonic sources," *Power Delivery, IEEE Transactions on,* vol. 9, pp. 1632-1638, Jul. 1994.

[65] Y. Baghzouz, R. F. Burch, A. Capasso, A. Cavallini, A. E. Emanuel, M. Halpin*, et al.*, "Time-varying harmonics. II. Harmonic summation and propagation," *Power Delivery, IEEE Transactions on,* vol. 17, pp. 279-285, Jan. 2002.

[66] A. Cavallini and G. C. Montanari, "A deterministic/stochastic framework for power system harmonics modeling," *Power Systems, IEEE Transactions on,* vol. 12, pp. 407-415, Feb. 1997.

[67] P. T. Staats, W. M. Grady, A. Arapostathis, and R. S. Thallam, "A statistical method for predicting the net harmonic currents generated by a concentration of electric vehicle battery chargers," *Power Delivery, IEEE Transactions on,* vol. 12, pp. 1258-1266, Jul. 1997.

[68] P. T. Staats, W. M. Grady, A. Arapostathis, and R. S. Thallam, "A statistical analysis of the effect of electric vehicle battery charging on distribution system harmonic voltages," *Power Delivery, IEEE Transactions on,* vol. 13, pp. 640-646, Apr. 1998.

[69] M. Bell, M. Swinton, E. Entchev, J. Gusdorf, W. Kalbfleisch, R. Marchand*, et al.*, "Development of micro combined heat and power technology assessment capability at the Canadian Centre for Housing Technology," Ottawa, ON, Canada2003.

[70] J. Janssen and R. de Dominicis, "Finite non-homogeneous semi-Markov processes: Theoretical and computational aspects," *Insurance: Mathematics and Economics,* vol. 3, pp. 157-165, Jul. 1984.

[71] A. Platis, N. Limnios, and M. L. Du, "Hitting time in a finite non-homogeneous Markov chain with applications," *Applied Stochastic Models and Data Analysis,* pp. 241-253, 1998.

[72] F. Eicker, "A multivariate central limit theorem for random linear vector forms," *The Annals of Mathematical Statistics,* pp. 1825-1828, Feb. 1966.

[73] H. Kobayashi, B. L. Mark, and W. Turin, *Probability, random processes, and statistical analysis*: New York : Cambridge University Press, 2012.

[74] S. J. Julier and J. K. Uhlmann, "New extension of the Kalman filter to nonlinear systems," in *AeroSense'97*, Orlando, Florida, USA, 1997, pp. 182-193.

[75] E. A. Wan and R. Van der Merwe, "The unscented Kalman filter for nonlinear estimation," in *2000 IEEE Adaptive Systems for Signal Processing,*

Communications, and Control Symposium, Lake Louise, Alta., USA, 2000, pp. 153-158.
[76] S. J. Julier and J. K. Uhlmann, "Unscented filtering and nonlinear estimation," *Proceedings of the IEEE,* vol. 92, pp. 401-422, Mar. 2004.
[77] IPSOS-RSL and Office for National Statistics, “United Kingdom Time Use Survey, 2000” (computer file), 3rd ed. Colchester, Essex, U.K., U.K. Data Archive (distributor), 2003.
[78] Statistics Canada, 2011 Census of Population, Statistics Canada Catalogue no. 98-313-XCB2011026. [Online]. Available: http://www12.statcan.gc.ca/datasets/Index-eng.cfm?Temporal=2011&Theme=91
[79] Natural Resources Canada, Micro-Hydro Systems - A Buyer's Guide [Online]. Available: https://www.nrcan.gc.ca/energy/publications/sciences-technology/renewable/6487
[80] C. Jiang, "A probabilistic bottom-up technique for modeling and simulation of residential distributed harmonic sources," M. Sc. thesis, Dept. Elect. Comput. Eng., Univ. Alberta, Edmonton, AB, Canada, 2012.
[81] Y. H. Lin and M. S. Tsai, "Non-intrusive load monitoring by novel neuro-fuzzy classification considering uncertainties," *Smart Grid, IEEE Transactions on,* vol. 5, pp. 2376-2384, Sept. 2014.
[82] E. Garcia, "Cosine similarity and term weight tutorial," *Information retrieval intelligence,* 2006.
[83] W. Jewell, W. L. Miller, and T. Casey, "Filtering dispersed harmonic sources on distribution," *Power Delivery, IEEE Transactions on,* vol. 15, pp. 1045-1051, Jul. 2000.
[84] C. J. Wu, J. C. Chiang, S. S. Yen, C. J. Liao, J. S. Yang, and T. Y. Guo, "Investigation and mitigation of harmonic amplification problems caused by single-tuned filters," *Power Delivery, IEEE Transactions on,* vol. 13, pp. 800-806, Jul. 1998.
[85] H. L. Jou, J. C. Wu, K. D. Wu, W. J. Chiang, and Y. H. Chen, "Analysis of zig-zag transformer applying in the three-phase four-wire distribution power system," *Power Delivery, IEEE Transactions on,* vol. 20, pp. 1168-1173, Apr. 2005.
[86] E. Larsen, "Filter for removing harmonic current from a neutral conductor," US Patent 5 914 540, Jun. 22, 1999.
[87] P. Bagheri and W. Xu, "A technique to mitigate zero-sequence harmonics in power distribution systems," *Power Delivery, IEEE Transactions on,* vol. 29, pp. 215-223, Feb. 2014.
[88] "IEEE Guide for Application and Specification of Harmonic Filters," *IEEE Std 1531-2003,* pp. 0_1-60, 2003.
[89] J. C. Das, "Passive filters - potentialities and limitations," *Industry Applications, IEEE Transactions on,* vol. 40, pp. 232-241, Jan./Feb. 2004.
[90] H. Hu, Z. He, and S. Gao, "Passive filter design for China high-speed railway with considering harmonic resonance and characteristic harmonics," *Power Delivery, IEEE Transactions on,* vol. 30, pp. 505-514, Feb. 2015.
[91] S. V. Kulkarni and S. Khaparde, *Transformer engineering: design and practice* vol. 25: CRC Press, 2004.
[92] P. Anderson, *Analysis of Faulted Power Systems*: Wiley-IEEE Press, 1995.

[93] "IEEE Application Guide for AC High-Voltage Circuit Breakers Rated on a Symmetrical Current Basis," *ANSI/IEEE C37.010-1979,* pp. 1-54, 1979.
[94] "IEEE Standard for Shunt Power Capacitors," *IEEE Std 18-2012 (Revision of IEEE Std 18-2002),* pp. 1-39, 2013.
[95] "IEEE Guide for Application and Specification of Harmonic Filters," *IEEE Std 1531-2003,* pp. 1-60, 2003.
[96] T. Ding and W. Xu, "A filtering scheme to reduce the penetration of harmonics into transmission systems," *Power Delivery, IEEE Transactions on,* vol. 31, pp. 59-66, Feb. 2016.
[97] R. Abu-Hashim, R. Burch, G. Chang, M. Grady, E. Gunther, M. Halpin*, et al.*, "Test systems for harmonics modeling and simulation," *Power Delivery, IEEE Transactions on,* vol. 14, pp. 579-587, Apr. 1999.
[98] L. Helle, J. Nieuwenuizen, and M. Lidholm, "Low-voltage harmonic filter for full-scale converter systems," US Patent 2010/0118568 A1, May 13, 2010.
[99] C. J. Chou, C. W. Liu, J. Y. Lee, and K. D. Lee, "Optimal planning of large passive-harmonic-filters set at high voltage level," *Power Systems, IEEE Transactions on,* vol. 15, pp. 433-441, Feb. 2000.
[100] S. Boyd and L. Vandenberghe, *Convex optimization*: Cambridge university press, 2004.
[101] G. Lemieux, "Power system harmonic resonance-a documented case," *IEEE Transactions on Industry Applications,* vol. 26, pp. 483-488, May/Jun. 1990.
[102] J. R. Macedo Jr., J. W. Resende, and M. I. Samesima, "Design and performance of shunt tuned filter on the MV side of distribution systems," in *13th International Conference on Harmonics and Quality of Power (ICHQP)*, Wollongong, Australia, 2008, pp. 1-5.
[103] "IEEE Guide for the Application of Shunt Power Capacitors," *IEEE Std 1036-2010 (Revision of IEEE Std 1036-1992),* pp. 1-88, 2011.
[104] S. H. E. Abdel Aleem, A. F. Zobaa, and M. Mamdouh Abdel Aziz, "Optimal C-type passive filter based on minimization of the voltage harmonic distortion for nonlinear loads," *Industrial Electronics, IEEE Transactions on,* vol. 59, pp. 281-289, Jan. 2012.
[105] R. Horton, R. Dugan, and D. Hallmark, "Novel design methodology for C-type harmonic filter banks applied in HV and EHV networks," in *2012 IEEE PES Transmission and Distribution Conference and Exposition (T&D)*, Orlando, FL, USA, 2012, pp. 1-6.
[106] E. W. Kimbark, *Direct Current Transmission* vol. I. USA: John Wiley & Sons, Inc., 1971.
[107] C. H. Stanley, J. J. Price, and G. L. Brewer, "Design and performance of AC filters for 12 pulse HVDC schemes," *IEE Power Electronics - Power Semiconductors and Their Application,* vol. 154, 1977.
[108] S. C. Chapra and R. P. Canale, *Numerical Methods for Engineers*, 7th ed. New York: McGraw-Hill Education, 2015.
[109] T. Ding, W. Xu, and H. Liang, "Design method for third-order high-pass Filter," *Power Delivery, IEEE Transactions on,* vol. 31, pp. 402-403, Feb. 2016.

[110] Y. Tian, J. Yong, and W. Xu, "Using short-circuit programs to simulate basic capacitor switching transients," *Power Delivery, IEEE Transactions on,* vol. 31, pp. 2332-2341, Oct. 2016.

[111] Information Technology Research Council, ITI (CBEMA) curve application note. [Online]. Available: http://www.itic.org.

[112] G. W. Chang, H. L. Wang, G. S. Chuang, and S. Y. Chu, "Passive harmonic filter planning in a power system with considering probabilistic constraints," *Power Delivery, IEEE Transactions on,* vol. 24, pp. 208-218, Jan. 2009.

[113] C. Kawann and A. E. Emanuel, "Passive shunt harmonic filters for low and medium voltage: a cost comparison study," *Power Systems, IEEE Transactions on,* vol. 11, pp. 1825-1831, Nov. 1996.

[114] A. F. Zobaa, "The optimal passive filters to minimize voltage harmonic distortion at a load bus," *Power Delivery, IEEE Transactions on,* vol. 20, pp. 1592-1597, Apr. 2005.

[115] G. W. Chang, S. Y. Chu, and H. L. Wang, "A new method of passive harmonic filter planning for controlling voltage distortion in a power system," *Power Delivery, IEEE Transactions on,* vol. 21, pp. 305-312, Jan. 2006.

Appendix A: Derivations for Resonance-Free Shunt Capacitors

This appendix presents the derivations and proofs for resonance-free shunt capacitors.

A.1 Equation to Determine R for C-type Filter Configured Shunt Capacitor

According to Figure 5.3 (b), the impedance of C-type filter is

$$Z_F(\omega) = \frac{1}{j\omega C_1} + \left(\frac{1}{j\omega C_2} + j\omega L \right) // R \ . \tag{A.1}$$

Accordingly, the reactive component $X_F(\omega)$ and resistive component $R_F(\omega)$ of C-type filter impedance are

$$\begin{cases} X_F(\omega) = \operatorname{Im}(Z_F(\omega)) = \dfrac{a_1\omega^4 + b_1\omega^2 - 1}{(\omega^2 (RC_2)^2 + (\omega^2 LC_2 - 1)^2)\omega C_1} \\ R_F(\omega) = \operatorname{Re}(Z_F(\omega)) = \dfrac{R(\omega^2 LC_2 - 1)^2}{\omega^2 (RC_2)^2 + (\omega^2 LC_2 - 1)^2} \end{cases}, \tag{A.2}$$

where

$$\begin{cases} a_1 = R^2 LC_2^2 C_1 - L^2 C_2^2 \\ b_1 = 2LC_2 - R^2 C_1 C_2 - R^2 C_2^2 \end{cases} . \tag{A.3}$$

As can be seen from equation (A.2), the denominator of $X_F(\omega)$ is always positive, $X_F(\omega_H) = 0$ is equivalent to that the numerator polynomial of $X_F(\omega)$ equals to zero when $\omega = \omega_H$, i.e.,

$$a_1\omega_H^4 + b_1\omega_H^2 - 1 = 0 . \tag{A.4}$$

Take equation (5.7) and equation (A.3) into equation (A.4), then we can get

$$\left(\frac{R^2C_1C_2}{\omega_1^2}-\frac{1}{\omega_1^4}\right)\omega_H^4+\left(\frac{2}{\omega_1^2}-R^2C_1C_2-R^2C_2^2\right)\omega_H^2-1=0\,. \tag{A.5}$$

Let $n_H=\omega_H/\omega_1$. Substitute it into equation (A.5) and rearrange the equation by taking R as the unknown variable. Then we have

$$n_H^2\omega_1^2\left((n_H^2-1)C_1C_2-C_2^2\right)R^2=(n_H^2-1)^2\,. \tag{A.6}$$

Since $n_H>1$, both sides of equation (A.6) are positive, which means

$$(n_H^2-1)C_1C_2-C_2^2>0\Rightarrow C_2<(n_H^2-1)C_1\,. \tag{A.7}$$

Then we can take square root of both sides of equation (A.6) and substitute $n_H\omega_1$ by ω_H. By moving all other terms to the left side of the equation except for *R*, equation (5.11) is obtained.

A.2 Proof of Inductive Impedance Condition for C-type Filter

Substitute equation (5.7) and equation (5.11) into equation (A.3), then

$$a_1=\left((n_H^4-2n_H^2+1)/\left(n_H^4-(1+C_2/C_1)n_H^2\right)-1\right)\omega_1^{-4}\,. \tag{A.8}$$

According to equation (5.9),

$$n_H^4-(1+C_2/C_1)n_H^2\le n_H^4-2n_H^2+1\,. \tag{A.9}$$

Hence

$$\frac{n_H^4-2n_H^2+1}{n_H^4-(1+C_2/C_1)n_H^2}\ge 1\,. \tag{A.10}$$

Therefore,

$$a_1 \geq 0 \Leftrightarrow R^2 L C_2^{\,2} C_1 - L^2 C_2^2 \geq 0 \Leftrightarrow R \geq \sqrt{L / C_1}\ . \tag{A.11}$$

Let $x = \omega^2$. Then the numerator polynomial of $X_F(\omega)$ can be represented by

$$g_H(x) = a_1 x^2 + b_1 x - 1 \tag{A.12}$$

When $a_1 > 0$, according to Vita's formulas, $g_H(x) = 0$ has one negative root x_1 and one positive root $x_2 = \omega_H^2$. Accordingly, $g_H(x)$ can be further represented as

$$g_H(x) = a_1 (x - x_1)(x - x_2)\,. \tag{A.13}$$

Then it can be seen when $x \geq x_2$, $g_H(x) \geq 0$. Since as aforementioned that the denominator of $X_F(\omega)$ is always positive, correspondingly when $\omega \geq \omega_H$, $X_F(\omega) \geq 0$.

When $a_1 = 0$, i.e., $C_2 = (n_H^2 - 1) / n_H^2 C_1$, $R = \sqrt{L / C_1}$, then $b = \omega_H^{-2}$. Hence

$$g_H(x) = x \omega_H^{-2} - 1\,. \tag{A.14}$$

As can be seen from equation (A.14), when $x \geq \omega_H^2$, $g_H(x) \geq 0$. Accordingly when $\omega \geq \omega_H$, $X_F(\omega) \geq 0$.

In summary, when equation (5.9) and equation (5.10) (or equation (5.11)) are satisfied, $a_1 \geq 0$ and $X_F(\omega) \geq 0$ for $\omega \geq \omega_H$.

A.3 Frequency to Reach Maximal *HAR*worst for C-type Filter

This section first presents the equivalent condition to reach maximal *HAR*worst, which simplifies solving maximal *HAR*worst to an easier problem and then derives the frequency to reach maximal *HAR*worst for C-type filter.

Let

$$\delta(\omega) = \frac{X_F(\omega)}{R_F(\omega)}. \tag{A.15}$$

Then according to equation (5.5), $HAR_{\text{worst}}(\omega) = \sqrt{1+\delta^2(\omega)}$. The derivative of $HAR_{\text{worst}}(\omega)$ with respect to ω is given by

$$HAR'_{\text{worst}}(\omega) = \frac{dHAR_{\text{worst}}(\omega)}{d\delta(\omega)}\delta'(\omega). \tag{A.16}$$

Since $R_F(\omega) > 0$ and $X_F(\omega) > 0$ for $\omega > \omega_H$ according to the established design condition, and the derivative of $HAR_{\text{worst}}(\omega)$ with respect to $\delta(\omega)$ is

$$\frac{dHAR_{\text{worst}}(\omega)}{d\delta(\omega)} = \frac{2\delta(\omega)}{\sqrt{1+\delta^2(\omega)}} > 0. \tag{A.17}$$

Therefore,

$$\begin{cases} HAR'_{\text{worst}}(\omega) = 0, \text{ when } \delta'(\omega) = 0 \\ HAR'_{\text{worst}}(\omega) > 0, \text{ when } \delta'(\omega) > 0 \\ HAR'_{\text{worst}}(\omega) < 0, \text{ when } \delta'(\omega) < 0 \end{cases}. \tag{A.18}$$

Accordingly, $HAR_{\text{worst}}(\omega)$ achieves its extrema when $\delta(\omega)$ achieves its extrema, that is,

$$\arg\max_{\omega \geq \omega_H} HAR_{\text{worst}}(\omega) = \arg\max_{\omega \geq \omega_H} \delta(\omega). \tag{A.19}$$

Therefore, solving the frequency to reach maximal HAR_{worst} is transformed into solving the frequency to reach maximal $\delta(\omega)$.

Substitute equation (A.2) into equation (A.15), then we can obtain

$$\delta(\omega) = \frac{a_1\omega^4 + b_1\omega^2 - 1}{\omega R C_1(\omega^2 L C_2 - 1)^2}. \tag{A.20}$$

The derivative of $\delta(\omega)$ with respect to ω is given by

$$\delta'(\omega) = \frac{d_1\omega^6 + 3e_1\omega^4 + g_1\omega^2 - 1}{\omega^2 RC_1(\omega^2 LC_2 - 1)^3}, \tag{A.21}$$

where

$$\begin{cases} d_1 = L^3C_2^3 - R^2L^2C_2{}^3C_1 \\ e_1 = R^2LC_2{}^3 - L^2C_2{}^2 \\ g_1 = R^2C_2{}^2 + R^2C_1C_2 + 3LC_2 \end{cases}. \tag{A.22}$$

As can be seen from equation (A.21), the denominator of $\delta'(\omega)$ is always positive. Hence whether $\delta'(\omega)$ is positive, zero or negative is exclusively determined by its numerator.

Let $\alpha = R^2/(L/C_1)$, $\beta = R^2/(L/C_2)$ and $x = (\omega/\omega_1)^2$. Then the numerator of $\delta'(\omega)$ can be further represented by

$$g_C(x) = (1-\alpha)x^3 + 3(\beta - 1)x^2 + (\alpha + \beta + 3)x - 1. \tag{A.23}$$

When $a_1 > 0$, $R > \sqrt{L/C_1}$, then, $1 - \alpha < 0$. Accordingly,

$$g_C(-\infty) > 0,\ g_C(\infty) < 0,\ g_C(0) < 0. \tag{A.24}$$

Further, as $X_F(\omega_H) = 0$, and $X_F(\omega_H) > 0$, when $\omega > \omega_H$; $X_F(\omega) < 0$, when $\omega < \omega_H$ per the proof in Appendix A.2, as can be seen from equation (A.20), $\delta(\omega_H) = 0$, $\delta(\omega) > 0$, when $\omega > \omega_H$; $\delta(\omega) < 0$, when $\omega < \omega_H$. Correspondingly, $\delta'(\omega_H) > 0$, which also means

$$g_C(n_H^2) > 0. \tag{A.25}$$

By equation (A.24) and equation (A.25), we can see $g_C(x) = 0$ has three roots x_1, x_2 and x_3, which are governed by $-\infty < x_1 < 0 < x_2 < n_H^2 < x_3$. Accordingly $g_C(x)$ can also be represented by its root form as

$$g_C(x) = (1-\alpha)(x-x_1)(x-x_2)(x-x_3)\,. \tag{A.26}$$

It can be seen from equation (A.26), when $x > x_3$, $g_C(x) < 0$; when $x < x_3$, $g_C(x) > 0$. Accordingly, when $\omega > \sqrt{x_3}\omega_1$, $\delta'(\omega) < 0$, when $\omega < \sqrt{x_3}\omega_1$, $\delta'(\omega) > 0$. Therefore, $\delta(\omega)$ achieves its maximum extrema at $\omega = \sqrt{x_3}\omega_1$ for $\omega \geq \omega_H$. So is $HAR_{\text{worst}}(\omega)$ per equation (A.19). By the general formula for roots of cubic equation, x_3 can be obtained as

$$x_3 = (A+B)^{1/3} + D(A+B)^{-1/3} + (\beta-1)/(\alpha-1)\,, \tag{A.27}$$

Then as $\omega_{\max} = \sqrt{x_3}\omega_1$, equation (5.13) is obtained.

When $a_1 = 0$, $R = \sqrt{L/C_1}$ and $C_2 = (n_H^2 - 1)/n_H^2 C_1$, take them with equation (5.7) into equation (A.20), then

$$\delta(\omega) = \frac{\sqrt{n_H^2 - 1}\,\omega_1^3(\omega^2 - \omega_H^2)}{n_H^3\omega(\omega^2 - \omega_1^2)^2}\,. \tag{A.28}$$

The derivative of $\delta(\omega)$ with respect to ω is given by

$$\delta'(\omega) = -\frac{\sqrt{n_H^2 - 1}\,\omega_1^3 g_{C0}(\omega)}{n_H^3\omega^2(\omega^2 - \omega_1^2)^3}\,, \tag{A.29}$$

where

$$g_{C0}(\omega) = 3\omega^4 + (\omega_1^2 - 5\omega_H^2)\omega^2 + \omega_1^2\omega_H^2\,. \tag{A.30}$$

As can be seen from equation (A.29), the other terms except $g_{C0}(\omega)$ in $\delta'(\omega)$ is always positive. Hence, whether $\delta'(\omega)$ is positive, zero or negative is exclusively determined by $g_{C0}(\omega)$. Let $x = \omega^2$, then

$$g_{C0}(x)=3x^2+(\omega_1^2-5\omega_H^2)x+\omega_1^2\omega_H^2=3(x-x_1)(x-x_2)\,, \tag{A.31}$$

where $x_1<\omega_1^2<\omega_H^2<x_2$, since $g_{C0}(\omega_1^2)<0$, $g_{C0}(\omega_H^2)<0$.

It can be seen from equation (A.31), when $x>x_2$, $g_{C0}(x)>0$; when $x<x_2$, $g_{C0}(x)<0$. Accordingly, when $\omega>\sqrt{x_2}$, $\delta'(\omega)<0$, when $\omega<\sqrt{x_2}$, $\delta'(\omega)>0$. Therefore, $\delta(\omega)$ achieves its maximum at $\omega=\sqrt{x_2}$ for $\omega\geq\omega_H$. So is $HAR_{\text{worst}}(\omega)$ per equation (A.19). Further, by the general formula for roots of quadric equation, we can obtain

$$x_2=\omega_1^2(\sqrt{25n_H^4-22n_H^2+1}+5n_H^2-1)/6\,. \tag{A.32}$$

Then as $\omega_{\max}=\sqrt{x_2}$, (5.12) is obtained.

A.4 Frequency to Reach Maximal *HAR*worst for 3rdHP Filter

This section presents the derivation of the frequency to reach maximal *HAR*worst for 3rdHP filter.

According to Figure 5.4 (b), the impedance of 3rdHP filter is

$$Z_F(\omega)=\frac{1}{j\omega C_1}+\left(\frac{1}{j\omega C_2}+R\right)//\,j\omega L\,. \tag{A.33}$$

Accordingly, the reactive component $X_F(\omega)$ and resistive component $R_F(\omega)$ of 3rdHP filter impedance can be derived as

$$\begin{cases} X_F(\omega)=\mathrm{Im}(Z_F(\omega))=\dfrac{a_2\omega^4+b_2\omega^2-1}{(\omega^2(RC_2)^2+(\omega^2LC_2-1)^2)\omega C_1} \\ R_F(\omega)=\mathrm{Re}(Z_F(\omega))=\dfrac{RL^2C_2{}^2\omega^4}{\omega^2(RC_2)^2+(\omega^2LC_2-1)^2} \end{cases}, \tag{A.34}$$

where

$$\begin{cases} a_2 = R^2 L C_2{}^2 C_1 - L^2 C_2 C_1 - L^2 C_2^2 \\ b_2 = L C_1 - R^2 C_2^2 + 2 L C_2 \end{cases}. \tag{A.35}$$

As shown in Appendix A.3, for 3rdHP filter under the established design condition, its $HAR_{\text{worst}}(\omega)$ also achieves its extrema when $\delta(\omega)$ achieves its extrema. So the following is just to solve the frequency to reach maximal $\delta(\omega)$.

Substitute equation (4.35) and equation (A.34) into equation (A.15) , then we can obtain

$$\delta(\omega) = \frac{(R^4 C_1{}^2 - R^2 L C_1 - L^2) L C_1 \omega^2 - (R^2 C_1 - L)^2}{R L^4 C_1^3 \omega^5}. \tag{A.36}$$

The derivative of $\delta(\omega)$ with respect to ω is given by

$$\delta'(\omega) = \frac{-3(R^4 C_1{}^2 - R^2 L C_1 - L^2) L C_1 \omega^2 + 5(R^2 C_1 - L)^2}{R L^4 C_1^3 \omega^6} \tag{A.37}$$

Let $\delta'(\omega) = 0$, we can obtain equation (5.16). As $\delta'(\omega) > 0$, when $\omega < \omega_{\max}$; $\delta'(\omega) < 0$, when $\omega > \omega_{\max}$. Therefore, $\delta(\omega)$ achieves its maximum extrema at $\omega = \omega_{\max}$ for $\omega \geq \omega_H$. So per equation (A.19), $HAR_{\text{worst}}(\omega)$ also reaches its maximum at $\omega = \omega_{\max}$.

Appendix B: RLC Component Cost Estimation

This appendix documents how the RLC component cost estimation was done.

B.1 Input Data

The cost data for two C-type filters and one capacitor collected from the local utility are given in Table B.1. It should be noted that the cost of a 144 kV, 15 MVAr capacitor is 20%~25% less than that of a 144 kV, 30 MVAr C-type filter.

Table B.1: Cost Data Collected

No.	Type	Voltage Level	Capacity	Cost	Year
1	C-type Filter	144 kV	25 MVAr	$453,000	?
2	C-type Filter	144 kV	30 MVAr	$568,000	2015
3	Capacitor	144 kV	22 MVAr	$96,000	?

B.2 Assumptions

The following assumptions are made to perform cost estimation.

1) No. 1 and No. 3 were manufactured in 2010
2) The cost of RLC components is linearly related to their MVAr or MW capacity.
3) The cost of the filter and capacitor is composed of the cost of the RLC components and CTs, but excludes the cost of the switchgear. The C-type filter has four sets of CTs while the capacitor only has one set of CT. The cost of each set of CT is the same.
4) All C-type filters are tuned to 3rd harmonic and designed by using our proposed method with HAR_{limit}=1.2.

B.3 Estimation Method and Result

The estimation procedure is as follows.

1) Convert the cost in 2010 into the cost in 2015

   The inflation rate from 2010 to 2015 was around 8.35% according to the inflation calculator (2015 Nov, http://inflationcalculator.ca/).

   Therefore, the costs of No. 1 C-type filter and NO. 3 capacitor are 453*(1+8.35%)=490.81 (k$) and 96*(1+8.35%)=104.01 (k$) when converted to 2015, respectively.

2) Calculate the RLC component capacity

   According to assumption 4), the capacities of the RLC components in the C-type filter are calculated as follows.

Table B.2: RLC Component Capacity

	30 MVar C-type filter	25 MVar C-type filter	15 MVar C-type filter
Capacitor (MVAr)	34.62	28.85	17.31
Inductor (MVAr)	4.64	3.87	2.32
Resistor (MW)	0.10548	0.09184	0.06043

3) Establish cost equation

   Let c, l, r and f represent the cost of the capacitor per MVAr, the cost of inductor per MVAr, the cost of resistor per MW, and the cost of each set of CT, respectively. Then according to the Input Data and Assumptions, the following equation set can be built:

$$\begin{cases} 22c + f = 104.01 \\ 34.62c + 4.64l + 0.10548r + 4f = 568 \\ 28.85c + 3.87l + 0.09184r + 4f = 490.81 \\ 568*(1-25\%) \le 17.31c + 2.32l + 0.06043r + 4f \le 568*(1-20\%) \end{cases} \tag{B.1}$$

Equation set (B.1) has no feasible solutions, i.e., c, l, r and f cannot be all positive and meaningful values. As the last inequity of equation set (1) is just vague information, it is further relaxed as $568*(1-45\%) \le 17.31c + 2.32l + 0.06043r + 4f \le 568*(1-20\%)$. Then we can obtain a set of reasonable RLC component costs as

$$\begin{cases} c = 3.591 \\ l = 70.503 \\ r = 158.271 \\ f = 25.000 \end{cases} \tag{B.2}$$

which means the cost of the capacitor is $3,591/MVAr; the cost of the inductor is $70,503/MVAr; the cost of the resistor is $158,271/MW; and the cost of each set of CT is $25,000.